THE UNIVERSITY OF QUEENSLAND

AUSTRALIA

Radar Target Identification based on Complex Natural Resonances

Wei Cher Chen

Bachelor of Electrical Engineering

A thesis submitted for the degree of Doctor of Philosophy at

The University of Queensland in 2015

School of Information Technology and Electrical Engineering

Abstract

Radars, as the name suggests, were traditionally used for radio detection and ranging. Nevertheless, advancement in technology has made it possible for using them as a sensor to identify or classify targets. The design of a reliable and robust (in term of noise and clutter) radar target recognition technique has long been the dream of many researchers.

Although target recognition based on Singularity Expansion Method (SEM) has been studied extensively for the last few decades, the feasibility of using the Complex Natural Resonances (CNRs) or poles to classify targets is further investigated in this thesis. CNRs are chosen for representing the target in this thesis as they are theoretically independent of the aspect angle between the radar and the target, and they form a minimal set of parameters by which the target can be identified thus assisting the classification problem.

This thesis focus on designing a reliable and robust resonance based target discrimination process by breaking down the resonance based target identification process into two parts. The first part involves addressing the computational issue of the poles extraction scheme and extracting the dominant poles of the target. In a resonance based target identification scheme, it is important to extract the contributing CNRs of the target and store them into a target feature reference library. Incorrectly determining the dominant poles of the target could result in a false alarm during the target identification step. The second part consists of designing a classifier that is capable of identifying the correct target from a set of targets in the presence of noise.

Matrix Pencil Method (MPM) is utilized in this thesis to extract the CNRs of the target. MPM is chosen due to its low sensitivity to background noise and its computational ease and efficiency. However, spurious poles as a result from overestimating the modal order of the system could deteriorate the performance of the MPM. A method has been proposed to overcome this issue and improve the performance of the MPM.

Two methods have been proposed in this thesis to extract the dominant poles of the target. The first novel approach uses Principle Component Analysis (PCA) to fuse the backscattering signatures of the target from either multiple incident aspects or multiple incident polarizations. The significant poles of the target could then be extracted from the fused signature. This method has the advantage

of reducing the noise of the target's signatures and thereby aiding the dominant CNRs extraction process. The second novel approach utilizes the energy of each of the extracted resonances of the target to identify the contributing poles of the target.

After extracting the significant CNRs of the target, the next step is to design a reliable and robust resonance based target identification technique. Two robust resonance based target identification schemes have been introduced in this thesis. The first unique method utilizes a standard tool in statistical analysis for target discrimination. Canonical Correlation Analysis (CCA), which has previously been used in economics and medical studies, has been proposed in this thesis for target identification. Numerical results show that this technique is comparable to the Generalized Likelihood Ratio Test (GLRT) in the presence of white Gaussian noise.

One of the issues related to resonance based target classifier is that it requires the commencement of the late time period for the unknown target response to be determined accurately, in order to avoid false alarms during the target classification process. For Automatic Target Recognition (ATR) applications, usually such information is not known *a priori*. In view of this problem, a modified GLRT technique that utilizes the Time-Frequency Analysis (TFA) is introduced in the second novel approach. The improved GLRT method does not require *prior* knowledge of the beginning of the late time period for the transient response of the unknown target. Simulation results show that the modified GLRT method is comparable to the original GLRT technique when the commencement of the late time period for the unknown target response is correctly determined and outperforms the original GLRT technique when the commencement of the late time period for the unknown target response is incorrectly determined.

Declaration by Author

This thesis is composed of my original work, and contains no material previously published or written by another person except where due reference has been made in the text. I have clearly stated the contribution by others to jointly-authored works that I have included in my thesis.

I have clearly stated the contribution of others to my thesis as a whole, including statistical assistance, survey design, data analysis, significant technical procedures, professional editorial advice, and any other original research work used or reported in my thesis. The content of my thesis is the result of work I have carried out since the commencement of my research higher degree candidature and does not include a substantial part of work that has been submitted to qualify for the award of any other degree or diploma in any university or other tertiary institution. I have clearly stated which parts of my thesis, if any, have been submitted to qualify for another award.

I acknowledge that an electronic copy of my thesis must be lodged with the University Library and, subject to the policy and procedures of The University of Queensland, the thesis be made available for research and study in accordance with the Copyright Act 1968 unless a period of embargo has been approved by the Dean of the Graduate School.

I acknowledge that copyright of all material contained in my thesis resides with the copyright holder(s) of that material. Where appropriate I have obtained copyright permission from the copyright holder to reproduce material in this thesis.

Publications during Candidature

Journal Papers

[J1] Wei Cher Chen, N. V .Z. Shuley, "Robust target identification in white Gaussian noise using canonical correlation analysis," *IEEE Trans. Antennas Propag.*, vol. 60, pp. 3533–3537, July 2012.

[J2] Wei Cher Chen, N. V. Z. Shuley, "Robust target identification using a modified generalized likelihood ratio test," *IEEE Trans. Antennas Propag.,* vol. 62, pp. 264–273, Jan. 2014.

International Conference Papers

[C1] Wei Cher Chen, N. V. Z. Shuley, "Utilizing the energy of each of the extracted poles to identify the dominant complex natural resonances of the radar target," *Proceedings of the IEEE Antenna and Propagation Society International Symposium*, pp. 69–72, June 2007.

[C2] Wei Cher Chen, N. V. Z. Shuley, "Resonance based radar target identification using principal component analysis," *Asia Pacific Microwave Conference*, pp. 1–4, Dec. 2008.

National Conference Abstracts

[A1] Wei Cher Chen, N. V. Z. Shuley, "Matrix pencil method for estimating parameters use in radar target identification," *Proceedings of 10th Australian Symposium on Antenna*, Sydney, Australia, 14-15 February, 2007.

[A2] Wei Cher Chen, N. V. Z. Shuley, "Resonance based radar target identification using information fusion technology," *Proceedings of 11th Australian Symposium on Antenna*, Sydney, Australia, 18-19 February, 2009.

Publications included in this Thesis

[A1] – Incorporated as Chapter 4

Contributor	Statement of Contribution
W. C. Chen (Candidate)	Designed experiments (100%) Wrote the paper (80%)
N. V. Z. Shuley	Wrote and edited the paper (20%)

[C1] – Incorporated as Chapter 4

Contributor	Statement of Contribution
W. C. Chen (Candidate)	Designed experiments (100%) Wrote the paper (80%)
N. V. Z. Shuley	Wrote and edited the paper (20%)

[C2] – Incorporated as Chapter 4

Contributor	Statement of Contribution
W. C. Chen (Candidate)	Designed experiments (100%) Wrote the paper (80%)
N. V. Z. Shuley	Wrote and edited the paper (20%)

[J1] – Incorporated as Chapter 5

Contributor	Statement of Contribution
W. C. Chen (Candidate)	Designed experiments (100%) Wrote the paper (80%)
N. V. Z. Shuley	Wrote and edited the paper (20%)

[J2] – Incorporated as Chapter 5

Contributor	Statement of Contribution
W. C. Chen (Candidate)	Designed experiments (100%) Wrote the paper (80%)
N. V. Z. Shuley	Wrote and edited the paper (20%)

Contributions by Others to the Thesis

A/Prof. Nicholas V. Z. Shuley contributed closely by defining the research problems and the direction of the thesis. A/Prof. Nicholas V. Z. Shuley and Prof. Andrew Bradley also provided valuable guidance in the process of writing the thesis.

Statement of Parts of the Thesis Submitted to Qualify for the Award of Another Degree

None

Acknowledgements

This dissertation could not have been completed without the support of a large number of people. Therefore, I would like to take this opportunity to express deepest appreciation and most sincere gratitude to those who have assisted me during my PhD candidature, in particular, to A/Prof. Nicholas V. Z. Shuley for his in-depth knowledge of the field. Without his constant encouragement and guidance on my research, this PhD project would not have been possible. He has also given me many degrees of freedom to explore different possibilities in this research and has always been supportive of my novel research ideas. I would also like to express my gratitude to my associate advisor, Prof. Andrew Bradley, and A/Prof. Aleksander Rakic for their fruitful discussions and suggestions to my work.

Thanks also go to my colleagues in the Target Identification Group, Dr Faisal Aldhubaib and Dr Hoi-Shun Lui for their friendship and discussions which has made this PhD journey more enjoyable.

The author would also like to thanks his manager, Khan Steffensen, from SuccessFactors for his support and understanding by giving the author time-off to finish up his PhD.

The author would like to acknowledge the scholarship supports from the Australian Postgraduate Awards (APA) and Australian Research Council (ARC).

I would like to take this opportunity to thanks my wife for her endless care, understanding, and support. She is the person who makes me feel relax again when I am under stress. I would also like to thanks my son for bringing joy to the family. His birth has motivated me to finish up my PhD as soon as possible.

Last but not least, I would like to thank my parents and my brother for their genuine support and encouragement throughout my PhD journey.

Keywords

complex natural resonances (CNRs), noise, target identification

Australian and New Zealand Standard Research Classifications (ANZSRC)

ANZSRC code: 090609, Signal Processing, 20%
ANZSRC code: 100501, Antennas and Propagation, 40%
ANZSRC code: 100505, Microwave and Millimetrewave Theory and Technology, 40%

Fields of Research (FoR) Classification

FoR code: 0906, Electrical and Electronic Engineering, 30%
FoR code: 1005, Communications Technologies, 70%

Table of Contents

List of Figures

List of Tables

List of Abbreviations

AR	Auto-Regressive
ARMA	Auto-Regressive Moving Average
ATR	Automatic Target Recognition
CCA	Canonical Correlation Analysis
CF	Correlation Factor
CNR	Complex Natural Resonance
DC	Direct Current
EDN	E-pulse Discrimination Number
EFIE	Electric Field Integral Equation
EM	Electromagnetic
E-pulse	Extinction-pulse
FCC	Federal Communications Commission
FDTD	Finite Difference Time Domain
GLRT	Generalized Likelihood Ratio Test
GPOF	Generalized Pencil-of-Function
GTD	Geometrical Theory of Diffraction
HRRP	High Resolution Range Profiling
HWSEM	Hybrid Wavefront Singularity Expansion Method
ICA	Independent Component Analysis
ICZT	Inverse Chip-Z Transform
IFFT	Inverse Fast Fourier Transform
ISAR	Inverse Synthetic Aperture Radar
JEM	Jet Engine Modulation
K-pulse	Kill-pulse
LP	Linear Prediction
LRT	Likelihood Ratio Test
LTI	Linear Time Invariant
MoM	Method of Moment
MPM	Matrix Pencil Method
NCTR	Non-Cooperative Target Recognition
PCA	Principle Component Analysis

PEC	Perfect Electrical Conductor
PO	Physical Optics
Q-Factor	Quality-Factor
RCS	Radar cross section
ROC	Receiver Operating Characteristics
SEM	Singularity Expansion Method
SNR	Signal-to-Noise Ratio
SNRs	Signal-to-Noise Ratios
STFT	Short-Time Fourier Transform
SVD	Singular Value Decomposition
TFA	Time-Frequency Analysis
TFD	Time-Frequency Distribution
TLS	Total Least Squares
UHF	Ultra High Frequency
UWB	Ultra Wide Band
UTD	Uniform Theory of Diffraction
VHF	Very High Frequency
WVD	Wigner-Ville Distribution

Chapter 1: Introduction

Chapter 1: Introduction

1.1 Introduction

The ability to quickly and accurately identify targets, either friends or foes, at long distances and under all weather conditions has the potential to greatly enhance the effectiveness of military and commercial sensor systems. Possible attack from military aircrafts and missiles can require decisions regarding lethal engagement to be made within seconds of detecting an unknown target. This decision often relies upon the process of Non-Cooperative Target Recognition (NCTR).

In the realm of radar NCTR, there are two main categories: imaging and feature based identification [1]. Imaging radars provide a visualization of the detected target utilizing techniques such as focus spot scanning, inverse synthetic aperture [2], tomography [3], and inverse scattering [4]. In order to reconstruct the image of the target, imaging identification techniques require information of the target to be gathered from multiple incident aspect angles. Feature based identification radars sense unique characteristics which are often not image related such as jet engine turbine rotation rates, hull vibration, or maneuvering patterns. Such radars typically utilize Doppler modulation of the received signal spectrum to sense differential motion of portions of the structure [1]. Jet Engine Modulation (JEM), High Resolution Range Profiling (HRRP), and Inverse Synthetic Aperture Radar (ISAR) are some examples of the NCTR techniques used for recognizing aircraft targets [5].

The main disadvantage of these techniques is that the extracted images or features may vary as the incident aspect angle changes. Therefore, in order to correctly identify the target, a large database that contains the extracted images or features of the target, from multiple incident aspect angles, is needed. For most radar target identification problems, usually the incident aspect angles to the target are not known *a priori*. Therefore, it is preferable to have a target's signature that is purely dependent on the target itself and independent of the incident aspect angles.

In this thesis, the Complex Natural Resonances (CNRs) or poles will be used for representing the target. CNRs are chosen as they overcome the drawbacks highlighted previously. Natural resonance frequencies contained in a target's radar signature are determined by its structure and can serve to

identify the target. Furthermore, the full sets of CNRs depend only upon the target's geometry and composition [1], [6]. They are independent of the target's position or orientation to the radar [1], [7] and incident polarization states [1], [8]. These are appealing properties which have lead many researchers into using them as a feature set to characterize radar targets. While the poles are mathematically aspect independent, their associated residues are angle dependent and thus will require more than one radar measurement to be made to collect a complete set of poles to correctly represent the target [8], [9]. The feasibility of using the CNRs for target classification has also been successfully demonstrated in the literature [7], [9], [11].

Natural resonance NCTR is most effective using frequencies within the resonant region of the target [1]. In order to find the maximal number of poles to represent the target, it is necessary to use Ultra Wide Band (UWB) radar system which excites the full structure resonances of the target. Moreover, the target is excited at a frequency band for which the wavelength of the excitation corresponds approximately to the size of the target. Therefore, resonance based target identification is the only approach that is being considered. This will imply long wavelength for many targets (i.e. aircrafts etc.). For example, for a radar target of characteristic dimension equal to 1 meter, we use the Very High Frequency (VHF) band [30MHz - 300MHz] and, similarly, for a target of characteristic dimension of 0.1 meter, we use the Ultra High Frequency (UHF) band [300MHz - 3GHz].

Several assumptions are made in this thesis. First, it is assumed that only stationary Perfect Electrical Conductor (PEC) targets will be used in this research, therefore, any Doppler information will be ignored. Furthermore, the scope of this thesis is limited to ground-to-air scenario where the targets are illuminated by an UWB signal (i.e. Gaussian pulse, Rayleigh monocycle etc.) in the free space environment. It is also noted that the research presented in this thesis only dealt with numerical simulations or simulated wire model and ellipsoid targets. A lot of researchers around the world have used wire model targets (i.e. bent wire target, wire model aircraft etc.) in their research [8], [16], [24], [32], [39], [92]. This is necessary in the first instance to relate resonances to various dimensions. In a sense, they are canonical problems that go some way to verify the performance of the various target identification techniques. Simple shaped 3D target, ellipsoid, has also been introduced in this thesis to quantify the performance of the proposed techniques. To the author knowledge, there are only few instances in the literature where full 3D objects have been investigated. [44] and [93] are some of the works that used full 3D targets. The idea of this thesis is

not to investigate complicated geometries, but to get a sense of what can be achieved in successful identification using the proposed techniques. The work presented in this report concerns the design and development of an efficient and robust resonance based target identification system for Automatic Target Recognition (ATR) applications.

A brief summary of some of the target discrimination methods will be established in the next section follow by a discussion of the development and limitations of the resonance based target identification system. Last but not least, the motivation and scope of the research will be presented followed by an outline of the thesis.

1.2 Radar Target Recognition Methodologies

A general radar target recognition method consists of several discrete stages as shown in Figure 1.1: data acquisition (measuring radar returns or computing profiles within a simulated environment), pre-processing (i.e. scaling, noise reduction etc.), feature extraction, and finally using a suitable classifier to identify the target. The work presented in this thesis will concentrate on the final two stages (feature extraction and designing a robust classifier to identify the target) of the ATR system.

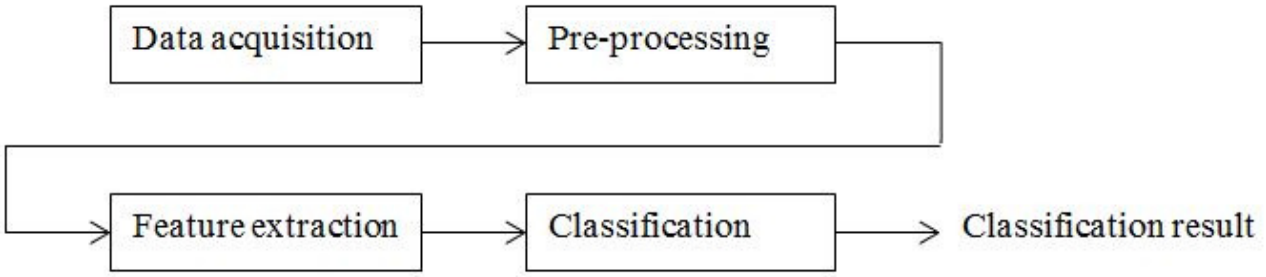

Figure 1.1: A typical ATR system.

Some of the well-known target recognition methodologies are listed below. There techniques are classified based on the transmitted waveforms used by the Radar [28], [86].

1. Recognition of targets with Narrow band signals:
   (a) Polarization features of radar echoes [87].
   (b) Target recognition using intensity of received signals.
2. Recognition of targets using multi-frequency signals [86]:

(a) Methods using impulse function and transfer function of target including use of response to step and ramp functions.

(b) Use of natural resonances as target feature at multiple frequencies.

(c) Combination of natural resonances and frequency dependence of radar cross section (RCS).

(d) Using polarization and frequency dependence of RCS.

(e) Using RCS at different frequencies.

3. Recognition of targets using UWB signals [26]:

(a) Using high resolution range profile of targets so that all of the major scatterers of the target can be resolved individually, thereby generating the image of the target.

(b) Using CNRs: this method illuminated the target with a sufficiently broadband signal to be able to excite the target's resonance frequencies.

Lin and Kiang [88] have demonstrated target discrimination for the cases of prolate spheroids based on the concept of natural frequencies. Chen and Walton [89] have used the multi-frequency radar returns for classification of targets in both the time and frequency domains. They have concluded that the use of resonance region (1.0 to 20.0 MHz) has great potential for radar target discrimination between targets of different class. Baum [7], [9] has reported that the Singularity Expansion Method (SEM) is useful for the aspect independent nature of the pole locations in the complex frequency plane/ S-plane. SEM is a way to represent the solution of the scattering problems in terms of singularities in the S-plane. An example of the poles of the metallic thin straight wire targets in the S-plane could be found in Figure 1.2 below.

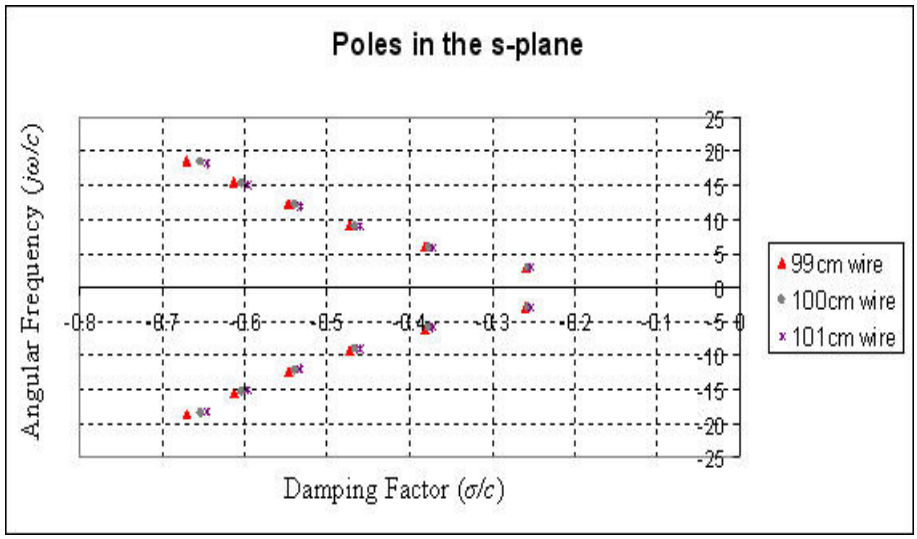

Figure 1.2: Normalized poles of the metallic thin straight wire targets in the S-plane.

Out of the above mentioned methodologies, the target recognition based on CNRs of the target is of major interest to the radar designer due to the appealing properties of the CNRs as mentioned in Section 1.1. Therefore, we will be using CNRs as a feature set for target recognition in this thesis.

1.3 Development and Limitations of the Resonance Based Radar Target Identification System

Extracting the complex resonances from the target response accurately is critical for the success of resonance based target recognition, as the target identification process is based solely on these resonances. The development of resonance based radar target recognition is based on the SEM initially developed in 1971 by C. E. Baum [7], [9]. Baum was the first to demonstrate that the target resonances can be extracted by searching for singularities in the Method of Moment (MoM) matrix that result from a frequency domain integral equation formulation [7]. The disadvantages of this method are that it is limited to the frequency domain formulation and its computational cost is too high.

In view of these problems, Van Blaricum and Mittra [10] proposed using Prony's algorithm to extract the target resonances from the late time of the time domain target response. This approach has drawn substantial attention in the literature as the extraction procedures can be applied to any

computed or measured target response. However, it is well known that the accuracy of the extracted CNRs from the Prony's method is significantly degraded when the data is corrupted by noise. Therefore, researchers around the world have been introducing better methods for resonance extractions. Least Square Prony's Method [11], Continuation Method [12], and Matrix Pencil Method (MPM) [13], [14] are some examples of the improved resonance extractions techniques. Apart from these poles extraction techniques, there are also target recognition schemes that extract poles as part of the identification process. Kill-pulse (K-pulse) technique [15] and Extinction-pulse (E-pulse) technique [16], [17] are some examples of the target recognition schemes. Most of these techniques are capable of determining the number of poles embedded in the late time of the target signature and accurately extracting the CNRs, provided that the target response has a minimum Signal-to-Noise (SNR) ratio of 20dB or better [13]. A perturbation analysis of the MPM can be found in [19]. In particular, the perturbation of the variance of the extracted resonant frequency, $Var(\delta f_1)$, as a function of SNR can be found in Figure 2 of [19]. At a SNR of 20dB, $Var(\delta f_1) = 10^{-5}$.

Identifying the correct portion of the target response for extracting the CNRs is another issue of the resonance based target identification system. It is well established that the damped exponential model only applies to the late time period of the target response, thus inclusion of any early time samples in the extraction procedure would significantly degrade the accuracy of the extracted CNRs. Therefore, it is important to correctly determine the commencement of the late time period. Ilavarasan [81] has formulated a method to calculate the late time commencement for a given target, provided that the excitation pulse width, the time when the pulse hits the target and the one way transit time of the pulse along the line of sight under that particular incident aspect, are known in advance. However, such information is usually not known a *priori* for ATR applications. Therefore, determination of the commencement of the late time period automatically has always been the dream of researchers around the world.

Other than the process of resonance extraction, another research interests have focussed on the development of target recognition schemes for ATR applications. The key requirement for high performance ATR is the separability of the extracted features in the feature space. The CNRs which characterize an object are found to be excitation invariant. The positions of the resonances in the complex frequency plane or S-plane do not shift as the same object is viewed along different

incident directions or with different polarizations, which permits a minimum amount of data to be used in object discrimination [1], [6]-[8]. According to the SEM, the CNRs are purely dependent on the target's geometry and composition [1], [6]. Differences in the target attributes from target to target will result in different sets of CNRs and target recognition could then be achieved based on such differences between the CNRs. Mittra, Pearson, and Van Blaricum first proposed using the S-plane for target discrimination [21]. Some of the resonance based ATR schemes that are popular in the literature include K-pulse [22], [23], E-pulse [16], [17], and Generalized Likelihood Ratio Test (GLRT) [24], [25]. Amongst them, the GLRT has produced a better identification result, in the presence of noise [24], [25]. Therefore, it will be used as the reference classifier in this research.

Other than radar targets in free space, the concept of using target resonances has also been applied to subsurface targets or targets below an interface. The motivation of this research originates from the topic of Unexploded Ordnance (UXO) detection using Ground Penetrating Radar (GPR). Extensive theoretical studies of CNRs for targets below realistic soil models have been conducted by Lawrence Carin's research group [69], [90] and Wang [91]. Chen [11] has successfully extracted the CNRs of UXOs from experimental data. Baum [70] has conducted some analytical studies on the resonant behaviour of subsurface dielectric targets. Recently, the concept of using target resonances has also been applied to biomedical targets [71]-[74]. In conclusion, the behaviour and extraction of CNRs for subsurface targets are quite well documented in the open literature.

1.4 Motivation and Scope of this Research

The main motivation behind this research is to design and develop a reliable and robust resonance based target identification system that could enhance the effectiveness of the current military and commercial sensor systems.

The resonance based target identification process is broken down into two parts in this research. The first part involves identifying the dominant poles of the target. In a resonance based target identification scheme, it is crucial to extract the contributing CNRs of the target and store them into a target feature reference library. Incorrectly determining the dominant poles of the target could result in a false alarm during the target recognition step. The second part consists of designing a

classifier that is capable of identifying the correct object from a set of targets under all weather conditions.

1.4.1 Dominant Poles Extraction Process

Precise extraction of the complex resonances from the target response is critical for the success of resonance based target recognition, as the target recognition process is based solely on these resonances. However, in real world application, noise (i.e. antenna ringing etc.), clutter (i.e. ground, sea etc.), and multipath could be source of interferences to the ATR system. Noise will appear in the early time region as well as the late time region. The CNR extraction process is then forced to fit the early-time non-resonant signals into the SEM and results in erroneous CNR [11]. Any clutter appearing in the late time region will also cause error. The effect of clutter on the ATR system is smaller in the ground-to-air scenario as compared to the ground-to-ground or air-to-ground scenario. This is due to the fact that the reflection from the ground is larger than the reflection from the target.

All these interferences would result in erroneous CNRs and cause false alarm during target classification process [11]. Therefore, they should be removed before the poles extraction process. Some of the noise, clutter, and multipath removal techniques include Singular Value decomposition (SVD), Principle Component Analysis (PCA), Independent Component Analysis (ICA), and CLEAN and spatial location diversity [75]-[78]. As mention previously, it is assume in this thesis that the targets are illuminated by an UWB signal in the free space environment. However, in order to quantify the performance of the proposed resonance based target discrimination process, white Gaussian noise is added to the target signature.

Amongst all the existing poles extraction techniques (shown in Section 1.3), MPM is chosen to extract the CNRs of the target in this thesis. MPM is chosen as vigorously studied in the literature has proven its computational ease and efficiency and that it is less sensitive to background noise [18]-[20]. However, extraneous poles as a result from overestimating the modal order of the system could deteriorate the performance of the MPM. In view of this issue, a method has been proposed in Chapter 4 to improve the performance of the MPM.

Before storing the target's CNRs into the target feature reference library, it is important to ensure that only the contributing poles of the target are extracted. This is needed to prevent a false alarm during target classification process. Two methods have been proposed in this thesis to extract the dominant poles of the target. The first novel approach uses PCA to fuse the backscattering signatures of the target from either multiple incident aspects or multiple incident polarizations. The significant poles of the target could then be extracted from the fused signature. The second novel approach utilizes the energy of each of the extracted resonances of the target to identify the contributing poles of the target. These two methods will be discussed in detail in Chapter 4.

1.4.2 Robust Resonance based Target Recognition Schemes

After extracting the significant CNRs of the target, the next important step to the creation of a reliable and robust resonance based target discrimination system is to design an efficient and robust resonance based target identification technique for ATR applications.

Two novel and robust resonance based target identification schemes have been introduced in this thesis. The first unique method utilizes a standard tool in statistical analysis for target discrimination. Canonical Correlation Analysis (CCA) which has previously been used in economics and medical studies has been proposed in this thesis for target identification. A detail discussion of the CCA based technique can be found in Chapter 5.

One of the issues related to resonance based target classifier is that it requires the commencement of the late time period for the unknown target response to be determined accurately. It is well established that the damped exponential model only applies to the late time portion of the target response. Therefore, inclusion of any early time samples in the identification process would significantly degrade the performance of the classifier. However, for ATR applications, usually the late time period for the unknown target response is not known *a priori*. In light of this problem, a modified GLRT technique that utilizes the Time-Frequency Analysis (TFA) is introduced in Chapter 5.

1.5 Organisation of the Thesis

As mentioned before, the resonance based target identification process is divided into two parts in this research. The first part of the thesis focuses on developing methods to identify the dominant poles of the target, while the second part concentrates on designing and developing efficient and robust classifiers for ATR applications. This thesis is organised as follows.

Chapter 2 gives a literature review of the resonance based target identification process. The theoretical background of the CNRs, SEM, CNR extraction methods such as the MPM, and target recognition schemes such as the GLRT method will be presented in this chapter.

In Chapter 3, we will look at some of the signal processing techniques, CCA, PCA, and Wigner-Ville Distribution (WVD), that are utilized in this research to enhance the resonance based target identification scheme. The theoretical background of these three techniques will be described in detail in this chapter.

Chapter 4 will present the works that have been done to identify the contributing poles of the target. These include addressing the computational issue of the MPM and developing two novel techniques to extract the dominant CNRs of the target. The first novel method utilizes the PCA to obtain the fused signature of the target from either multiple incident aspects or multiple incident polarizations. The significant poles of the target could then be extracted from the fused signature. The second unique method uses the energies of the extracted CNRs to identify the dominant poles of the target.

Last but not least, two unique reliable and robust resonance based target classifiers will be presented in Chapter 5. The first classifier uses a novel statistical method based on CCA to perform target classification. The second classifier introduces WVD to the original GLRT method to enhance the performance of the classifier. Numerical examples show that the performance of both of the target identification techniques is comparable to the original GLRT method in the presence of noise.

Finally, a summary of the works presented in this thesis and recommendations for further research are given in Chapter 6.

Chapter 2: Resonance Based Rader Target Identification

Chapter 2: Resonance Based Rader Target Identification

2.1 Introduction

A typical ATR system could be found in Figure 1.1. The problem of interest here is to identify a specific target based on the noisy backscattered field from a "wide-band" transmitted pulse. First of all, the target is illuminated by an electromagnetic (EM) pulse or UWB signal. The backscattering signature of the target is then collected by the receiver. Next, signal processing techniques are applied to the received signal for pre-processing (i.e. removing any unwanted components like noise and clutter, combining the signatures of the target from multiple aspects using data fusion techniques etc.) purposes before the desire feature of the target is being extracted. The extracted feature of the target is then stored into a reference library for classification purposes. Last of all, a classifier is used to identify the unknown target.

In this thesis, the target identification scheme makes use of the complex resonances embedded in the target signature as a feature set to distinguish one target from another. This chapter presents an overview of the resonance based radar target identification. The theoretical background of the CNRs, SEM, CNRs extraction methods such as the MPM, and target recognition schemes such as the GLRT method will be provided in this chapter.

2.2 Complex Natural Resonances

In order to understand the concept of CNRs, we first have to understand what resonance is. To illustrate the concept of resonance, consider a tuning fork. When it is struck, it produces an initial transient, which almost instantaneously changes to a simple relatively pure note or tone. The frequency of the vibration and the tone that it produces is purely dependent on the physical shape, size and material of the tuning fork.

The term CNRs arises when an object (i.e. string etc.) vibrates and produces more complex waves with a set of frequencies instead of just one frequency as in the case of tuning fork. The same thing

happens for EM scattering. The incident field (i.e. ultra-short pulse etc.) induces current on the radar target. CNRs are then formed corresponding to the shape, size and material of the radar target.

As mentioned in Section 1.1, in order to study the feasibility of the proposed techniques, the scope of this thesis has been limited to free space stationary PEC targets. For dielectric targets, the situation becomes more complicated due to the existence of both the external and internal resonances. The internal resonances are caused by the internal waves that experience multiple internal reflections, whereas the external modes are caused by the surface creeping waves [95]. In Chapter 4 of [70], Baum studied the general properties of the external and internal resonances of the dielectric target. It was concluded that the external resonances are quite similar to the resonance of the PEC target in the same geometry and the external resonance of the target inside the medium can be approximated using the Baum's Transform [70]. For internal resonance, the mechanism is essentially the internal bouncing of the radiation within target. Experimentally it can be measured by coating the target with metal foil, and coupling into the target using a small hole then measuring the resonance using electric and magnetic probes. Chen [95] has studied the resonance behaviour of the spherical target within a lossless environment using modal analysis and obtained similar conclusions to Baum for the relationship of the external and internal resonances for PEC and PMC targets.

The underlying advantages of using the CNRs for target identification are as follow:

- The CNRs are theoretically independent of the aspect angle between the radar and the target. This means that the same poles will be extracted from different transient signatures, for different incident angle, of the same target [1], [7]-[11], [55].
- They are polarization independent [8].
- They form a minimal set of parameters by which the target can be identified thus assisting the classification problem [11], [55].
- They are formed corresponding to the physical and geometrical properties of the target. Therefore, every target has its own unique set of poles [1], [7]-[11], [55].
- A target's RCS is enhanced in the resonance region [26].

Some of the disadvantages of using the CNRs for target identification are as follows:

- For certain incident aspect angles or incident polarization states some poles cannot be excited sufficiently and the corresponding polar-residue patterns show deep nulls at certain aspects indicating that, while the poles are aspect independent themselves, the excitation mechanism for producing them is not [8], [9]. This could cause false alarms during target classification process.
- It is a challenging process to identify the dominant CNRs of the target if interferences such as noise, clutter, and multipath are present as they would result in erroneous CNRs. These interferences could result in false alarm during classification process [11].
- It is also difficult to identify the significant CNRs of concealed targets and dielectric targets due to the heterogeneous dispersive nature of the half-space and additional resonant modes from internal bouncing respectively [70].
- The identification of the complex resonances associated with the structures with high radiation damping is a difficult proposition, even with relatively noise-free data [94].
- It is a challenging process to determine the correct portion of the target response for extracting the CNRs. It is well established that the damped exponential model only applies to the late time period of the target response, thus inclusion of any early time samples in the extraction procedure would significantly degrade the accuracy of the extracted CNRs. However, such information is usually not known a *priori* for ATR applications [11], [94].

2.3 Excitation Pulse

In order to find the maximal number of poles to represent the target, it is necessary to use UWB radar system which excites the full structure resonances of the target. UWB signals are used for detecting echoes from the local scattering centers of the target and hence require the pulse width to be of the order of a nanosecond to meet the resolution criteria for a typical target [28]. This low pulse width will result in a low energy bandwidth product which will lower the detection range of the radar. For achieving a detection range of 100km, the peak power of the transmitted signal should be of the order of few tens of gigawatts [96]. The peak power is determined by multiplying the power of the transmitted pulse by the bandwidth duration product of the signal and the energy of the transmitted signal [96].

Chapter 2: Resonance Based Rader Target Identification

UWB system is defined with respect to the spectrum property of the transmitted signals [97], rather than any other properties. This indicates the importance of the pulse in the UWB system [98]. According to the definition of UWB signals by the Federal Communications Commission (FCC), any pulse with a fractional bandwidth ≥ 0.20 or a 10dB UWB bandwidth ≥ 500MHz can be used as a basic UWB pulse [97]. In practice, the selection of pulses depends on many factors. The radiation efficiency and spectrum shape are two of the general concerns. Since the transmitted UWB signal is usually a baseband signal, the basic pulse should not have a Direct Current (DC) component to allow effective radiation. In addition, to maximize the radiated power within the FCC constraints, the pulse should have a flat spectrum over the desired bandwidth [98]. Among pulses with definite mathematical expressions, typically used pulses include Gaussian monocycles, Gaussian doublet, Rayleigh monocycles and Manchester monocycles [98].

In this research, plane wave excitation will be considered. Although any temporal waveform may be used, a plane wave impulse is perhaps the most useful. With the impulse response known, the response due to any other plane wave incident from the same direction may be obtained by a convolution operation. However, it is impractical to obtain an ideal impulse response since its frequency spectrum extends from zero to infinity. Hence, a Gaussian pulse excitation with a rapid decay to a negligible value in both the time and frequency domains is considered. This type of pulse is effectively band limited and is well suited for numerical computation [27].

The time domain formulation for the Gaussian plane wave is given by [27]

$$E^i(r,t) = E_0 \frac{4}{T\sqrt{\pi}} e^{-\gamma^2} \tag{2.1}$$

with

$$\gamma = \frac{4}{T}\left(ct - ct_0 - r \cdot a_k\right) \tag{2.2}$$

where a_k is the unit vector in the direction of propagation of the plane wave, T is the pulse width of the Gaussian impulse, r is a position vector relative to the origin, c is the velocity of propagation in the external medium, and t_0 is a time delay which represents the time at which the pulse peaks at the origin. The time delay is introduced to ensure a smooth rise of the incident field

from a zero value. An example of the time and frequency profiles of the Gaussian pulse can be found in Figure 2.1.

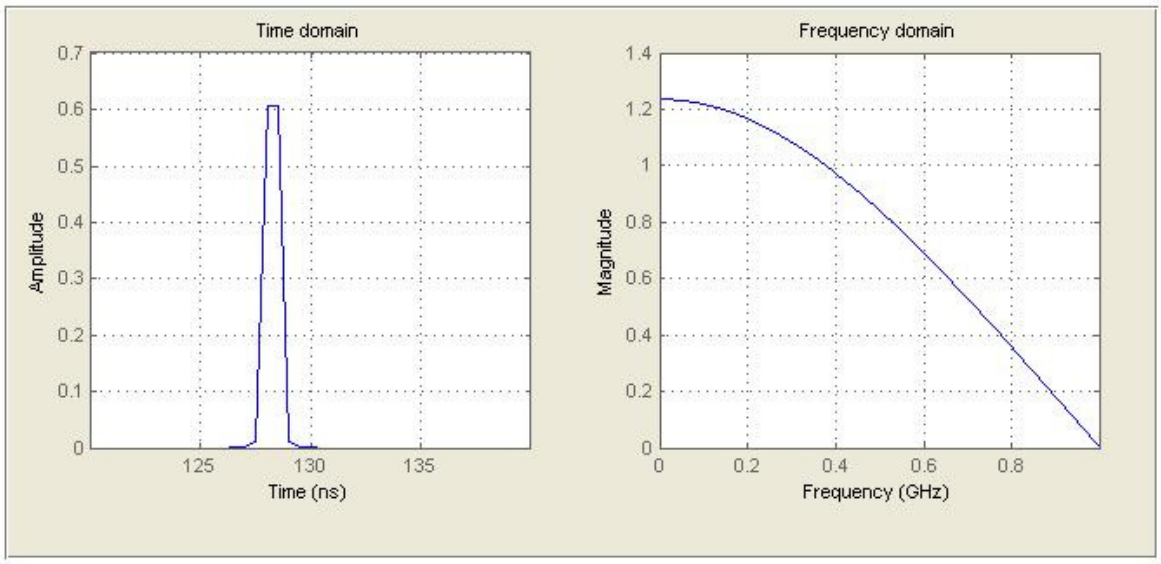

Figure 2.1: Time and frequency profiles of a Gaussian pulse with a bandwidth of 1GHz.

2.4 Target Response

Upon the plane wave excitation, current is induced on the target. The response of the target due to plane wave excitation can be obtained either by direct measurement or by simulation. Computational electromagnetics software such as FEKO (Field Computations Involving Bodies of Arbitrary Shape) and XFDTD could be used to obtain the target response.

FEKO implements the frequency domain method of MoM solution of the Electric Field Integral Equation (EFIE) for low frequencies problem, and the Physical Optics (PO) Geometrical Theory of Diffraction (GTD) and Uniform Theory of Diffraction (UTD) for high frequencies problem [28]. Electromagnetic fields are obtained by calculating the electric surface currents on the conducting surfaces. The currents are calculated using a linear combination of basis functions, where the coefficients are obtained by solving a system of linear equations. Once the current distribution is known, further parameters, such as far field of the target, can be obtained. The frequency samples obtained can be converted to time samples by either using an Inverse Fast Fourier Transform (IFFT)

or an Inverse Chirp-Z Transform (ICZT). Further details on the MoM can be found in Section 2.5 below.

In FEKO, many small triangular patches are used to form the target. The current distribution on the conducting surface of the target is then obtained by calculating the current distribution of each of the small triangular patch.

XFDTD is a three-dimensional full wave electromagnetic solver based on the Finite Difference Time Domain (FDTD) method. The FDTD method belongs in the general class of differential time domain numerical modelling methods. The Maxwell's (differential form) equations are solved in a leap-frog manner; that is, the electric field is solved at a given instant in time, then the magnetic field are solved at the next instant in time, and the process is repeated over and over again until a state of convergence has been reached. This typically means that all field values have decayed to essentially zero or a steady-state condition has been reached. The amount of interest devoted to time domain numerical methods to solve electromagnetic problems have been increasing dramatically in recent years. This is due partly to its conceptual simplicity and great flexibility to treat practical problems (i.e. modeling of biological tissues etc.). Further details on FDTD can be found in [27].

While the FDTD algorithm is an excellent tool for the analysis of the transient scattering from general two dimensional target, it is computationally intensive for the three dimensional problem of interest [106]. Thus, FEKO will be used to obtain the target response in this thesis.

2.5 Method of Moments

In general, integral equation methods are known to have several advantages over those based on differential equations [82]. In the context of solving the scattering problem, all the integral equation formulations implicitly incorporate the radiation condition at infinity through a properly chosen Green's function. The MoM introduced by Harrington [29] is an integral equation based method for the scattering problem. In this method, the integral equations are reduced to a set of complex valued system of linear equations. This is achieved by expanding the unknown currents using a known set of basis functions. An inner product is formed with this expansion and by defining a set of weighting functions [83]. This results in a matrix equation of the form of

$$[Z][I]=[V] \tag{2.3}$$

where the matrix $[Z]$ is the approximation for the integral equation operator and is only dependent on the geometry and constitutive parameters of the problem. Vector $[I]$ is the unknown current distribution on the wire and vector $[V]$ is the excitation. The excitation $[V]$ will normally vary according to different excitations.

The matrix equation is then solved for $[I]$ using either the direct methods (i.e. LU decomposition or Gaussian elimination methods), or iterative methods (i.e. conjugate gradient and fast multipole methods [84], [85]). For an object under consideration with X unknowns, the computational load is X^3 for the direct methods. For the iterative methods, this requirement is somewhat lower depending on the algorithm. The number of unknowns increases with the frequency of operation. This enforces a limit on the electrical size of the object that may be considered using a single computer. The numerical procedure of MoM could be found in [29].

2.6 Early Time and Late Time Target Responses

It is well known that when a radar target is illuminated by a short pulse, the scattered transient signal may be divided into an early time component and a late time component as shown in Figure 2.2. When an incident EM pulse first strikes a target, some of its energy will be reflected in the reverse direction to the incident field. This is known as backscattering. The interval during which this occurs and before a resonance condition can be established is known as the early time period. The early time response of the transient scattered filed is characterized by time varying coefficients determined by local features of the scattering object and is due to direct physical optics fields, as well as a sum of temporally modulated natural modes [30]. The early time scattering phenomenon is local, aspect dependent, and target dependent. In some instances and orientations, the early time response components of the return signal can be of much larger peak amplitude than the resonance or late time responses. Due to its aspect dependent nature, it is well known in the literature that modelling of the time varying early time response is complicated [31]-[33].

As the exciting field is passing by the target, it induces current on the target's conducting surface. The finite surface area of the target limits the current flow and causes it to flow back and forth on

the body. When the frequency coincides with the period of oscillation of the induced currents, a strong resonance will occur. The interval during which this occurs is called the late time period. The beginning of the late time period is given by [7]

$$T_L = T_b + T_p + 2T_{tr} \quad \textbf{(2.4)}$$

where T_b is an estimate of the time when the incident wave strikes the leading edge of the target, T_p is the effective pulse duration used in the system, and T_{tr} is the maximum transit time of the target. In other words, the beginning of the late time period is defined as the time when the pulse has transited through the whole target by one round trip along the line of sight after hitting the target. For complex targets or targets containing highly damped CNR's, it is difficult to separate the early time and late time responses [11]. The presence of noise, a non-resonant signal, in the target signature could also affect the separation of the early time and late time responses as noise will appear in both the early time and late time regions of the target response [11]. Auto-Regressive Moving Average (ARMA) model [34] and Half Fourier Transform [32] are some of the methods used to separate the early time and late time responses.

Compared to the complexity of modelling the early time response, modelling the late time response is much simpler. This is because the scattering phenomenon in the late time period is dominated by global resonances and theoretically such global phenomena are purely target dependent and aspect independent. Late time scattering can be described by the SEM, which is used to model the late time response of the target by a sum of complex exponentials. The CNRs can then be directly extracted from the complex exponentials.

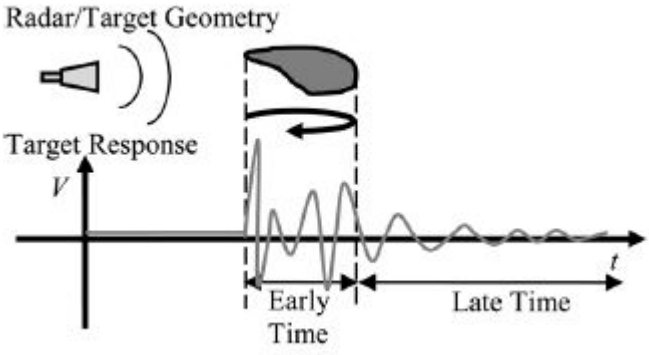

Figure 2.2: Early time and late time responses of a target.

2.7 Complex Natural Resonances Extraction Techniques

Target identification based on CNRs requires an accurate and reliable method for extracting the poles. There are two methods for extracting the CNRs from the received signature of the target. The first method is based on the formulation of the scattering problem. The induced current on the target can be solved for by using MoM as shown in Equation 2.3.

For CNRs, which are purely dependent on the target rather than the excitation field, the MoM equation can be rewritten as

$$[Z][I] = [0] \tag{2.5}$$

A solution exists only when $\det(Z) = 0$ [7]. The CNRs can then be solved for by any complex root searching scheme such as Mueller's method [7], [79]. However, this technique is limited to frequency domain formulations and the computational cost is usually too high. Therefore, this method for extracting the CNRs is not use in this research.

The second method for extracting the CNRs is based on linear time signal's model. Two of the linear time signals' models used for extracting the CNRs from the transient response of the target are Auto-Regressive (AR) and ARMA models [34], [80]. The SEM, which has provided a convenient way to model the late time response of the target as a sum of complex exponentials, employs the AR model [34]. The SEM based techniques for estimating the parameters are further divided into either non-iterative or iterative. For the former, representations include the Prony's method, the E-pulse technique and the MPM. Examples of the iterative technique include least squares curve fitting and genetic algorithms [35]. In this research, the non-iterative technique will be used. In particular, the MPM is chosen as it is more robust to noise in the sampled data and it is proven to have better computational efficiency [18]-[20].

In contrast to AR model, the use of the ARMA model has eliminated the need to determine the start of the late time period for the transient response of the target [34].

2.7.1 Singularity Expansion Method

In circuit theory and using the Linear Time Invariant (LTI) model, the impulse response characterizes the behaviour of linear circuits or systems. For most linear circuits, the impulse response can be determined from the singularities of the response function in the complex frequency plane and the corresponding residues according to the resistive, inductive and capacitive elements of the circuits [36], [37]. The impulse response can be modelled as a sum of all residues multiplied by exponentially damped sinusoids.

In the 1960s, Kennaugh and Moffatt [38] extended the concept of impulse response and applied it to transient scattering from the radar targets. Based on their work, Baum [7] introduced the SEM in the early 1970's to describe the transient electromagnetic scattering phenomena.

The development of the SEM has provided a convenient way to model the late time response of the target as a sum of complex exponential. The CNRs or poles can then be directly extracted from the complex exponentials. It is to be noted that the SEM does not directly provide the transient response, but rather is an alternative method of looking at the broadband time domain response of boundary value problems and as such is a procedure to be used in conjunction with an analysis procedure [39].

2.7.2 Matrix Pencil Method

As mentioned previously in Chapter 1, researchers around the world have been looking for alternative methods which provide better resonance extraction performance as compared to the Prony's method. Among them, the MPM [13] has been extensively studied in the literature. MPM is also known as Generalized Pencil-of-Function (GPOF) method [13].

MPM is relatively new, even though its roots go back to the Pencil-of-Function (POF) approach [40]-[42], which has been in use for years. The term "pencil" originated with Gantmacher, in 1960 [13]. The basic difference between the MPM and the POF is that the MPM is computationally more efficient even though they both start from the same philosophy. The original POF method was a variation of the polynomial method and hence it has the same bottlenecks as associated with

Prony's method, which requires two distinct steps. However, the MPM as presented in [13], [19], [20] is a one-step process and thus it is more computational efficient. More importantly, the original POF method deals with continuous time signals, while the MPM is designed for discrete time signals [43]. In this thesis, the computed target signatures are discrete time signals and thus the MPM is employed.

A number of versions of the MPM are available in the literature [18]. The one that is presented and used in this thesis is the one with a Linear Prediction (LP) and SVD, given by [13]. The SVD gives a prediction of the desired number of poles and also removes noise from the sample data [18].

In general, the observed late time of the electromagnetic energy scattered from an object in free space can be modelled by

$$y(t) = x(t) + n(t) = \sum_{i=1}^{M} R_i e^{s_i t} + n(t) \qquad \textbf{(2.6)}$$

where $y(t) =$ observed time response, $x(t) =$ signal, $n(t) =$ noise in system, $R_i = r_i e^{j\theta_i}$ is the residue or complex amplitude of the i^{th} mode, $s_i = \sigma_i \pm j\omega_i$ is the Complex Natural Resonance (CNR) or pole of the i^{th} mode, $M =$ desired number of poles to be extracted, $r_i =$ aspect dependent amplitude of the i^{th} mode, $\theta_i =$ aspect dependent phase of the i^{th} mode, $\sigma_i =$ aspect independent damping factor of the i^{th} mode, and $\omega_i =$ aspect independent angular frequency of the i^{th} mode.

Note that Equation 2.6 only applies to the late time response of the target. Inclusion of any non-resonant signals (i.e. early time signal, noise etc.) could result in erroneous poles [11]. It is assumed that the interferences such as clutter and multipath are removed before applying Equation 2.6 as they could also result in erroneous poles.

The sampled version of the above expression can be written as

$$y(kT_s) = x(kT_s) + n(kT_s) = \sum_{i=1}^{M} R_i z_i^k + n(kT_s) \qquad \text{for } k = 0,1,2,\ldots,N-1 \qquad \textbf{(2.7)}$$

where $z_i = e^{s_i T_s}$ is the roots of the system, $k =$ late time sample for the target, T_s is the sampling period which should satisfy the Nyquist sampling criteria to avoid higher mode aliasing, and N is the total number of late time data samples in the discrete time domain.

To combat noise, the Total Least Squares (TLS) MPM has been found to be superior [18]. In this implementation, one forms the data matrix $[Y]$ from the noise contaminated $y(t)$ as show below:

$$[Y] = \begin{bmatrix} y(0) & y(1) & \cdots & y(L) \\ y(1) & y(2) & \cdots & y(L+1) \\ \vdots & \vdots & & \vdots \\ y(N-L-1) & y(N-L) & \cdots & y(N-1) \end{bmatrix}_{(N-L)\times(L+1)} \quad \textbf{(2.8)}$$

where L is the pencil parameter, which is chosen to be $\frac{N}{3} \le L \le \frac{N}{2}$ such that the variance in the parameters z_i, due to noise, has been found to be minimum [13], [18].

Next, apply SVD to matrix $[Y]$,

$$[Y] = [U][\Sigma][V]^T \quad \textbf{(2.9)}$$

where $[U]$ is the $(N-L)\times(N-L)$ unitary matrix whose columns are the eigenvectors of $[Y][Y]^T$, $[V]$ is the $(L+1)\times(L+1)$ unitary matrix whose columns are the eigenvectors of $[Y]^T[Y]$, $[\Sigma]$ is the $(N-L)\times(L+1)$ diagonal matrix containing the singular values of $[Y]$, and "T" denotes the conjugate transpose.

The choice of the desired number of poles, M, is done at this stage [13]. One looks at the ratio of the various singular values of $[Y]$ to the largest one. Typically, the singular values beyond M are discarded. Selection of M is done by considering the singular value, σ_c, such that

$$\frac{\sigma_c}{\sigma_{max}} \approx 10^{-p} \quad \textbf{(2.10)}$$

where p is the number of significant decimal digits in the data [13]. For instance, if the data is accurate up to 3 significant digits, then the singular values for which the ratio in Equation 2.10 is below 10^{-3} are essentially noisy singular values, and they should not be used in the data reconstruction.

Define $[\Sigma']$ as the $M \times M$ diagonal matrix with M largest singular values of $[Y]$ on its main diagonal in descending order. Further, define $[U']$ and $[V']$ as the 'filtered' matrices that contain only M dominant left singular vectors of $[U]$ and $[V]$ respectively.

The matrices $[Y_1]$ and $[Y_2]$ are then constructed by

$$[Y_1] = [U'][\Sigma'][V_2']^T \quad \textbf{(2.11)}$$

$$[Y_2] = [U'][\Sigma'][V_1']^T \quad \textbf{(2.12)}$$

where $[V_1']$ and $[V_2']$ are equal to $[V']$ without the last and first row respectively and "T" denotes the conjugate transpose. Using Equations 2.11 and 2.12, the roots of the system, z_i, are given by the nonzero eigenvalues of $\{[V_1']^T\}^+[V_2']^T$. Here, "+" is the Moore-Penrose pseudo-inverse operator.

The values of the poles, s_i, can then be extracted from z_i as follow:

$$s_i = \frac{\ln z_i}{T_s} \quad \textbf{(2.13)}$$

Once M and z_is are known, the residues can be solved for from the following least squares problem:

$$\begin{bmatrix} y(0) \\ y(1) \\ \vdots \\ y(N-1) \end{bmatrix} = \begin{bmatrix} 1 & 1 & \cdots & 1 \\ z_1 & z_2 & \cdots & z_M \\ \vdots & \vdots & & \vdots \\ z_1^{N-1} & z_2^{N-1} & \cdots & z_M^{N-1} \end{bmatrix} \begin{bmatrix} R_1 \\ R_2 \\ \vdots \\ R_M \end{bmatrix} \quad \textbf{(2.14)}$$

Equation 2.14 can be rewritten in parametric form as follow:

$$\mathbf{y} = \mathbf{ZR} \quad \textbf{(2.15)}$$

A solution to the above least squares problem is

$$\mathbf{R} = \mathbf{Z}^+\mathbf{y} \quad \textbf{(2.16)}$$

where "+" is the Moore-Penrose pseudo-inverse operator.

Unlike the CNRs, the residues or complex amplitudes are aspect (incident angle) and polarization dependent [8].

After performing the poles extraction, pre-filtering of the spurious poles can be done by eliminating the poles which are outside the range of excitation frequencies, not in complex conjugate pairs and with damping factors greater or equal to zero.

2.8 Resonance based Target Recognition Techniques

In an ATR system, it is important to have a target recognition scheme that is robust to noise in the sampled data. During the past twenty years, a number of target discrimination techniques that utilize the CNRs have been proposed. Perhaps the most popular of these methods is the E-pulse technique which operates by annihilating the late time response from a specific target [16], [17], [44], [81]. The aspect independent E-pulse is a discriminatory waveform which, when convolved with the late time response of a matched target, produce an almost null response. When an E-pulse tailored to one target is convolved with a different target, a larger response results. By designing a bank of filters to annihilate late time responses from known targets, the E-pulse discriminator selects the target filter whose output has the minimum energy as the correct target. Obviously, this can be done by doing a visual check. However, it could be difficult to do a visual check when the targets are too similar. Therefore, to quantify the performance of the E-pulse technique, the E-pulse Discrimination Number (EDN) is introduced in [81]. Target recognition is achieved by thresholding the output of the convolution signal. The target is then identified by the E-pulse yielding the minimum EDN. Though the E-pulse technique is an intuitively sensible approach, it has several design disadvantages as follow:

- An E-pulse for each of the candidate targets needs to be formed using the CNRs of the targets.
- In order to avoid a false alarm in the target discrimination process, the received signature of the unknown target needs to be re-sampled to ensure that it has the same sampling interval as the E-pulse itself [45].
- In order to select the correct target, computation of the E-pulse Discrimination Number (EDN) is needed for each of candidate targets.

Therefore, the computational cost for the E-pulse technique is high.

Recently, the use of a GLRT, which is based on maximum likelihood estimation of the model parameters in white Gaussian noise, was shown to perform better than the E-pulse technique [24], [25]. Moreover, the GLRT method is more computationally efficient than E-pulse technique. Therefore, it will be used as the reference classifier in this research.

2.8.1 Generalized Likelihood Ratio Test

Using the SEM representation of the late time scattered field from a radar target as the signal model, the GLRT provides a decision criterion for target discrimination. Before we look at the mathematical definition of GLRT, a few assumptions have to be made. In order to test the performance of the GLRT method, first off all, as in almost all target discrimination studies, we assume that a target has been detected and only a single target is responsible for the returned scattered field. In addition, the target producing the return belongs to a family of P known targets for which we know *a priori* the poles of each for classification purposes. The mathematical definition of GLRT can be found in the literature [24], [25].

Using Equations 2.6 and 2.7, the SEM representation of the return from the gth target in the presence of noise can be rewritten as

$$y(t) = x^{(g)}(t) + n(t) = \sum_{i=1}^{M_g} R_i^{(g)} z_i^{(g)}(t) + n(t), \quad t \geq T_{L_g}, \quad 1 \leq g \leq P \tag{2.17}$$

where $z_i^{(g)}(t) = e^{s_i^{(g)} t}$ and T_{L_g} is the start of the late time period for the transient response of target g.

The various signals in Equation 2.17 can then be denoted by

$$\mathbf{y} = \begin{bmatrix} y(T_{L_g}) \\ y(T_{L_g} + T_{S_g}) \\ y(T_{L_g} + 2T_{S_g}) \\ \vdots \end{bmatrix} \tag{2.18}$$

$$Z_i^g = \begin{bmatrix} z_i^{(g)}(T_{L_g}) \\ z_i^{(g)}(T_{L_g} + T_{S_g}) \\ z_i^{(g)}(T_{L_g} + 2T_{S_g}) \\ \vdots \end{bmatrix} \quad \textbf{(2.19)}$$

$$\mathrm{n} = \begin{bmatrix} n(T_{L_g}) \\ n(T_{L_g} + T_{S_g}) \\ n(T_{L_g} + 2T_{S_g}) \\ \vdots \end{bmatrix} \quad \textbf{(2.20)}$$

where T_{S_g} is the sampling interval for the transient response of target g.

Using the sampled version of the signal in Equation 2.17, the response from the gth target can be written in parametric form as

$$\mathbf{y} = \mathbf{R}_g \mathbf{Z}_g + \mathbf{n}, \qquad 1 \le g \le P \quad \textbf{(2.21)}$$

where

$$\mathbf{R}_g = \begin{bmatrix} R_1^g & R_2^g & \cdots & R_{M_g}^g \end{bmatrix}^T \quad \textbf{(2.22)}$$

is an unknown, non-random vector containing the residues, "T" denotes the transpose operator, and

$$\mathbf{Z}_g = \begin{bmatrix} Z_1^g & Z_2^g & \cdots & Z_{M_g}^g \end{bmatrix}_{q \times M_g} \quad \textbf{(2.23)}$$

denotes the matrix containing the known signal modes, CNRs. The late time response of the target in Equation 2.17 is assumed to be sampled q times at a uniform rate.

Without loss of generality, a Bayes criterion can be used to develop a Likelihood Ratio Test (LRT) [46] to decide between two targets. The likelihood function for the gth target is proportional to

$$p(\mathbf{y} \mid \text{target } g) \propto \exp\left(-\frac{1}{2\sigma^2} (\mathbf{y} - \mathbf{R}_g \mathbf{Z}_g)^H (\mathbf{y} - \mathbf{R}_g \mathbf{Z}_g) \right) \quad \textbf{(2.24)}$$

where σ^2 is the noise variance and "H" denotes the complex conjugate transpose.

Though the LRT is a very useful tool in a number of applications, resonance based target identification cannot benefit directly since orientation dependency results in the unknown parameter vector $\mathbf{R}_g$. An alternative solution is to use the GLRT. When the maximum likelihood estimate of $\mathbf{R}_g$ is used in the LRT, the resulting test is referred to as the GLRT [24]. Assuming that each target

has equal probability of being present and when uniform cost (zero for a correct decision and one for an incorrect decision) is assumed, the GLRT leads to the following decision rule for P targets discrimination [24]

$$\text{decide}\{y(t)\} = \text{target } g \text{ if } \| (\mathbf{Z}_g^H \mathbf{Z}_g)^{-1/2} \mathbf{Z}_g^H \mathbf{y} \|^2 \text{ is maximum} \quad \textbf{(2.25)}$$

where $\|\cdot\|$ denotes the vector 2-norm or Euclidean norm and "H" denotes the complex conjugate transpose.

2.9 Classifier Performance

The confusion matrix and Receiver Operating Characteristics (ROC) graphs have been widely used in ATR for organizing classifiers and visualizing their performance [100]-[103]. A confusion matrix displays the number of correct and incorrect predictions made by the model compared with the actual classifications in the test data. Each column of the matrix represents the instances in a predicted class, while each row represents the instances in an actual class. The name stems from the fact that it makes it easy to see if the system is confusing the two classes. A ROC curve is a graph of a relation which summarizes the possible performances of a signal detection system faced with the task of detecting a signal (target) in the presence of noise and/or clutter. This relation is usually used to relate the detection or "hit" rate to the false alarm rate as an internal decision threshold is carried [102]. For a typical ROC curve, the decision threshold is carried from a very conservative value (i.e. a value that results in zero detection rate and zero false alarm rate) to a very aggressive value (i.e. a value that results in 100% detection rate and 100% false alarm rate) [102]. The mathematical definition of the confusion matrix and ROC could be found in [100].

To the author knowledge, both of the methods have not been used in the literature to quantify the performance of the resonance based classifier. Instead of using the confusion matrix or ROC plot to quantify the performance of the resonance based target identification scheme, most of the researchers around the world have used "the number of correct identifications per number of test trials" or "correct recognition rate" methods [24], [25], [104], [105]. In this thesis, the performance of the proposed resonance based classifiers was evaluated by using the "the number of correct identifications per number of test trials" method.

2.10 Conclusion

An overview of the various disciplines related to resonance based radar target recognition has been presented in this chapter. These include discussing the advantages of using the CNRs as a feature set to distinguish one target from another and choosing the appropriate resonance extraction and target recognition schemes for use in this research. MPM and GLRT methods are chosen for CNRs extraction and target classification respectively because of their robustness to noise and their computational efficiency.

In the following chapter, we will look at some of the signal processing techniques that will be used in this thesis to enhance the target identification process.

Chapter 3: Signal Processing Techniques

Chapter 3: Signal Processing Techniques

3.1 Introduction

In this chapter, we will look at some of the signal processing techniques that are utilized in this research to enhance the resonance based target detection scheme described in Chapter 2.

3.2 Motivation behind the Chosen Techniques

SEM was one of the first models to describe the transient scattering behaviour of a radar target in the free space. In this model, late time period of the target response is presented as a sum of damped exponentials with natural resonant frequencies that purely correspond to the target attributes. This advantageous feature has allowed the resonances to be used as feature sets for target recognition.

Based on the SEM model, resonances extraction and resonance based target identification could only be carried out in the late time portion of the target response. Inclusion of early time samples could result in accuracy degradation of the CNRs extraction and affect the performance of the resonance based target classifier. Therefore, determination of the late time commencement is crucial for the resonance based target identification process. However, for ATR applications, usually the commencement of the late time period for the unknown target response is not known *a priori*. Therefore, it is important to determine the resonance region for the unknown target and this can be achieved by using the TFA. A robust resonance based target classifier that utilizes the TFA will be presented in Chapter 5.

In addition to the issue of late time commencement, mere existence of particular resonant modes is another issue related to the resonance based target identification process. It is well known that the late time resonances are target dependent and are theoretically independent of the incident aspect and polarization state. In other words, the contributing resonances of the target can be extracted from any incident aspect or polarization state. However, there are cases where some of the resonance modes cannot be properly extracted. Blaricum [47] has shown that for certain aspect angles some poles cannot be excited sufficiently and the corresponding polar-residue patterns show deep nulls at certain aspects indicating that, while the poles are aspect independent themselves, the

excitation mechanism for producing them is not. Shuley and Longstaff [8] had proven that a similar scenario also occurs for different incident polarizations. Therefore, in order to ensure that all of the dominant CNRs of the target are extracted so as to avoid false alarms during the target identification process, target responses from multiple incident aspect angles and/or multiple incident polarizations are used. A dominant poles extraction scheme that uses both the information fusion technology and multiple datasets will be introduced and discussed in Chapter 4.

3.3 Time-Frequency Analysis

There continues to be high interest in the development of signal analysis techniques that can improve both the detect ability and the detailed characterization of signals, particularly those with a high degree of complicated non-stationary (statistically time varying) behavior. Recently, the use of TFA techniques to analyse complicated nonlinear and/or non-stationary signals has become increasingly popular due to the fact that in the time versus frequency plot or joint Time-Frequency Distribution (TFD), one can determine the frequencies and their relative intensities as time progresses. In other words, more information regarding the signal can be extracted from the joint TFD as compare to either using the time domain or frequency domain plot of the signal. Figure 3.1 shows an example of the time-frequency plot.

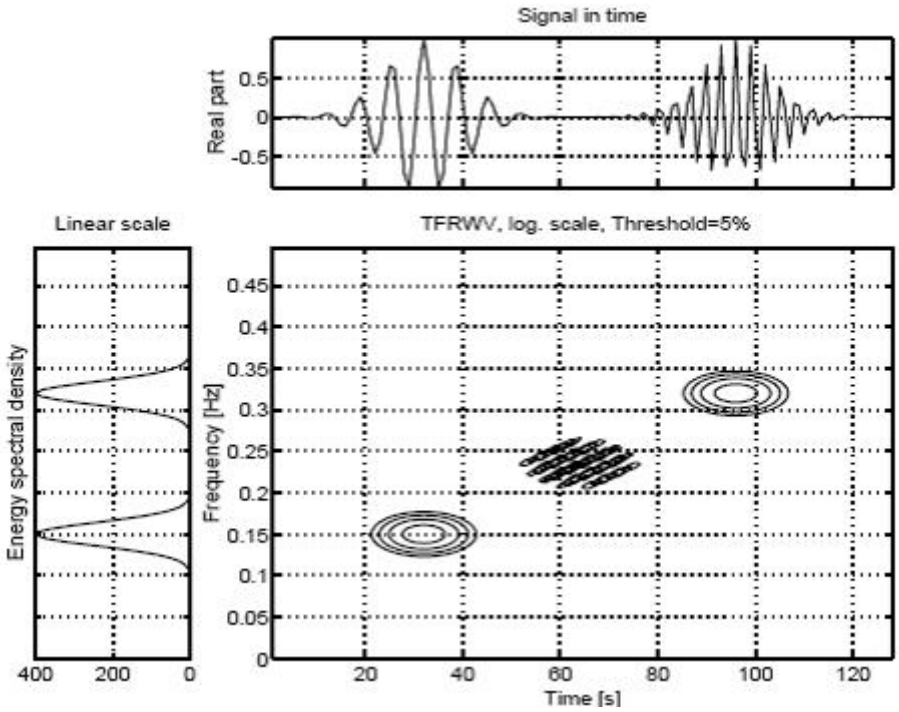

Figure 3.1: Time-frequency representation of two Gaussian atoms.

The evolvement of resonances of a target has been studied by a lot of researchers around the world [67], [107]-[110]. One of the most well-known descriptions for transient electromagnetic scattering in the resonance region if the SEM [7]. In extending the SEM, Felsen *et al.* [107]-[110] proposed a Hybrid Wavefront Singularity Expansion Method (HWSEM). The HWSEM essentially formulates the transient scattering as a series of wavefront events. In the early time period, the target is partially excited and the dominant scattering phenomena can be described by wavefronts (progressing waves) [110] which correspond to diffractions from various parts of the target. In the late time period, formation of global resonances can be regarded as a consequence of the multiple interactions between the various wavefronts. The connection between wavefront and resonance descriptions in the late time period is thus established and such a connection has been further verified in [67], [107]-[110]. As compared to the well-known "full body resonance" in the late time period, the HWSEM has also suggested the term "partial resonance", which corresponds to the resonances of the substructure of the target [107], [110]. In terms of a wavefront description, this is the consequence of the interaction between at least two wavefront events [107], [110]. As a result, partial resonances may also appear when the target is partially excited in early time period or due to the substructure of a complex target [111]. Furthermore, it has also been shown that each resonant mode (both full body resonance and partial resonance) has its own "turn-on time" [67], [107].

Therefore, the TFD can be considered as an important alternative means of studying the transient scattering, especially for complex targets from which analytical solutions are usually not available.

The TFDs are divided into two main classes: linear and bilinear. The Short-Time Fourier Transform (STFT), which belongs to the linear class, was one of the first tools to be used for analysing time variant signals. Compared to standard Fourier analysis which takes the entire duration of the signal in time and then takes the transform, the signal is first windowed with a time-limited window and then transformed to the frequency domain via a Fourier Transform. The resultant distribution is known as the STFT [48], [49]. The STFT is essentially a windowed version of the Fourier transform, which considers the frequency spectrum within a short period of time.

One of the well-known shortcomings about the STFT is that it is not able to achieve fine time and frequency resolution simultaneously due to the constraint of the uncertainty principle [48], [49]. In other words, if one would like to achieve fine resolution in the time domain, the resolution in the frequency domain would be correspondingly degraded and vice versa. One way to handle this resolution issue is to use the WVD [48], [49] which belongs to the bilinear class. WVD will be used in this thesis to determine the resonance region of the unknown target as it is capable of producing the best time-frequency resolution as compared to the other TFDs.

3.3.1 Wigner-Ville Distribution

WVD is belonged to the Cohen's class of TFD. In contrast with the linear time-frequency representations which decompose the signal on elementary components (atoms), the purpose of the energy distributions is to distribute the energy of the signal over the two description variables: time and frequency. As the energy is a quadratic function of the signal, WVD will be in general quadratic representation. The Wigner-Ville energy distribution in terms of the signal, $x(t)$ or its spectrum, $X(\omega)$, is defined by [48]-[50]

$$T_x(t,f) = \int_{-\infty}^{+\infty} x(t+\frac{\tau}{2}) x^*(t-\frac{\tau}{2}) e^{-j2\pi f\tau} d\tau \qquad \textbf{(3.1)}$$

or equivalently by

$$T_x(t,f) = \int_{-\infty}^{+\infty} X(f+\frac{\theta}{2}) X^*(f-\frac{\theta}{2}) e^{-j2\pi\theta t} d\theta \qquad \textbf{(3.2)}$$

Among all the quadratic time-frequency representations, the WVD satisfies a large number of desirable mathematical properties. For example, the WVD is always real-valued and it preserves the time shifts and frequency shifts of the signal. The WVD also satisfies the marginal properties, that is, the frequency or time integrals of the WVD correspond to the signal's instantaneous power and its spectral energy density respectively. Hence, the WVD can be loosely interpreted as a two dimensional distribution of signal energy over the time-frequency plane [50]. However, it should be emphasized that this interpretation is only approximately valid, as the uncertainty principle does not allow infinite resolution in time and in frequency simultaneously. Presence of the cross-terms in the WVD output at some points in the time-frequency domain, for instance, contradicts with the proper energy density interpretation. Nevertheless, it appears that these cross-terms must be present or the desirable properties of the WVD cannot be satisfied. In other words, there is a trade-off between the quantity of interferences and the number of desired properties.

3.4 Information Fusion Technology

Information fusion technology is one of the emerging technologies of data processing. Among the three levels of information fusion (pixel level, feature level, and decision level), the decision level fusion, delegated by multi-classifier combination, has been one of the hot research fields on pattern recognition. It has also achieved successful application in the aspects of handwritten character and face recognition [51]. Although the research of the feature level fusion starts not as early as other fusion methods, it received a delightful development.

The advantage of feature level fusion is obvious. Different feature vectors extracted from the same pattern always reflects the different characteristic of patterns. By optimizing and merging these different features, it not only keeps the effective discriminatively information of multi-feature, but also eliminates the redundant information to a certain degree [52]. This is especially important to classification and recognition.

In general, the existing feature fusion techniques for pattern classification can be subdivided into two basic categories. One is feature selection based, and the other is feature extraction based [53]. In the former, all feature sets are first grouped together and then a suitable method is used for feature selection. One examples of this method can be found in [54]. In the latter, the multiple feature sets are combined into one set of feature vectors that are input into a feature extractor for

fusion. Although there are quite a few feature extraction techniques available in the literature [52], only the PCA will be used and presented in this thesis. PCA is used to combine the backscattered signatures of the target from different incident aspect angles. The dominant CNRs of the target are then extracted from the fused signature. Details on using PCA to extract the dominant poles of the target could be found in the next chapter.

3.4.1 Principal Component Analysis

PCA is a useful statistical technique that has found application in fields such as data analysis, data compression, redundancy and dimensionality reduction and feature fusion. It is a way of identifying patterns in the data and expressing the data in such a way as to highlight their similarities and differences. To describe the basic procedure of PCA based feature fusion technique, let consider the following real valued data matrix of size $N \times K$:

$$F = \begin{bmatrix} \mathbf{x}_1 & \mathbf{x}_2 & \cdots & \mathbf{x}_K \end{bmatrix}, \tag{3.3}$$

where

$$\mathbf{x}_i = \begin{bmatrix} x_1 - mean(\mathbf{x}_i) \\ x_2 - mean(\mathbf{x}_i) \\ \vdots \\ x_N - mean(\mathbf{x}_i) \end{bmatrix}, \qquad i = 1,2,\ldots K \tag{3.4}$$

are zero mean data vectors of size $N \times 1$ each and K is the dimension of the data matrix.

The covariance matrix of the data matrix is a $K \times K$ symmetric, positive-definite matrix expressed in the general form

$$S_F = \begin{bmatrix} s_1^2 & s_{1,2} & \cdots & s_{1,K} \\ s_{2,1} & s_2^2 & \cdots & s_{2,K} \\ \vdots & \vdots & \vdots & \vdots \\ s_{K,1} & s_{K,2} & \cdots & s_K^2 \end{bmatrix} \tag{3.5}$$

The off-diagonal entries $s_{i,j} = s_{j,i}$ represent the covariance between the data vectors $\mathbf{x}_i$ and $\mathbf{x}_j$ while the diagonal entry s_i^2 represents the variance of the data vector $\mathbf{x}_i$. Accordingly, the correlation coefficient $r_{i,j}$ between the data vectors $\mathbf{x}_i$ and $\mathbf{x}_j$ can be defined as

$$r_{i,j} = \frac{s_{i,j}}{\sqrt{s_i s_j}} \tag{3.6}$$

Since the covariance matrix S_F is symmetric and positive-definite, it can be transformed into a diagonal matrix Λ through a similarity transformation

$$\Lambda = U^T S_F U = \begin{bmatrix} \lambda_1 & 0 & \cdots & 0 \\ 0 & \lambda_2 & \cdots & 0 \\ \vdots & \ddots & \ddots & \vdots \\ 0 & \cdots & 0 & \lambda_K \end{bmatrix} \tag{3.7}$$

where "T" denotes the conjugate transpose and U is the modal matrix which is a unitary matrix in the form

$$U = \begin{bmatrix} u_1 & u_2 & \cdots & u_K \end{bmatrix} \tag{3.8}$$

with u_i's being the normalized eigenvectors or characteristic vectors of size $K \times 1$ each, corresponding to the eigenvalues or characteristic values of the covariance matrix S_F.

The eigenvalues, λ_i, are solved by using the following equation:

$$\det(S_F - \lambda I) = 0 \tag{3.9}$$

where "det" denotes the determinant of the matrix and I is the identity matrix of size $K \times K$.

After ordering the computed eigenvalues such that $\lambda_1 > \lambda_2 > \cdots > \lambda_K$, the corresponding eigenvectors t_i are solved from the matrix equation

$$(S_F - \lambda_i I)t_i = 0 \qquad \text{for } i = 1,2,\ldots,K \tag{3.10}$$

These orthogonal eigenvectors are then normalized to obtain the orthonormal eigenvectors

$$u_i = \frac{t_i}{\sqrt{t_i^T t_i}} = \frac{t_i}{|t_i|} \tag{3.11}$$

It turns out that the eigenvector with the highest eigenvalue is the principal component of the data matrix F. Once the principal component has been chosen, the fused data, $\mathbf{x}_{fused}$, of size $1 \times N$ can be found by

$$\mathbf{x}_{fused} = u_1^T \times F^T \quad \textbf{(3.12)}$$

where "T" denotes the conjugate transpose.

3.5 Conclusion

In a feature based target identification scheme, it is important to pre-process (i.e. remove any unwanted components like noise etc.) the raw signature of the unknown target before extracting the desire feature of the target or performing the identification steps as shown in Figure ~~2~~1.1. In this chapter, we have introduced two signal processing techniques, WVD and PCA, to overcome the late time commencement and dominant CNRs extraction issues respectively of the resonance based target identification process. Their usages in this research will be presented in the upcoming chapters.

Chapter 4: Dominant Poles Extraction Schemes

Chapter 4: Dominant Poles Extraction Schemes

4.1 Introduction

As mentioned in the previous chapters, the CNRs are closely related to the physical attributes of the target, in this context the physical geometry and the material properties of that geometry. The resonant frequencies (the imaginary part of the CNRs) vary as the geometry of the target changes. Consider a library of targets of similar physical shape and structure. If we compare the CNRs of these targets, there must be some modes located quite closely to each other in the S-plane, due to the fact that those targets have similar physical shapes. On the other hand, there are also some resonant modes located in quite different positions in the S-plane due to the other differences in physical attributes (i.e. slight different in length etc.). Therefore, in the field of target recognition using CNRs as a feature set, it is important to extract the contributing poles of the target as incorrectly determining them could result in a false alarm during target identification process.

It is a rigorous process to extract the contributing CNRs of the target as at some incident aspects, some of the modes are not well excited and the accuracy of the poles could be affected by noise in the target signature. The well-known poles extraction technique, MPM, will be used in this research due to its robustness to noise and its computational ease. In order to ensure that the estimated poles will be more accurate and robust to different incident aspect and polarization state, Sarkar [14] had applied it to multiple datasets. Selection of the contributing poles of the target could also be done after the extraction process by eradicating parasitic CNRs that are outside the range of excitation frequencies, not in complex conjugate pairs, and with damping factors greater or equal to zero. Chauveau [55] had also proposed two criteria for selecting the dominant poles of the target based on weight and damping factors.

This chapter is divided into three sections. In the first section, a computational issue of the MPM will be discussed and an improved version of the MPM will be proposed. Following that, a dominant poles identification technique based on the energies of the extracted poles will be presented in detail with numerical examples provided. Last but not least, another novel dominant poles extraction scheme using PCA and multiple datasets will be proposed.

Chapter 4: Dominant Poles Extraction Schemes

4.2 Matrix Pencil Method Computational Issue

This section is based on publication [A1] and has been extended for this thesis.

4.2.1 Introduction

In a resonance based target identification process, most of the target classification techniques use only the pole information, due to their aspect independent nature. Although the residues are of seemingly little use in target identification process, due to their aspect dependent nature, correctly extracting their values is still necessary. If the target's orientation and antenna polarization are known *a priori*, target identification can be achieved by comparing the reconstructed transient response, using the extracted poles and residues, of the target with the simulated transient response of the target. There are also other applications where the residues are required involving polarization and multi-aspect scattering [8], [14]. In order to quantify that the correct residue information is indeed being extracted, the poles and residues extracted from the target, for a particular aspect, are used to reconstruct the transient response of the target in the late time period. The reconstructed signal of the target will be different from the original signal of the target if there is severe rank deficiency in the z-matrix, indicating that wrong residue information is being extracted.

In this section, the problem of the rank deficiency in the $\mathbf{Z}$ matrix, shown in Equation 2.15, of the MPM will be discussed. A solution to tackle the problem is proposed and simulation results are being used to evaluate the performance of the improved MPM.

4.2.2 Improved Matrix Pencil Method

In linear algebra, the rank of a matrix is defined by the maximal number of linearly independent rows or columns of the matrix. In the MPM, the $\mathbf{Z}$ matrix used for solving the least squares problem for the residues, is a $N \times M$ matrix of rank M. Equation 2.14 has a unique solution if and only if the rank of the $\mathbf{Z}$ matrix is equal to M. Rank deficiency of the $\mathbf{Z}$ matrix will occur if the rank of the $\mathbf{Z}$ matrix is less then M and if this happens, Equation 2.14 will have infinitely many solutions [56].

Chapter 4: Dominant Poles Extraction Schemes

It is stated in [57] that overestimating the modal order, M, is preferred to underestimating it, as underestimating M would lead to large errors. However, overestimating M could also result in spurious CNRs, which could cause rank deficiency in the $\mathbf{Z}$ matrix of the MPM. This will then led to incorrect residue information being extracted and result in a wrong target response being reconstructed.

It is assumed in this section that for the original MPM, parasitical poles (stated in Section 2.7.2) and their corresponding residues are removed after solving Equation 2.16. The flowchart for the original MPM is shown in Figure 4.1. The flowchart of the improved MPM is shown in Figure 4.2. It is shown in Figure 4.2 that the spurious poles are eradicated before solving the least squares problem for the residues. In this case, the rank of the matrix is reduced from M to $M-U$, where U is the number of spurious modes.

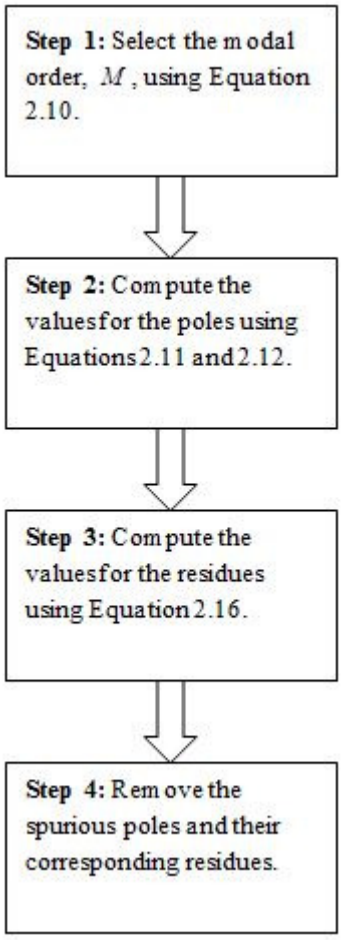

Figure 4.1: Flowchart of the original matrix pencil method.

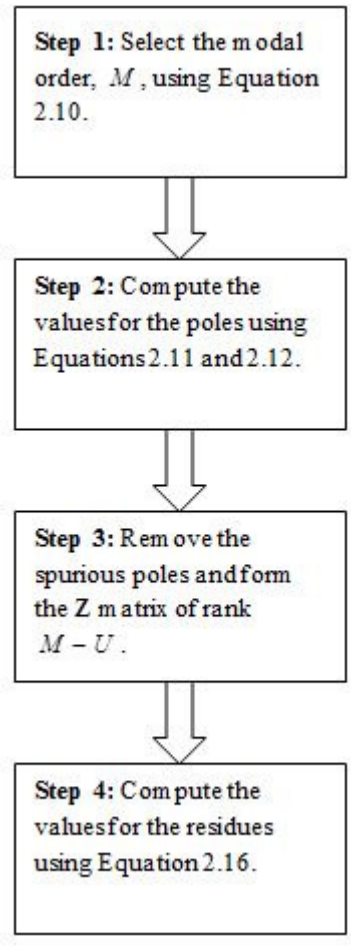

Figure 4.2: Flowchart of the improved matrix pencil method.

4.2.3 Signals Comparison

In order to ensure that the correct residue information is being extracted, the CNRs and residues extracted from the target, for a particular aspect, are used to reconstruct the impulse response of the target. The similarity between the reconstructed signal and the original signal can be found by using the following measure "Correlation Factor (CF)":

$$\mathrm{CF}=1-\frac{\sum_{k=1}^{N}[I(k)-\hat{I}(k)]^2}{\sum_{k=1}^{N}[I(k)]^2} \qquad \textbf{(4.1)}$$

where $I(k)$ and $\hat{I}(k)$ are the sampled version of the original signal and reconstructed signal respectively. It is observed that when the signals are identical, CF is 1. As there is more and more

difference between the signals, the CF decreases accordingly. This model is used frequently in model identification and control literature for validation of results.

4.2.4 Numerical Examples

Consider a simple PEC L-shaped wire of total length 1m (0.7cm in the z-direction and 0.3cm in the y-direction) in free space illuminated by a plane wave at an incident angle of $\theta = 150^\circ$ and $\phi = 0^\circ$. The 1m L-shaped in free space and its corresponding backscattering frequency and impulse responses are shown in Figure 4.3. The incident field was polarized with respect to the θ direction. The backscattered field is normally computed in the time domain, but for this example, data were obtained in the frequency domain. The frequency samples were then windowed by a Gaussian shaped window in the frequency domain, corresponding to a Gaussian pulse in the time domain. The Gaussian pulse in the time domain therefore acts as the time domain illuminating wave and acts as an approximation to the impulse response. The windowed data was then transformed to the time domain via either an IFFT or an ICZT. In this instance, 512 frequency samples were considered to a maximum frequency of 1GHz, resulting to 1024 time samples. After obtaining the time domain signature, the early time portion was removed and the MPM was applied to the remaining late time samples to extract the CNRs and their corresponding residues.

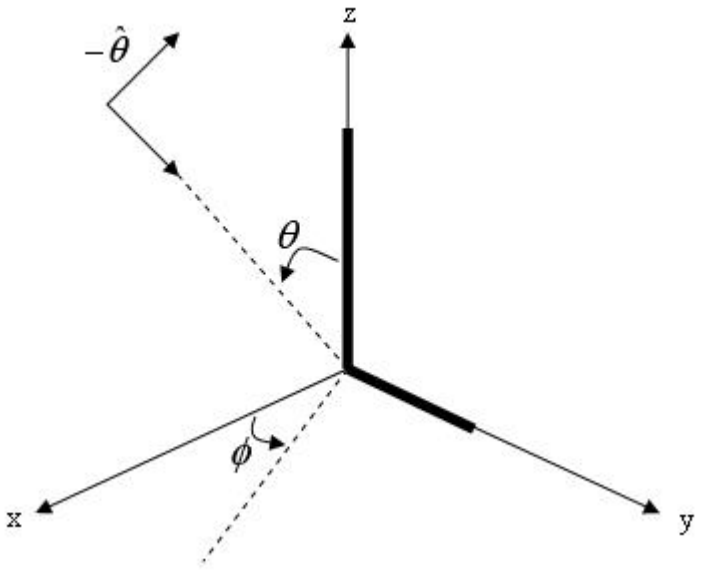

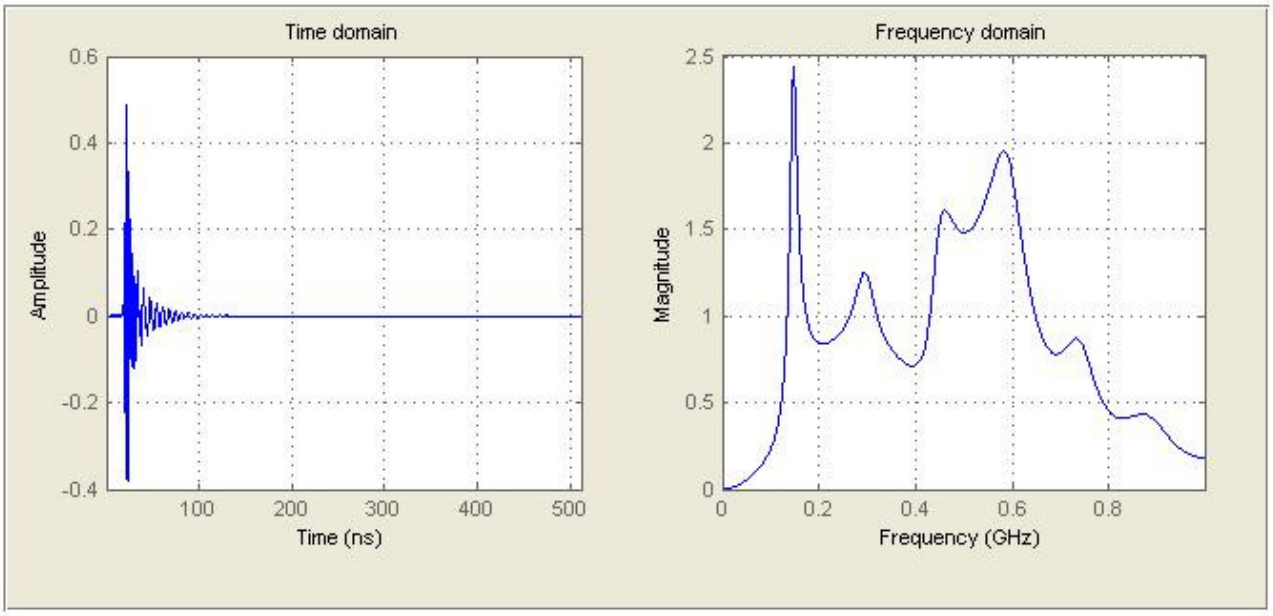

Figure 4.3: Geometry of the 1m L-shaped wire and its corresponding backscattering frequency and impulse responses as a result of an impulsive plane wave incident from $\theta = 150^{\circ}$.

Table 4.1 shows the computed poles and residues information for the 1m L-shaped wire. After filtering the singular values by using Equation 2.10, the modal order, $M = 16$, was chosen to perform the pole extraction. The modal order of $M = 16$ was chosen as the resonance peaks from the frequency response, shown in Figure 4.3, of the 1m L-shaped wire suggests that it contains 6 dominant CNRs or 12 dominant complex conjugate poles and it is preferred to overestimate the modal order instead of underestimating it. It can be seen from the results that the poles extracted by using the two different MPM solutions have almost the same values. However, the values of the residues computed by using the original MPM are different to the values of the residues extracted by using the improved MPM. By using the original MPM, 4 spurious modes were eliminated after solving Equation 2.16. The rank deficiency, $\text{rank} = 1$, in the $\mathbf{Z}$ matrix of the original MPM had caused the values of the residues to be zero. This in turn causes the reconstructed impulse response of the L-shaped wire, as shown in Figure 4.4, to be different to the original impulse response of the L-shaped wire. The CF between the original signal and the regenerated signal is 0.

By using the improved MPM, 4 spurious poles were eradicated before solving the least squares problem for the residues. Fig. 4.5 shows the reconstructed impulse response of the 1m L-shaped

wire using the poles and residues extracted by the improved MPM. The CF between the original signal and the reconstructed signal is 1.

It is demonstrated that rank deficiency in the **Z** matrix of the MPM will result in the wrong signal being reconstructed, indicating that incorrect residue information is being extracted. Therefore, careful measures have to be taken to prevent this problem.

	Original MPM	Improved MPM
$s_{1,2}/c$	$-0.181 \pm j3.044$	$-0.181 \pm j3.044$
$R_{1,2}/c$	0	$0.001 \mp j6.552 \times 10^{-4}$
$s_{3,4}/c$	$-0.313 \pm j6.241$	$-0.314 \pm j6.241$
$R_{3,4}/c$	0	$4.017 \times 10^{-4} \pm j9.892 \times 10^{-4}$
$s_{5,6}/c$	$-0.659 \pm j9.430$	$-0.659 \pm j9.430$
$R_{5,6}/c$	0	$-0.001 \mp j3.473 \times 10^{-5}$
$s_{7,8}/c$	$-0.792 \pm j12.571$	$-0.792 \pm j12.571$
$R_{7,8}/c$	0	$-2.114 \times 10^{-4} \mp j9.291 \times 10^{-4}$
$s_{9,10}/c$	$-0.763 \pm j15.788$	$-0.763 \pm j15.788$
$R_{9,10}/c$	0	$5.836 \times 10^{-4} \mp j7.740 \times 10^{-5}$
$s_{11,12}/c$	$-1.122 \pm j19.094$	$-1.122 \pm j19.094$
$R_{11,12}/c$	0	$-4.920 \times 10^{-5} \pm j3.457 \times 10^{-4}$

Table 4.1: Normalized poles and residues of the 1m L-shaped wire.

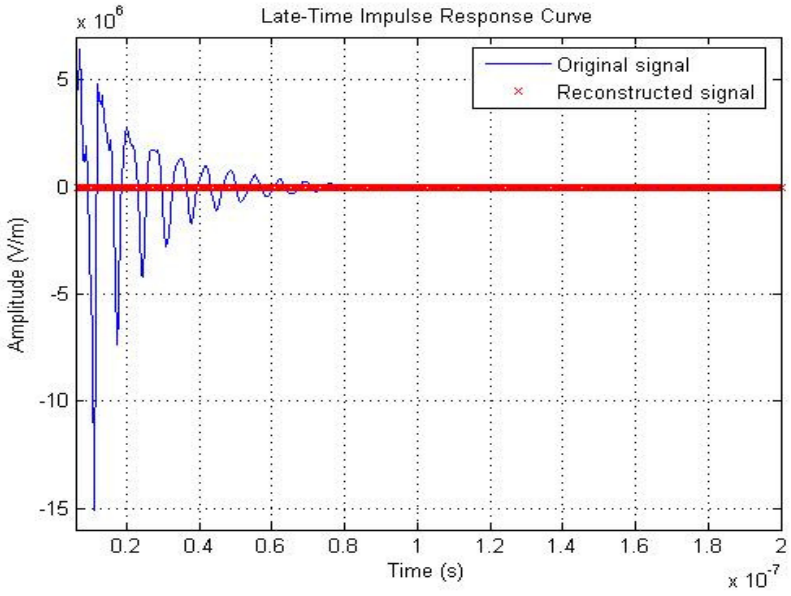

Figure 4.4: Reconstructed impulse response of the 1m L-shaped wire, using poles and residues extracted by the original matrix pencil method.

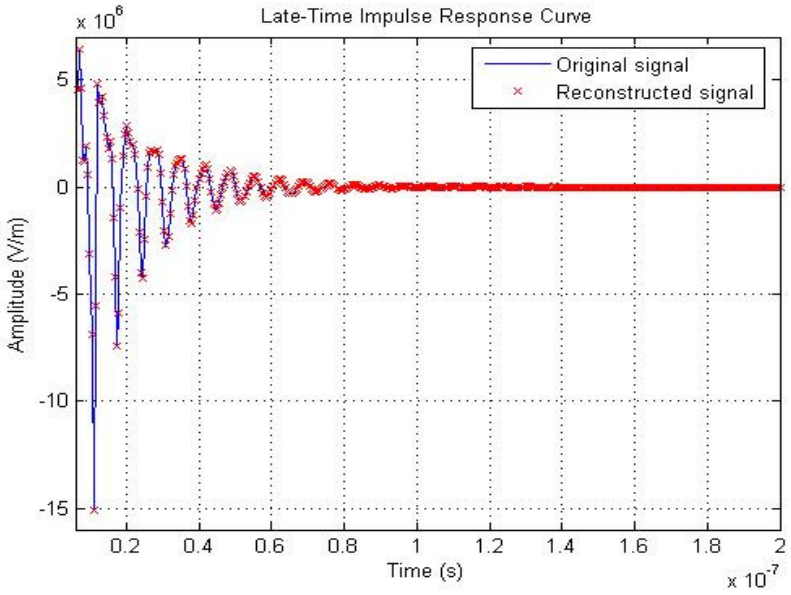

Figure 4.5: Reconstructed impulse response of the 1m L-shaped wire, using poles and residues extracted by the improved matrix pencil method.

4.2.5 Conclusion

The rank deficiency problem in the **Z** matrix of the MPM is examined in this section. The residues computed using the MPM are incorrect if there is severe rank deficiency in the **Z** matrix of the MPM. A solution has been proposed to solve the rank deficiency problem. Initial investigation, using a simple L-shape wire in free space, suggests that the proposed solution would improve the performance of the current MPM methods. In order to further quantify the performance of the proposed technique, future investigation should include applying the improved MPM method to low Q-Factor target, dielectric target and more complex target such as the wire aircraft model.

4.3 Identifying the Dominant Complex Natural Resonances of the Radar Target Based on the Energies of the Extracted Poles

This section is based on publication [C1].

4.3.1 Introduction

As mentioned previously, determining the modal order of the system is one of the major problems related to CNRs extraction. Incorrectly determining the modal order of the system may result in spurious poles. Moreover, if the received signature is corrupted by noise, identifying the significant poles of the target will become an even more complex problem to solve. In this section, a post processing technique, based on examining the energies of the extracted CNRs, will be applied to identify the dominant CNRs of the target.

The extraction for the dominant poles of the target is done without *prior* knowledge of the modal order of the system. The proposed dominant CNRs identification scheme is validated by using a PEC wire target in free space with different Signal-to-Noise Ratios (SNRs).

4.3.2 Dominant Poles Identification Scheme

In order to avoid false alarms during target classification process, it is important to identify the significant poles of the system. The actual number of significant modes is usually unknown and is determined by the system bandwidth, geometry and material properties of the target, sensitivity and

radar look angle. As stated previously in [57], it is preferable to overestimate the modal order as underestimating it will lead to large errors. If the received signature of the target is further corrupted by noise, noisy unwanted poles that are in complex conjugate pairs and within the range of excitation frequencies may get extracted. Therefore, by using the spurious poles filtering criterions, stated in Section 2.7.2, alone are not enough to extract the dominant poles of the target. In this section, the dominant CNRs of the target are extracted, without *prior* knowledge of the modal order of the system, by examining the energy of each of the extracted poles.

Before calculating the energy for each of the extracted CNRs of the target, the received late time signature of the target is normalized *prior* to any processing such that the total energy of the signal is equal to unity. The energy for each of the extracted CNRs of the target can be found by using the following equation:

$$E_{s_i}(joule) = \sum_{k=0}^{N-1} \left| R_i e^{s_i k T_s} \right|^2 \qquad \text{for } k = 0,1,2,\ldots,N-1 \tag{4.2}$$

where R_i = residue of the i^{th} mode, $s_i = \sigma_i \pm j\omega_i$ is the pole of the i^{th} mode, σ_i = aspect independent damping factor of the i^{th} mode, ω_i = aspect independent angular frequency of the i^{th} mode, T_s = sampling period for the transient response of the target, and N = number of data samples.

In physics, resonance is the tendency of a system to oscillate with greater amplitude at some frequencies than at others. Resonance occurs when a system is able to store and transfer energy between two or more different storage modes (such as kinetic and potential energy in the case of a pendulum). However, there are losses from cycle to cycle, called damping. When damping is small, the resonant frequency is approximately equal to the natural frequency of the system. In another words, the dominant poles of the target have a lower damping factor, σ_i, and hence a higher energy level. Experimental results also show that the dominant poles of the target have higher energy level than the noisy spurious poles as noise is a non-resonant signal. Elimination of the noisy unwanted poles can be done by computing the energies for the CNRs, followed by finding the average energy for the CNRs. With that, the energy ratio for each pole can be found by dividing the energy of each pole by the average energy of the CNRs. Finally, poles that have energy ratio less than the reference energy ratio of 0.1 are eradicated. It is noted that the value for the reference energy ratio is derived based on empirical results on several simple PEC targets.

4.3.3 Numerical Examples

For discussion purposes, we will consider a thin wire target of length $L = 1\text{m}$. The wire radius a is given by $L/a = 200$. Figure 4.6 shows the 1m PEC wire in free space. The wire target was illuminated by a plane wave at an incident angle of $\theta = 150^\circ$ and $\phi = 0^\circ$. The incident field was polarized with respect to the θ direction. The frequency response for the 1m thin wire target was obtained by using the MoM technique. The frequency samples were then windowed by a Gaussian shaped window in the frequency domain, corresponding to a Gaussian pulse in the time domain. The windowed data were transformed to the time domain via an IFFT. In this instance, 512 frequency samples were considered to a maximum frequency of 1GHz, resulting to 1024 time samples. For noise simulation, each point of the impulse response of the target was perturbed by white Gaussian noise. The white Gaussian noise is added to the corresponding impulse signature, $x(t)$, of the target by using the following equation:

$$SNR(dB) = 10log_{10}\left(\frac{P_{signal}}{P_{noise}}\right) \quad \textbf{(4.3)}$$

where P_{signal} and P_{noise} are the average power of the uncorrupted signature and average noise power of the system respectively.

$$P_{signal} = \frac{1}{T}\int_0^T |x(t)|^2\, d(t) \quad \textbf{(4.4)}$$

where T is the end-time for the transient response of the target and $|\cdot|$ denotes the complex modulus. Note that the average power of the target signal is computed using both the early time and late time portions of the return.

The SNRs of $\text{SNR} = 20\text{dB}$ and $\text{SNR} = 10\text{dB}$ will be considered.

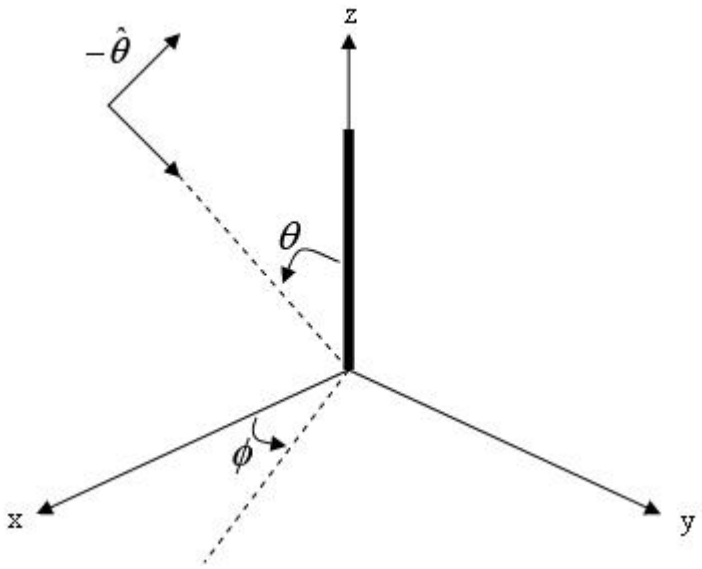

Figure 4.6: Geometry of the 1m thin straight wire.

Before performing poles extraction, the late time signature of the wire target was normalized such that the total energy of the signal is equal to unity. MPM was then applied to the late time period, sample 13 to 1024, to extract the poles and residues from the noise corrupted impulse responses of the wire target. In order to test the feasibility of the proposed scheme, the modal order, $M = 18$, was chosen to perform the CNRs extraction. After pre-filtering the spurious poles by using the criterions stated in Section 2.7.2, the remaining CNRs from the noise corrupted impulse responses of the wire target can be found in Figure 4.7. The energy of each of the extracted CNRs from the impulse responses of the 1m wire target with $\text{SNR} = 20\text{dB}$ and $\text{SNR} = 10\text{dB}$ is shown in Table 4.2. For the impulse response with $\text{SNR} = 20\text{dB}$, Table 4.2 shows that three of the positive poles with energy ratio less than the reference energy ratio of 0.1 were eliminated. For the impulse response with $\text{SNR} = 10\text{dB}$, Table 4.2 shows that two of the positive poles with energy ratio less than the reference energy ratio of 0.1 were eliminated. Figure 4.8 shows the dominant CNRs of the wire target in the S-plane after the noisy spurious poles elimination. It can be seen from Figure 4.8 that the imaginary parts of the dominant poles matches more well to the theoretical values [58] than the real parts as expected, since the damping factors are more sensitive to noise.

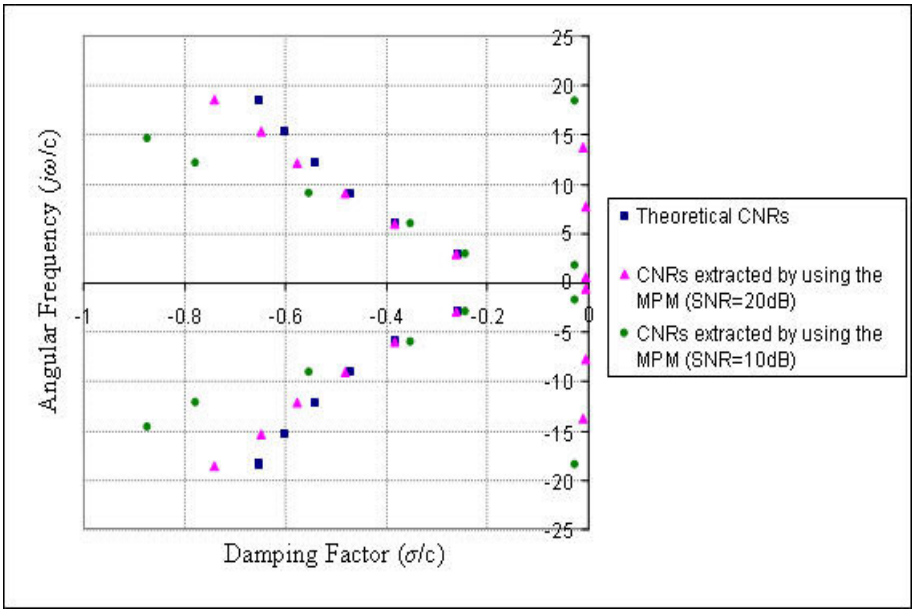

Figure 4.7: Theoretical and extracted poles for the 1m wire target before spurious modes eradication.

	SNR = 20dB				SNR = 10dB			
i	σ_i/c	ω_i/c	E_{s_i} (joule)	Energy ratio	σ_i/c	ω_i/c	E_{s_i} (joule)	Energy ratio
1	-0.740	18.553	0.006	0.165	-0.874	14.561	0.025	0.493
2	-0.647	15.300	0.019	0.521	-0.777	12.156	0.086	1.695
3	-0.577	12.152	0.052	1.426	-0.553	9.105	0.104	2.049
4	-0.481	9.047	0.094	2.578	-0.353	6.039	0.090	1.773
5	-0.385	5.949	0.102	2.797	-0.244	2.871	0.049	0.966
6	-0.263	2.877	0.055	1.508	~~-0.027~~	~~1.720~~	~~0.001~~	~~0.020~~
7	~~-0.011~~	~~13.700~~	~~9.118×10^{-5}~~	~~2.501×10^{-3}~~	~~-0.026~~	~~18.353~~	~~2.479×10^{-4}~~	~~4.885×10^{-3}~~
8	~~-0.004~~	~~0.559~~	~~4.495×10^{-5}~~	~~1.233×10^{-3}~~				
9	~~-0.004~~	~~7.753~~	~~2.644×10^{-5}~~	~~7.251×10^{-4}~~				

Table 4.2: Poles and corresponding energies information for the 1m wire target.

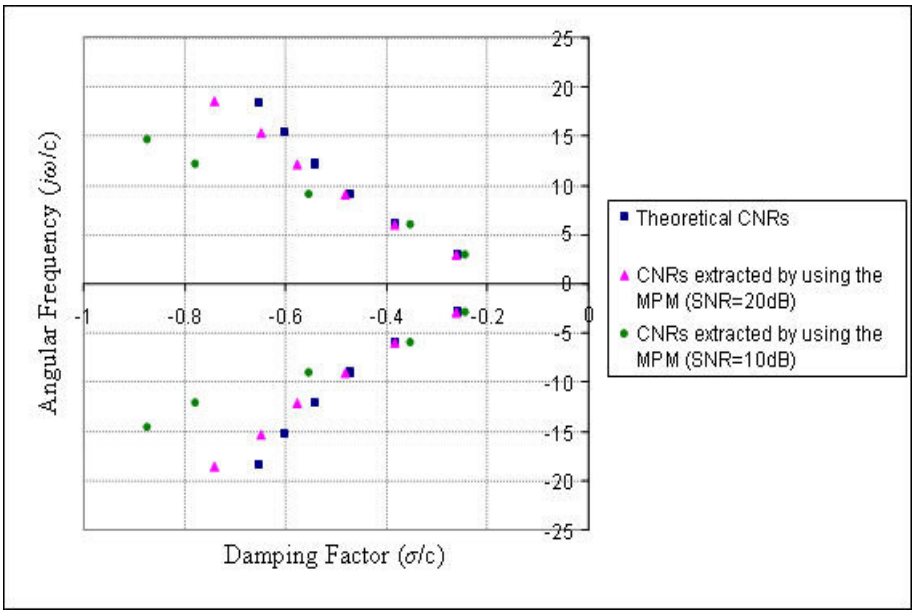

Figure 4.8: Theoretical and extracted poles for the 1m wire target after spurious modes eradication.

The reconstructed impulse responses (before and after noisy spurious poles elimination) for the 1m wire scatterer with $\mathrm{SNR} = 20\mathrm{dB}$ and $\mathrm{SNR} = 10\mathrm{dB}$ are shown in Figure 4.9 and Figure 4.10 respectively. Both of the reconstructed signals in Figure 4.9 have the same CF of 1 and both of the reconstructed signals in Figure 4.10 also have the same CF of 0.99. This indicates that the remaining CNRs, after spurious poles elimination using the proposed method, are indeed the dominant poles of the 1m wire target. This also shows that the noisy unwanted poles do not contribute much to the signal reconstruction, due to their low energy levels.

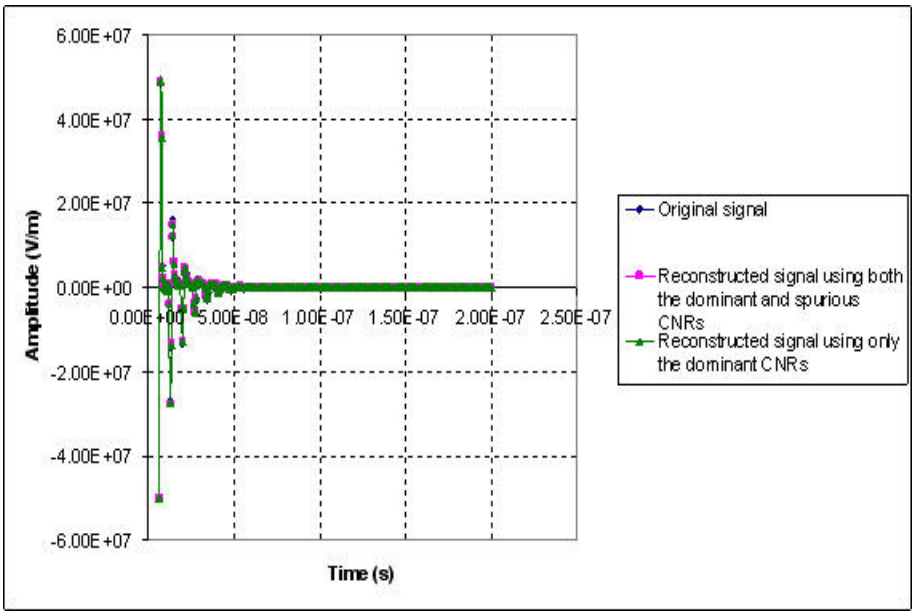

Figure 4.9: Reconstructed impulse response of the 1m wire target with SNR = 20dB .

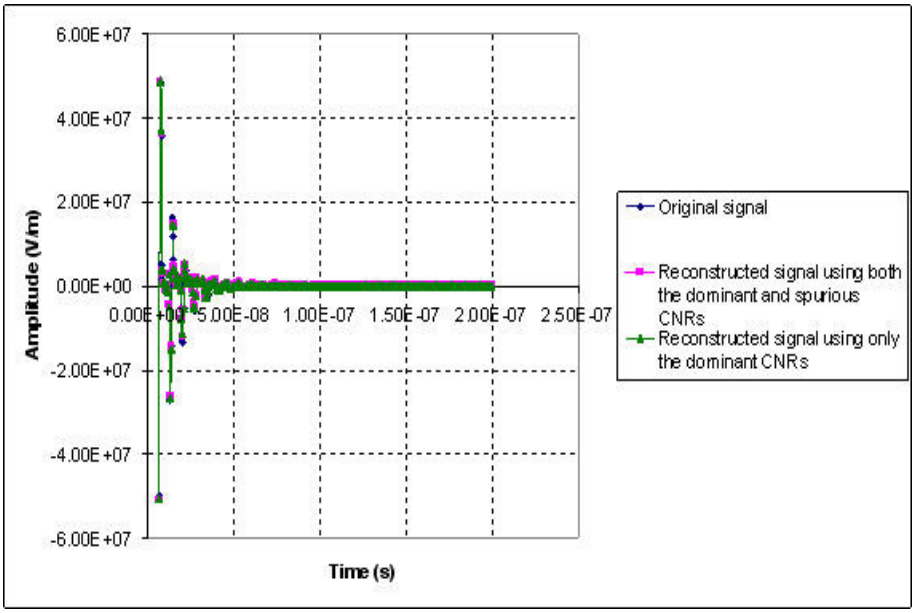

Figure 4.10: Reconstructed impulse response of the 1m wire target with SNR = 10dB .

4.3.4 Conclusion

A novel technique, based on utilizing the energies of the CNRs, has been introduced in this section to identify the dominant poles, from a pool of extracted CNRs, of a simple PEC target in free space with different SNRs. The proposed dominant poles identification scheme does not require any

knowledge of the modal order of the system. It is noted that the value for the reference energy ratio used in this research is derived based on empirical results on several simple PEC targets. In order to enhance the proposed dominant poles identification scheme, future research should include finding a way to auto determine the reference energy ratio regardless of the type of targets. Applying this new technique to low Quality-Factor (Q-Factor) target and dielectric target will also be the subject of further investigations.

4.4 Resonance Based Radar Target Identification Using Information Fusion Technology

This section is based on publications [A2] and [C2]. This section has been extended for this thesis.

4.4.1 Introduction

The main reason for interest in the resonance description is, no doubt, the theoretical aspect and polarization independence of the resonances, making them an ideal target feature parameter for ATR. However, due to the aspect dependency of the residues, some resonant modes will be weakly or not excited at all at some incident aspects [9] and incident polarization states [8]. Therefore, in order to ensure that all of the dominant CNRs of the target are extracted so as to avoid false alarms during target identification process, target's responses from multiple incident aspect angles and/or multiple incident polarizations are used.

In this section, a novel technique, based on PCA, is used to enhance the resonance based target identification process. PCA is used to combine the backscattered signatures of the target from different incident aspect angles. The dominant CNRs of the target are then extracted from the fused signature.

4.4.2 Significant Poles Extraction Using Multiple Data Sets

Currently, there are three methods for extracting the significant poles of the target from multiple data sets [59]. Conventionally, to estimate the SEM poles from multiple look angle data, one takes the average of all the various look directions waveforms and then obtains a single waveform. CNRs are then extracted from the averaged waveform. However, this is not a good approach if the SNRs of the different waveforms are different. For example, by taking an average of the signal along with

waveforms where the signal has died down may lead to an unnecessary contamination of the signal by noise [14]. This method of extracting the CNRs of the target from multiple data sets is shown in Figure 4.11.

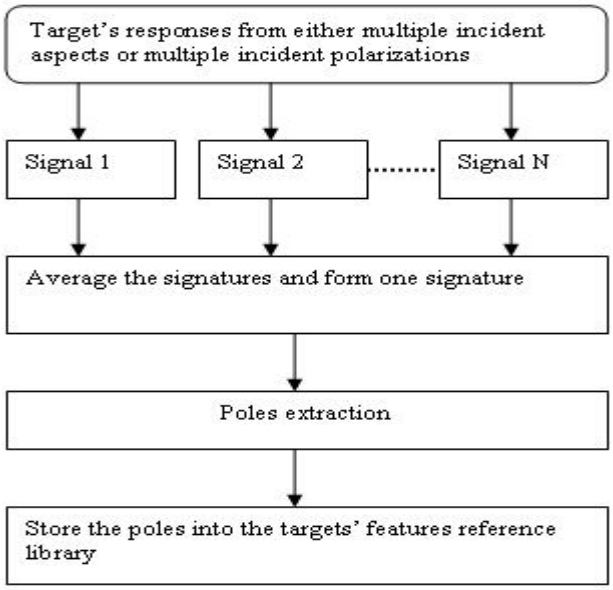

Figure 4.11: Method 1 – Poles extraction utilizing the averaged signature of the target.

The second approach, shown in Figure 4.12, to estimate the poles from the multiple data sets is done by extracting the CNRs from each target's response and selecting one pole to represent each resonant mode. This sounds more feasible and reasonable as compared to the first method, provided that a good pole selection technique is adopted. However, it is difficult to trace the CNRs when more than one mode is around a certain frequency. Some CNRs might be ignored if they are not properly selected.

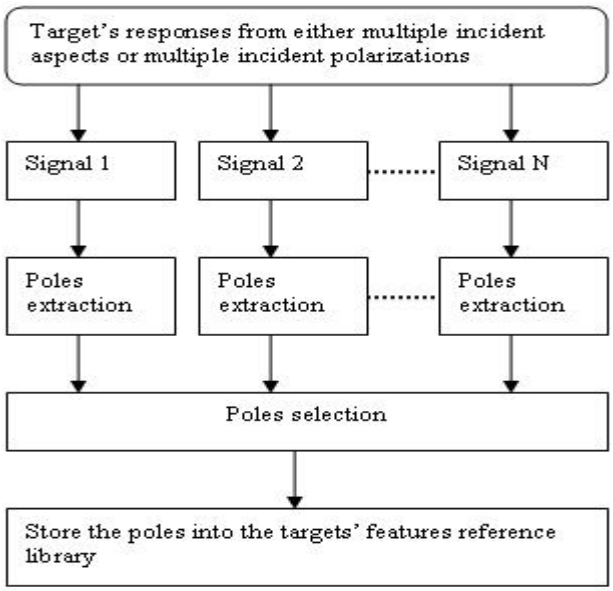

Figure 4.12: Method 2 – Extracting the poles from each target's response and selecting one pole to represent each resonant mode.

The third method for extracting the CNRs from the multiple data sets is accomplished by using Sarkar's modified MPM [14]. In this approach, shown in Figure 4.13, a modified MPM is applied to obtain a single estimate for the poles utilizing simultaneously all the transient waveforms from either multiple incident aspect angles or multiple incident polarizations. This technique for estimating the CNRs from the multiple data sets has eliminated the issues caused by the first two approaches. Nevertheless, higher computational cost is expected in the poles extraction process.

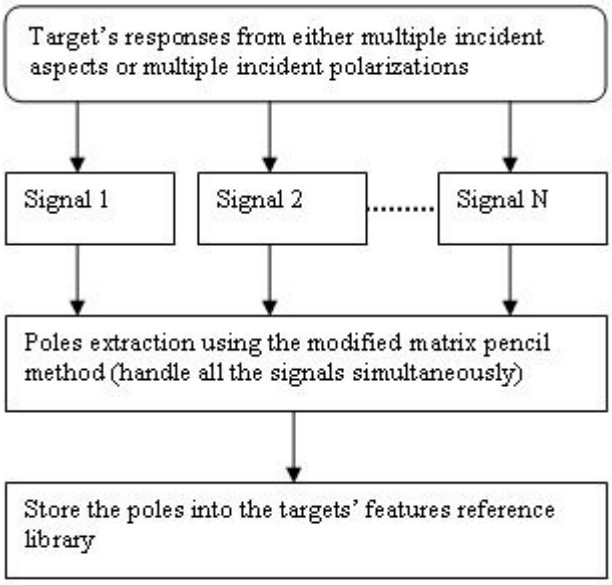

Figure 4.13: Method 3 – Poles extraction utilizing the modified matrix pencil method [14].

4.4.3 Proposed Method

In view of the disadvantages of the above three methods, a novel technique, shown in Figure 4.14, based on information fusion technology is introduced to enhance the CNRs extraction process from multiple data sets. First, PCA is applied to fuse the target's responses from multiple incident aspects and/or multiple incident polarizations. Next, the significant poles of the target are extracted from the fused signature. Although this approach is the same as method 1 in the sense that a single signature is formed, it has the advantage of eliminating the redundant information (i.e. noise) from the signatures of the target.

Chapter 4: Dominant Poles Extraction Schemes

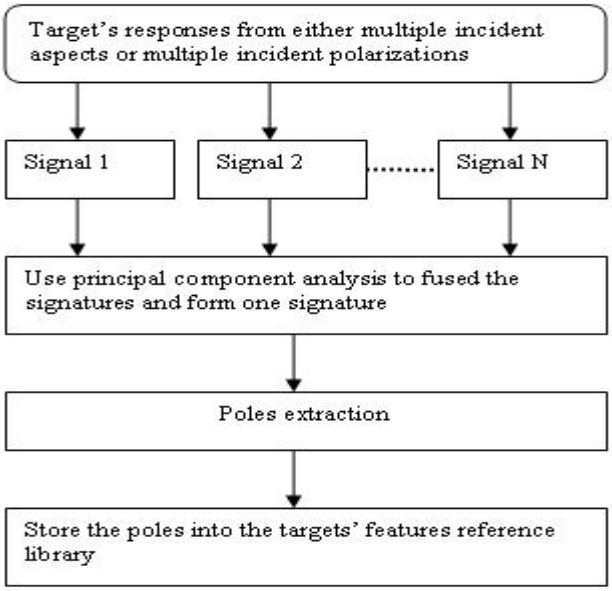

Figure 4.14: Proposed Method – Poles extraction utilizing the fused signature of the target.

4.4.4 Numerical Examples

In order to test the feasibility of our proposed method, we will consider two examples in this section. First, a thin wire target of length $L = 1\text{m}$, shown in Figure 4.6, in free space is being considered. The wire radius a is given by $L/a = 200$. In this example, the polarization angle of the incident field is fixed and various incident aspect angles are considered. Plane wave incident angles of $\theta = 20^\circ$ and $\phi = 0^\circ$, $\theta = 40^\circ$ and $\phi = 0^\circ$, $\theta = 60^\circ$ and $\phi = 0^\circ$, and $\theta = 80^\circ$ and $\phi = 0^\circ$ will be considered. The incident field was polarized with respect to the θ direction. The frequency response of the target was obtained by using the MoM technique, and transformed to the time domain via an IFFT algorithm. In this instance, 256 frequency samples were considered to a maximum frequency of 1GHz, resulting to 512 time samples. The received signatures of the wire target for the four different incident aspect angles are shown in Figure 4.15. It is assumed in this example that there is no noise in the received signatures of the wire target.

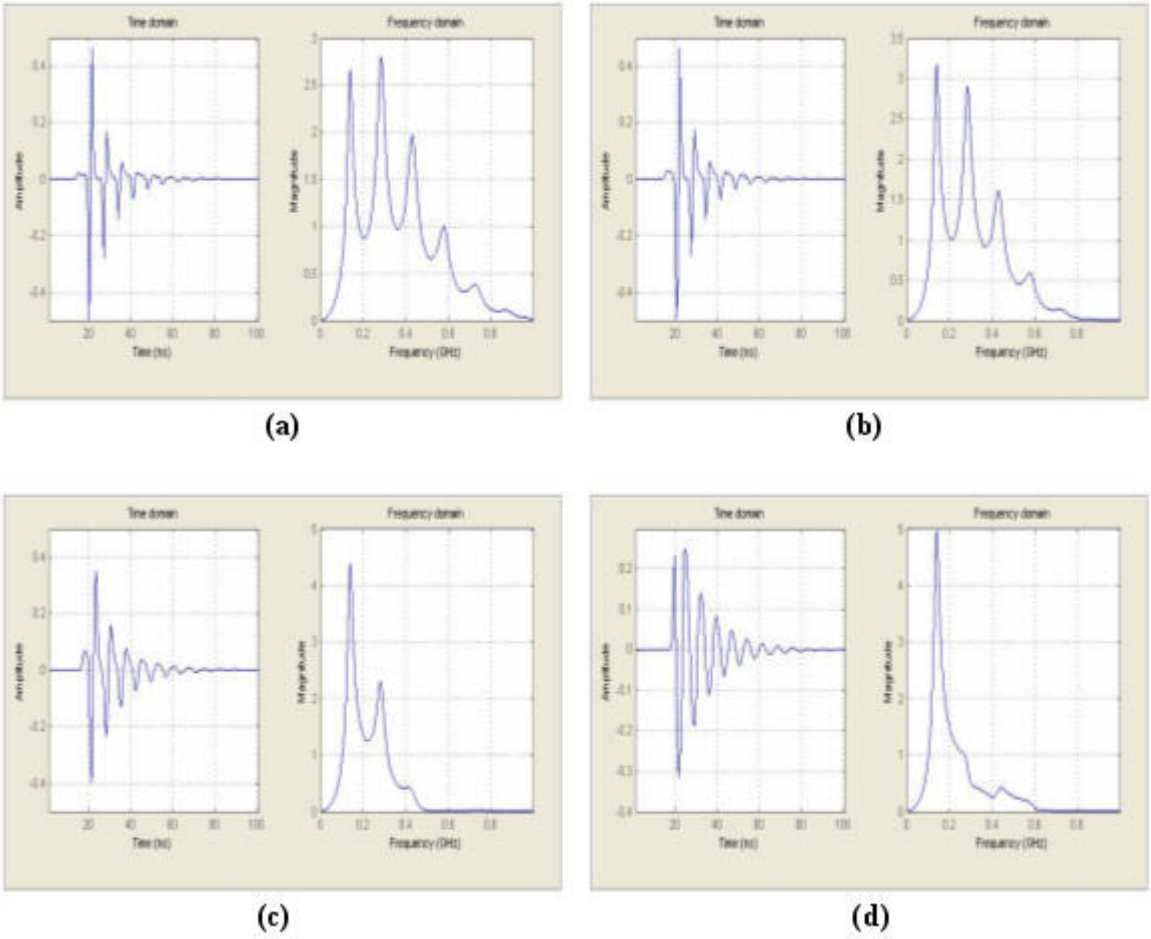

Figure 4.15: The impulse and magnitude responses of the 1m wire target excited by a plane wave at incident angles of (a) $\theta = 20^\circ$ and $\phi = 0^\circ$, (b) $\theta = 40^\circ$ and $\phi = 0^\circ$, (c) $\theta = 60^\circ$ and $\phi = 0^\circ$, and (d) $\theta = 80^\circ$ and $\phi = 0^\circ$.

It is observed from Figure 4.15 that the received signatures of the wire target are different for different incident aspect angles. As shown from the magnitude response waveforms, some of the resonance peaks are missing, indicating that the CNRs are weakly excited in some incident aspects.

PCA was then used for fusing the four different received signatures of the wire target. The fused signature of the 1m wire target is shown in Figure 4.16. Next, MPM was applied to the received signatures and fused signature to extract the first few dominant resonances of the wire target. The first few dominant normalized resonant frequencies of the 1m wire target are shown in Table 4.3 and Figure 4.17.

Chapter 4: Dominant Poles Extraction Schemes

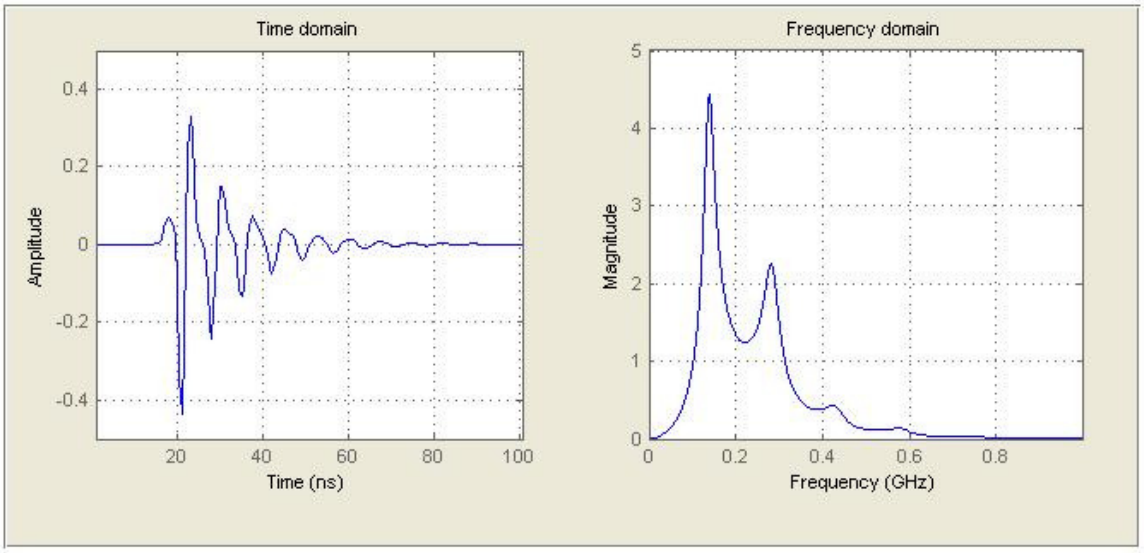

Figure 4.16: The fused signature of the 1m wire target.

Mode	**Theoretical CNRs [59]**	$\theta = 20^\circ$ **and** $\phi = 0^\circ$	$\theta = 40^\circ$ **and** $\phi = 0^\circ$	$\theta = 60^\circ$ **and** $\phi = 0^\circ$	$\theta = 80^\circ$ **and** $\phi = 0^\circ$	**Fused Signature**
i	ω_i / c	ω_i / c	ω_i / c	ω_i / c	ω_i / c	ω_i / c
1	2.910	2.880	2.880	2.880	2.880	2.880
2	6.010	5.947	5.947	5.948	5.948	5.947
3	9.060	9.047	9.046	9.046	9.046	9.046
4	12.200	12.168	12.167	–	12.159	12.168
5	15.300	15.312	15.313	15.301	–	15.311

Table 4.3: Dominant normalized resonant frequencies of the 1m metallic wire target.

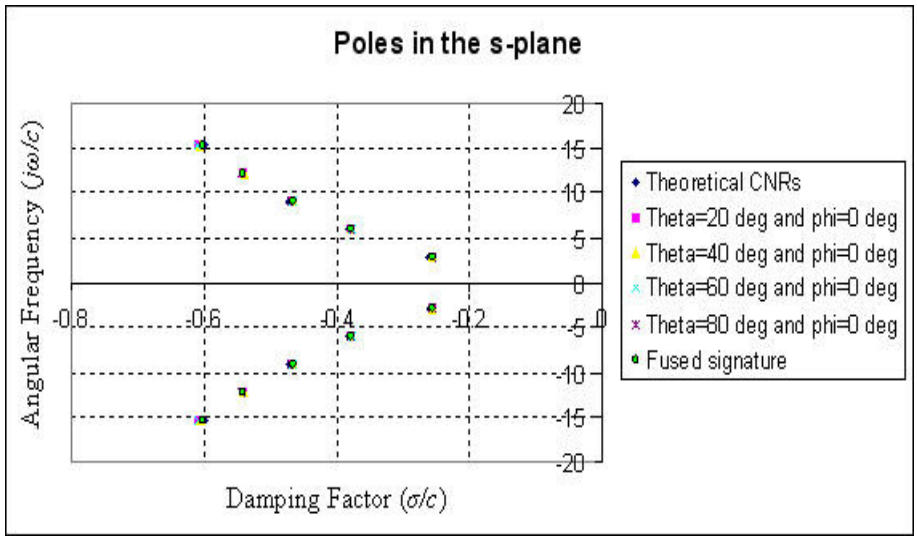

Figure 4.17: Dominant normalized poles of the 1m metallic wire target in the S-plane.

The first few dominant modes are at $\omega_i / c = 2.91$, 6.01, 9.06, 12.20, and 15.30 and they correspond to 139MHz, 287MHz, 432MHz, 582MHz, and 730MHz respectively. It can be seen from Table 4.3 and Figure 4.17 that at incident angles of $\theta = 60^\circ$ and $\phi = 0^\circ$, and $\theta = 80^\circ$ and $\phi = 0^\circ$, the normalized resonant frequencies of mode 4 and 5 are missing respectively. Whereas, all the dominant CNRs of the wire target were being extracted by using the fused signature.

For the second example, a PEC ellipsoid of dimension $a = b = 5$cm and $c = 30$cm in free space, shown in Figure 4.18, is being considered. The ellipsoid surface satisfies the following equation:

$$\frac{x^2}{a^2} + \frac{y^2}{b^2} + \frac{z^2}{c^2} = 1 \qquad \textbf{(4.5)}$$

In this example, the aspect angle of the plane wave is fixed at $\theta = 20^\circ$ and $\phi = 0^\circ$ and various polarization angles, ξ, are considered. Polarization angles of $\xi = 0^\circ$, $\xi = 30^\circ$, $\xi = 60^\circ$, and $\xi = 90^\circ$ will be considered. The frequency response of the target was obtained by using the MoM technique, and transformed to the time domain via an IFFT algorithm. In this instance, 256 frequency samples were considered to a maximum frequency of 1GHz, resulting to 512 time samples. The received signatures of the ellipsoid for the four different polarization angles are shown in Figure 4.19. It is assumed in this example that there is no noise in the received signatures of the ellipsoid target.

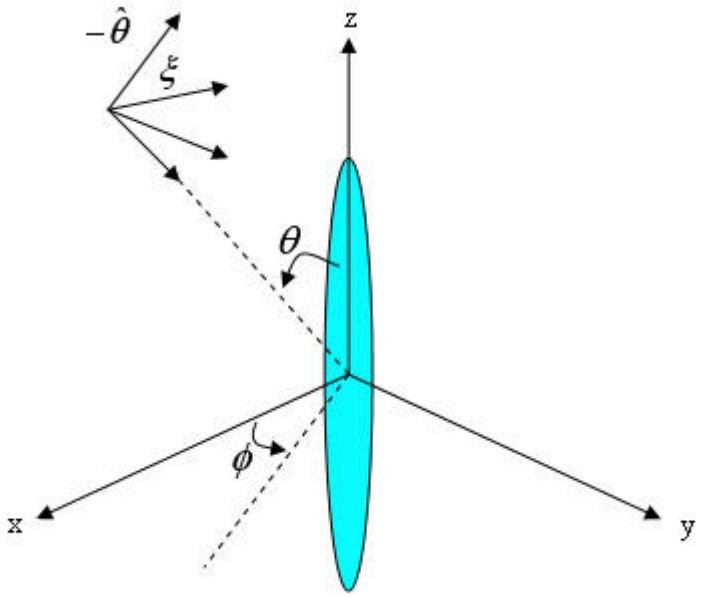

Figure 4.18: Geometry of the ellipsoid.

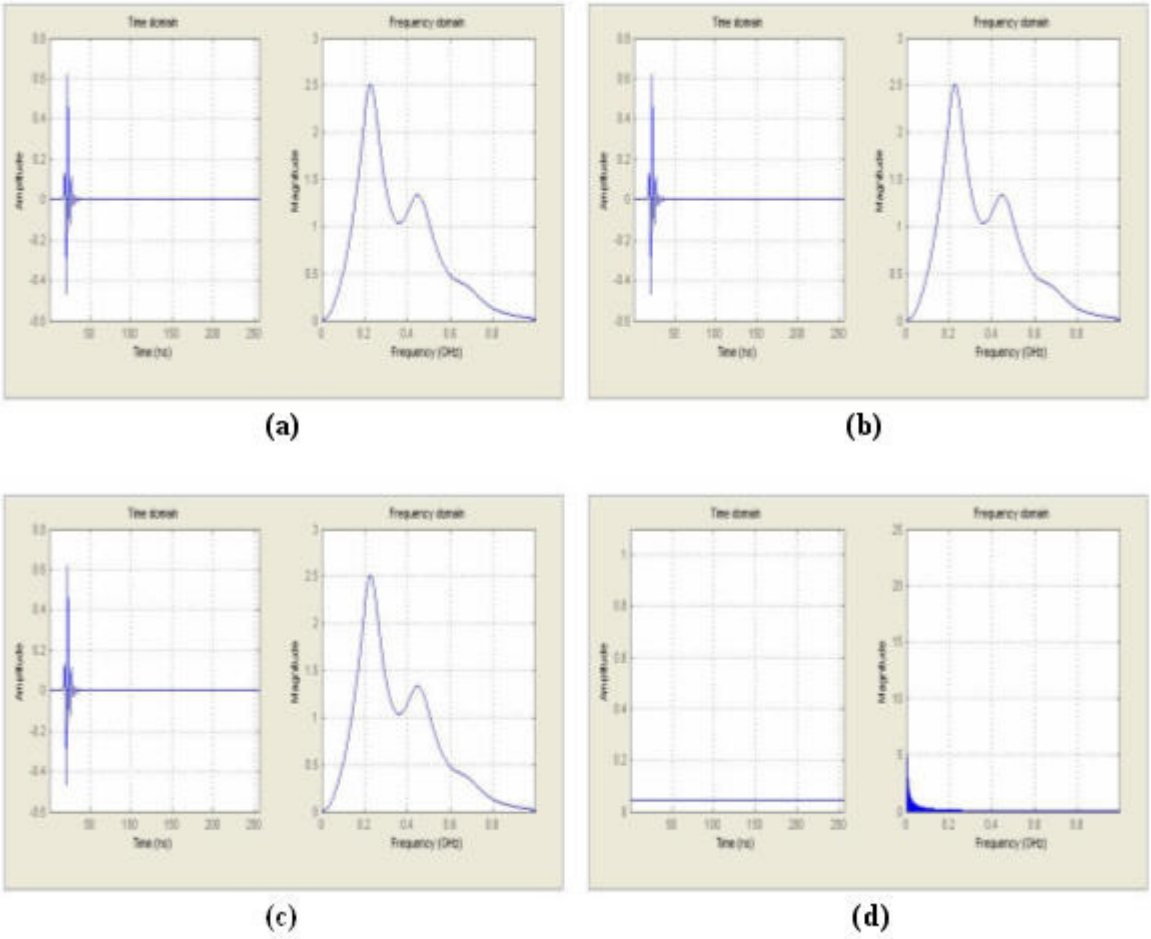

Figure 4.19: The impulse and magnitude responses of the ellipsoid excited by a plane wave at polarization angles of (a) $\xi = 0^\circ$, (b) $\xi = 30^\circ$, (c) $\xi = 60^\circ$, and (d) $\xi = 90^\circ$.

It is observed from Figure 4.19 that the received signature of the ellipsoid at a polarization angle of $\xi = 90^\circ$ is different from the rest of the received signatures as the ellipsoid was not excited properly at an incident polarization angle of $\xi = 90^\circ$. PCA was then used to fuse the four different received signatures of the ellipsoid. The fused signature of the ellipsoid target is shown in Figure 4.20. Next, MPM was applied to the received signatures and fused signature to extract the dominant resonances of the ellipsoid target. The dominant normalized resonant frequencies of the ellipsoid target are shown in Table 4.4 and Figure 4.21.

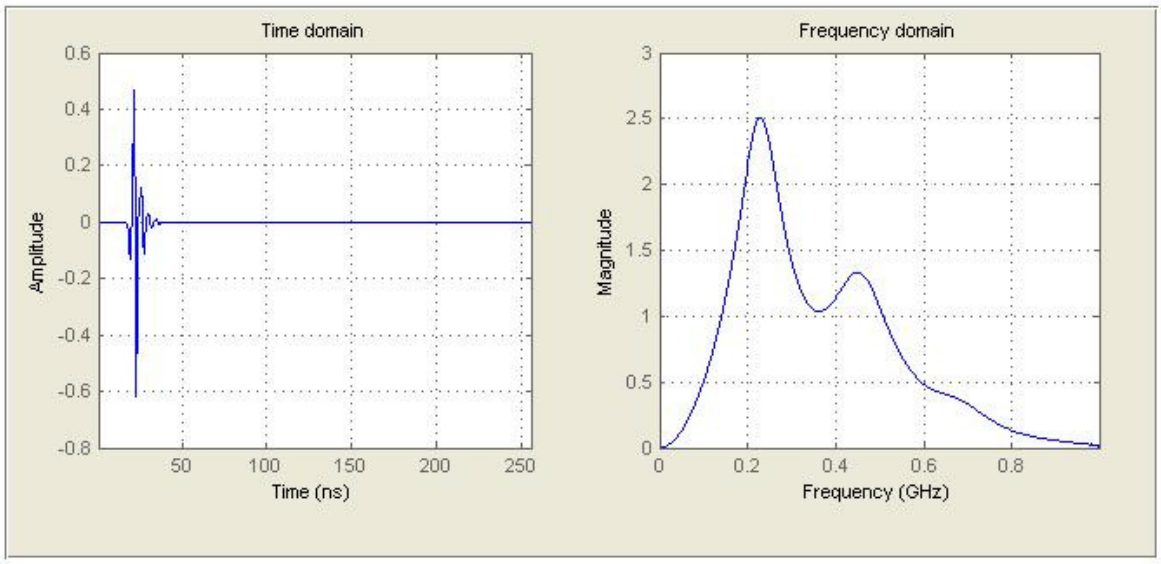

Figure 4.20: The fused signature of the ellipsoid target.

Mode	$\xi = 0^\circ$	$\xi = 30^\circ$	$\xi = 60^\circ$	$\xi = 90^\circ$	Fused Signature
i	ω_i / c	ω_i / c	ω_i / c	ω_i / c	ω_i / c
1	4.818	4.818	4.818	–	4.818
2	9.639	9.639	9.639	–	9.639
3	14.522	14.522	14.522	–	14.522

Table 4.4: Dominant normalized resonant frequencies of the metallic ellipsoid target.

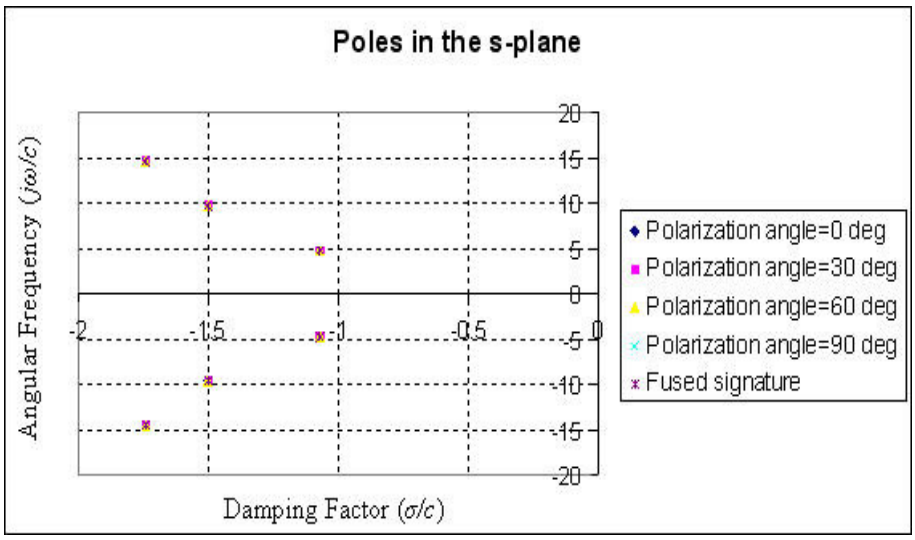

Figure 4.21: Dominant normalized poles of the metallic ellipsoid target in the S-plane.

It can be seen from Table 4.4 and Figure 4.21 that at a polarization angle of $\xi = 90^{\circ}$, the normalized resonant frequencies of all the modes are missing due to the weak excitation of the plane wave. Whereas, by using the fused signature, all the dominant CNRs of the ellipsoid were being extracted.

It is indicated from the above two examples that target classification with reduced aspect or polarization sensitivity can be achieved by using the PCA to obtain a single characteristic signature that contains the dominant CNRs of the target.

4.4.5 Remarks

A novel technique, based on PCA, has been introduced in this section to enhance the resonance based target identification process using multiple data sets. This new method has been successfully applied to identify the dominant CNRs of simple PEC targets in free space. In order to prove the robustness of this technique, further testing, using the noise contaminated signatures of the target, could be conducted. Applying this new technique to low Q-Factor target, dielectric target, and more complex target such as the aircraft model will also be the subject of further investigations.

4.5 Conclusion

In a resonance based target identification system, it is important that the contributing CNRs of the target are extracted *prior* to the target identification step as incorrectly identifying the dominant poles of the target could result in a false alarm during the target classification process. A robust and reliable pole extraction technique is needed to accomplish this task and MPM is chosen due to its robustness to noise in the sampled data and computational ease. However, the rank deficiency problem in the $\mathbf{Z}$ matrix, shown in Equation 2.15, of the MPM has degraded the performance of the MPM. In this chapter, a solution to the rank deficiency issue of the MPM has been presented and in order to further quantify the performance of the proposed technique, future investigation should include applying the improved MPM method to low Q-Factor target, dielectric target, and more complex target such as the aircraft model.

Two novel significant poles extraction schemes, that utilized the energies of the CNRs and PCA, have also been presented in this chapter. Numerical examples using PEC targets in free space have proven the feasibility of the proposed methods. However, in order to prove the reliability and

robustness of the proposed techniques, further investigation using a low Q-Factor target and a dielectric target is needed.

As mentioned previously in Chapter 1, the resonance based target identification process is broken down into two parts in this research. The first part, which involves identifying the dominant poles of the target, has been covered in this chapter. The second part, which involves designing a classifier that is capable of identifying the correct object from a set of targets under all weather conditions, will be presented in the following chapter.

Chapter 5: Robust Target Identification Techniques

Chapter 5: Robust Target Identification Techniques

5.1 Introduction

It can be seen from Figure 1.1 that the classification step forms an important part of the feature based target identification process. Other than the process of resonance extraction, another research interests have focussed on the development of target recognition schemes for ATR applications. It is also the dream of researchers around the world to develop a classifier that is reliable and can perform well in noisy environment.

Target recognition based on CNRs is popular due to the fact that the CNRs are purely dependent on target attributes. In other words, the differences in target attributes between two different targets would result in different CNRs for each target and target recognition can be achieved based on such differences between the CNRs. In order to automate the identification procedure, Moffatt and Mains [60] first proposed the concept of target identification based on target dependant CNRs using a predictor-correlator approach. A brief overview of some of the resonance based classifiers that are popular in the literature could also be found in Section 1.3. Amongst them, the GLRT has produced a better identification result, in the presence of noise. Therefore, it will be used as the reference classifier in this research to quantify the quality of the proposed classification techniques.

Two unique and efficient resonance based target identification schemes will be presented in this chapter. The first technique makes use of the correlation between the unknown target and the reference target in the identification process while the second method utilized both the WVD and GLRT to enhance the performance of the classifier. Numerical results have proven that both the proposed methods are comparable to the GLRT technique.

5.2 Target Classification Process

In a feature based target identification process, shown in Figure 1.1, it is important to have a classifier that is robust to noise in the sampled data. The problem of interest here is to identify a specific target based on the noisy backscattered field from a “wide-band” transmitted pulse. Several assumptions are made in order to simplify the target identification process in this chapter. First, we

assume that a target has been detected and the backscattered field contains only a single target. Furthermore, we assume that the reference target is within a set of targets and we know *a priori* the dominant poles of the reference target.

5.3 Robust Target Identification in White Gaussian Noise Using Canonical Correlation Analysis

This section is based on publication [J1].

5.3.1 Introduction

During the past, a number of target discrimination techniques that utilize the CNRs have been proposed. Perhaps the most popular of the techniques is the E-pulse technique [16] which operates by annihilating the late time response from a specific target. However, the disadvantages of the E-pulse, mentioned in Section 2.8, have degraded the target identification process. Therefore, statistical methods such as the GLRT [24], [25] were introduced to enhance the target identification process. In this section, we propose a new and robust resonance based target identification technique that is also based on hypothesis testing [46]. The performance of our method is evaluated by using various simulated targets in free space under different environmental conditions.

5.3.2 Overview of Canonical Correlation Analysis

CCA was developed by Hotelling [62]. It is a way of measuring the linear relationship between two multidimensional variables. It finds two bases, one for each variable, that are optimal with respect to correlations and, at the same time, it finds the corresponding correlations. In other words, it finds the two bases in which the correlation matrix between the variables is diagonal and the correlations on the diagonal are maximized. The dimensionality of these new bases is equal to or less than the smallest dimensionality of the two variables.

Being a standard tool in statistical analysis, canonical correlation has been used for example in economics, medical studies, and undersea target classification [63]-[65]. In this section, CCA will be used as a target identification tool to identify the reference target, based on its extracted poles' information, from a set of candidate targets.

5.3.3 Classification Using Canonical Correlation Analysis

The material presented here and much of the language and terminology are drawn from [63].

Given two sets of vectors, $X = [x_1, \cdots, x_M] \epsilon \mathbb{R}^{N \times M}$, and $Y = [y_1, \cdots, y_L] \epsilon \mathbb{R}^{N \times L}$, CCA seeks a pair of vectors, $a^*$and b^*, that maximize the correlation $\rho = corr(X_a, Y_b)$, such that

$$\rho^* = \max_{a,b} corr(Xa, Yb) \tag{5.1}$$

The covariance matrix of $\boldsymbol{X}$ and $\boldsymbol{Y}$ can be denoted as follow:

$$C = \begin{bmatrix} C_{xx} & C_{xy} \\ C_{yx} & C_{yy} \end{bmatrix} \tag{5.2}$$

where C_{xx} and C_{yy} are the within-sets covariance matrices of X and Y respectively and $C_{xy} = C_{yx}^T$ is the between-sets covariance matrix.

The solution to Equation 5.1 can be obtained by solving the following eigenvalue problems:

$$C_{xx}^{-1} C_{xy} C_{yy}^{-1} C_{yx} a^* = \rho^2 a^*$$
$$b^* = C_{xx}^{-1} C_{xy} a^* \tag{5.3}$$

where $C_{xx} = E[XX^T]$, $C_{yy} = E[YY^T]$, $C_{xy} = E[XY^T]$, $C_{yx} = E[YX^T]$, " E " denotes the expectation operator, and "T" denotes the transpose operator.

The square roots of the eigenvalues obtained from Equation 5.3 are called canonical correlations, and the vectors a^* and b^* are the canonical vectors.

To help explain the idea of CCA, we use a noiseless version of Equation 2.21 as follow

$$\mathbf{x} = \mathbf{R}_g \mathbf{Z}_g, \qquad 1 \le g \le P \tag{5.4}$$

where

$$\mathbf{R}_g = \begin{bmatrix} R_1^g & R_2^g & \cdots & R_{M_g}^g \end{bmatrix}^T \tag{5.5}$$

is an unknown, non-random vector, "T" denotes the transpose operator, and

$$\mathbf{Z}_g = \begin{bmatrix} Z_1^g & Z_2^g & \cdots & Z_{M_g}^g \end{bmatrix}_{q \times M_g} \tag{5.6}$$

denotes the matrix containing the known signal modes.

Chapter 5: Robust Target Identification Techniques

For the analysis presented here, $\mathbf{R}_g$ is an unknown parameter vector in the identification of target g. The only known parameters are the poles which determine $\mathbf{Z}_g$. Therefore, we will ignore $\mathbf{R}_g$ in our target identification process as it is orientation or polarization dependent.

The maximum canonical correlation between the noiseless return signal $\mathbf{x}$ and the known parameter $\mathbf{Z}$ is given by

$$\rho^* = \max_{a,b} corr(\mathbf{x}a, \mathbf{Z}b) \quad \textbf{(5.7)}$$

If $\emptyset$ denotes the empty set, we can see that

- Under $\mathcal{H}_0$, null hypothesis:
  $\mathbf{x} \cap \mathbf{Z} = \emptyset$, hence $\rho^* = 0$ if the subspaces spanned by $\mathbf{x}$ and $\mathbf{Z}$ are orthogonal.
- Under $\mathcal{H}_1$, alternative hypothesis:
  $\mathbf{x} \cap \mathbf{Z} \neq \emptyset$, hence $\rho^* = 1$ under noiseless condition.

Under noisy environment, if we assume that all targets are equally probable, the above decision rule can be generalized for P target discrimination as

$$decide\ y(t) = target\ g\ if\ \rho^*\ is\ maximum. \quad \textbf{(5.8)}$$

5.3.4 Numerical Examples

To demonstrate the effectiveness of the proposed CCA method, we will compare it against the GLRT technique.

5.3.4.1 Simulation Setup

In order to highlight the performance of the CCA method as a function of SNR, several simulations using PEC targets in free space were conducted.

The first example considers five 1m long thin bent wire targets with different bending angles of $\theta = 30°$, $\theta = 45°$, $\theta = 60°$, $\theta = 75°$, and $\theta = 90°$ as shown in Figure 5.1. The wires have equal lengths of 0.5m along both the X and Y axis.

The second example considers five ellipsoid targets with different lengths of $L = 0.56m, L = 0.60m, L = 0.64m$, $L = 0.68m$, and $L = 0.72m$ as shown in Figure 5.2. The ellipsoid surface satisfies Equation 4.5.

Also shown in Figure 5.1 and Figure 5.2 are the orientation of the incident field E_ϕ relative to each target.

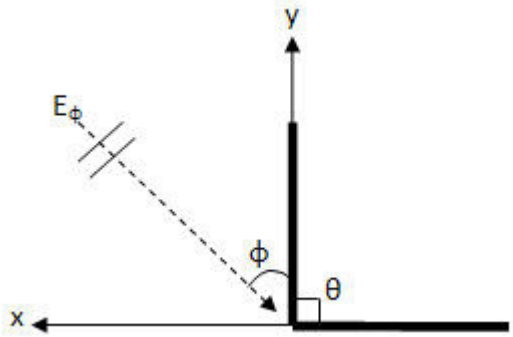

Figure 5.1: Geometry of the 1m long thin bent wire target with a bending angle of θ.

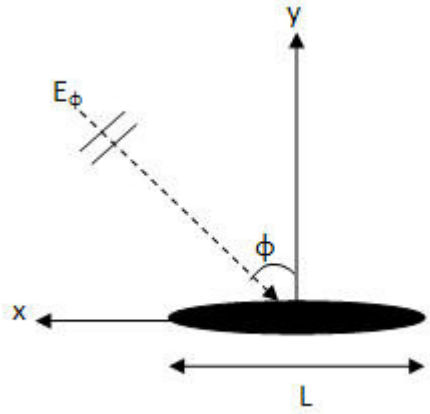

Figure 5.2: Geometry of the ellipsoid target with a length of L.

The scattering data used in the experiment are the theoretical impulse responses of the targets. The impulse response was obtained by first acquiring the frequency response of the target using the MoM technique. The frequency response was then windowed using a Gaussian window to approximate the Gaussian incident pulse. Finally, the impulse response of the target was obtained by transforming the windowed frequency domain data to the time domain via an IFFT technique.

Chapter 5: Robust Target Identification Techniques

After obtaining the impulse responses of the targets, the poles of each target were extracted using MPM algorithm. The extracted poles were then stored inside a targets' features reference library.

The experimental setup for the simulation process is illustrated in Figure 5.3. In our experiment, we will fix the reference target in each example by letting bent wire with a bending angle of $\theta = 60°$ and ellipsoid with a length of $L = 0.64m$ to be the reference targets.

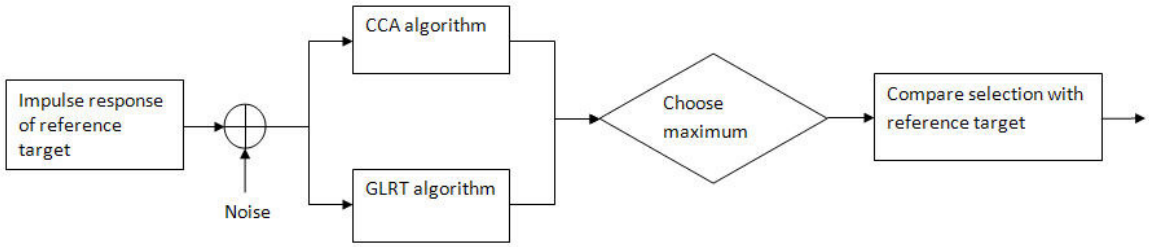

Figure 5.3: Experimental setup for demonstrating the performance of the CCA and GLRT techniques.

To simulate noisy environment, white Gaussian noise is added to the corresponding impulse signature, $x(t)$, of the reference target by using Equation 4.3.

After adding noise to the signature, the corrupted impulse response of the reference target is then fetched into either the CCA or GLRT detector, which then renders a decision as to which target is present. This process is repeated 30 times at each specified value of SNR. For the purposes of this experiment, the SNR values are chosen to range from -10dB to 20dB.

5.3.4.2 Bent Wire Targets of Different Bending Angles

For our first example, we will consider five bent wire targets. In this example, 512 frequency samples were considered up to a maximum frequency of 1GHz, resulting to 1024 time samples. Figure 5.4 shows the frequency and impulse responses of the reference target due to an impulsive plane wave incident from ϕ=45°. Late time commences at around $T_L = 23ns$ for the five bent wire targets. 12 dominant complex conjugate poles, tabulated in Table 5.1, were then extracted using the MPM algorithm.

Although this is an example that uses simple targets, it can be seen from Table 5.1 that the five bent wire targets have quite similar CNRs as there is only a slight different in bent angle between the five targets. Therefore, this increases the difficulty of identifying the reference target when noise is introduced into the system.

The simulation's results for this example are shown in Figure 5.5 for different target orientations.

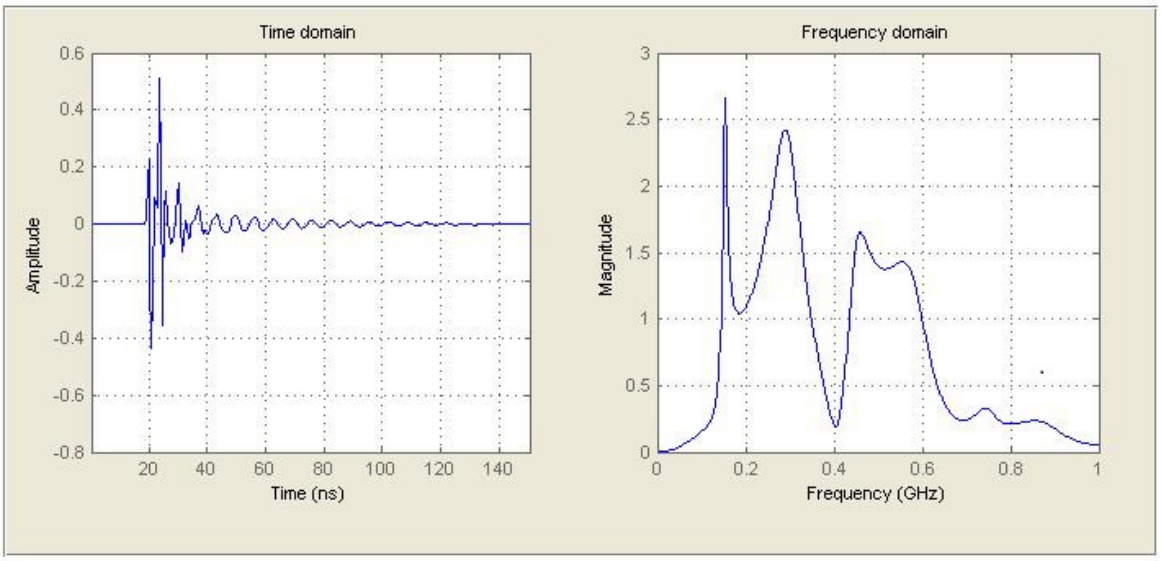

Figure 5.4: Backscattering frequency and impulse responses of the bent wire with a bending angle of $\theta = 60°$ as a result of an impulsive plane wave incident from ϕ=45^o.

	Bent wire with $\theta = 30°$	Bent wire with $\theta = 45°$	Bent wire with $\theta = 60°$	Bent wire with $\theta = 75°$	Bent wire with $\theta = 90°$
$\frac{s_{1,2}}{c}$	$-0.037 \pm j3.416$	$-0.064 \pm j3.287$	$-0.093 \pm j3.193$	$-0.121 \pm j3.119$	$-0.146 \pm j3.061$
$\frac{s_{3,4}}{c}$	$-0.883 \pm j5.895$	$-0.873 \pm j6.045$	$-0.774 \pm j6.171$	$-0.632 \pm j6.219$	$-0.508 \pm j6.202$
$\frac{s_{5,6}}{c}$	$-0.257 \pm j9.524$	$-0.407 \pm j9.384$	$-0.512 \pm j9.350$	$-0.543 \pm j9.363$	$-0.509 \pm j9.368$
$\frac{s_{7,8}}{c}$	$-1.087 \pm j12.249$	$-0.924 \pm j12.203$	$-0.974 \pm j12.154$	$-1.007 \pm j12.271$	$-0.917 \pm j12.410$
$\frac{s_{9,10}}{c}$	$-0.513 \pm j15.797$	$-0.617 \pm j15.768$	$-0.575 \pm j15.659$	$-0.646 \pm j15.526$	$-0.755 \pm j15.517$
$\frac{s_{11,12}}{c}$	$-1.276 \pm j18.489$	$-1.199 \pm j18.351$	$-1.209 \pm j18.381$	$-1.170 \pm j18.572$	$-1.071 \pm j18.500$

Table 5.1: Natural resonant frequencies of the five bent wire targets.

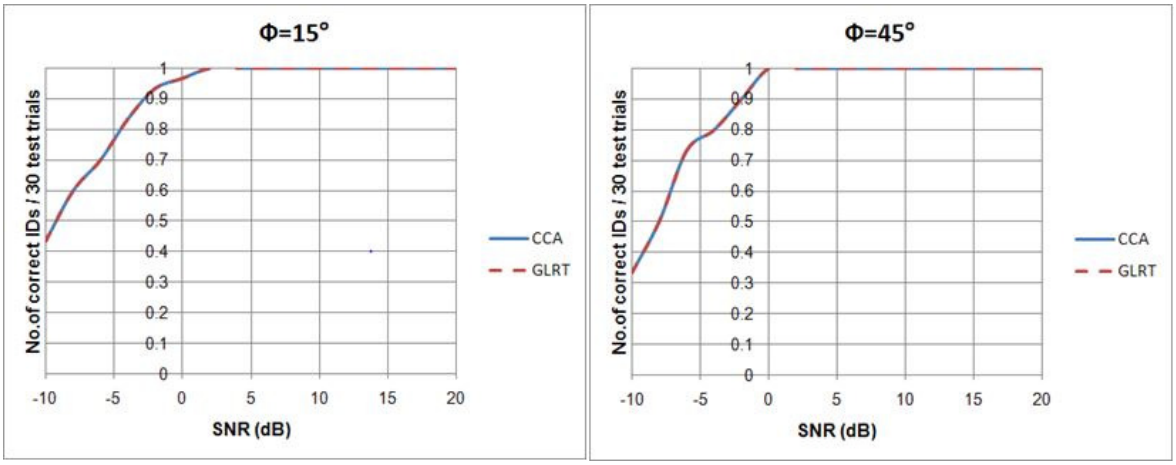

Figure 5.5: The performance of the CCA and GLRT methods as a function of SNR for two different incident angles using the five bent wire targets.

5.3.4.3 Ellipsoid of Different Lengths

For our second example, we will consider five ellipsoid targets. In this example, 512 frequency samples were considered up to a maximum frequency of 4GHz, resulting to 1024 time samples. The frequency and impulse responses of the reference target, due to an impulsive plane wave incident from ϕ=45^o, can be found in Figure 5.6. Late time commences at around $T_L = 4.5ns$ for the five ellipsoid targets. 4 dominant complex conjugate poles, tabulated in Table 5.2, were then extracted using the MPM algorithm.

The simulation's results for this example are shown in Figure 5.7 for different plane wave incident angles.

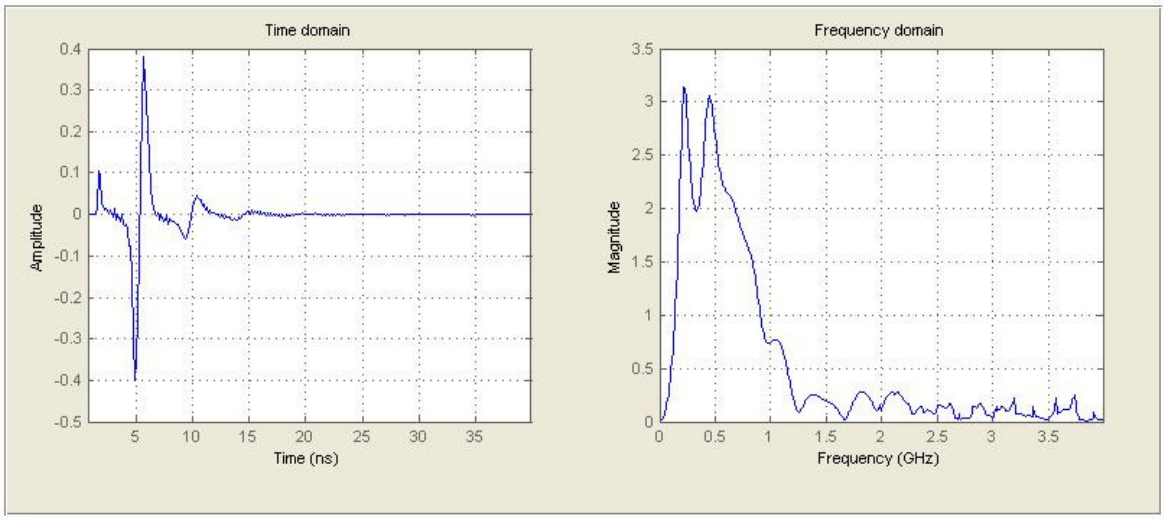

Figure 5.6: Backscattering frequency and impulse responses of the ellipsoid with a length of $L = 0.64m$ as a result of an impulsive plane wave incident from ϕ=45^o.

	Ellipsoid with L = 0.56m	Ellipsoid with L = 0.60m	Ellipsoid with L = 0.64m	Ellipsoid with L = 0.68m	Ellipsoid with L = 0.72m
$\frac{s_{1,2}}{c}$	$-1.539 \pm j4.193$	$-1.474 \pm j3.718$	$-1.307 \pm j3.568$	$-1.200 \pm j3.624$	$-1.223 \pm j3.795$
$\frac{s_{3,4}}{c}$	$-3.941 \pm j13.665$	$-3.938 \pm j13.045$	$-3.490 \pm j12.174$	$-2.934 \pm j11.430$	$-2.434 \pm j10.958$

Table 5.2: Natural resonant frequencies of the five ellipsoid targets.

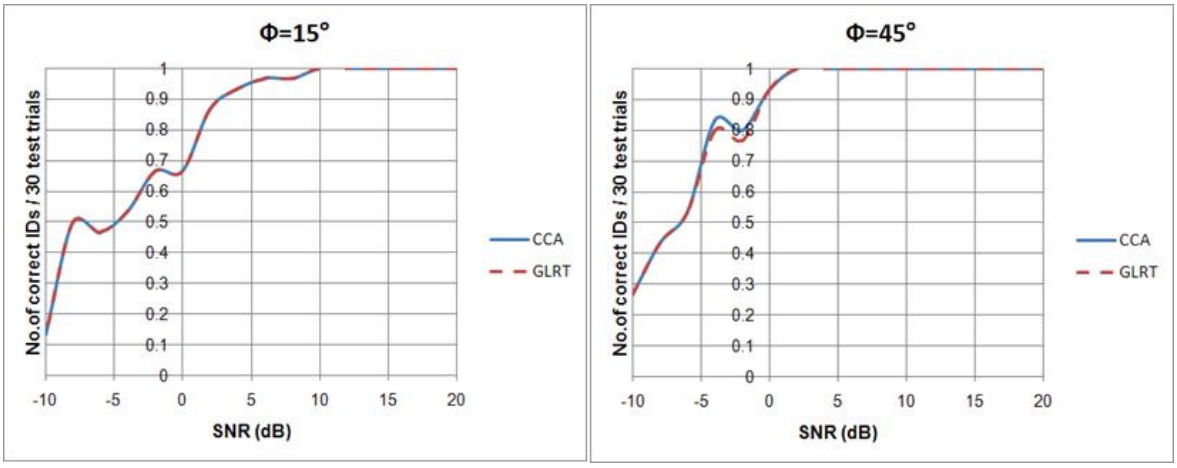

Figure 5.7: The performance of the CCA and GLRT methods as a function of SNR for two different incident angles using the five ellipsoid targets.

5.3.5 Discussion

A Q-Factor is use to describe how under-damped a resonator is [66]. Higher Q indicates a lower rate of energy loss relative to the stored energy of the oscillator. Therefore, the oscillations die out more slowly.

In order to demonstrate the effectiveness of the CCA technique, we have utilised both the high Q-Factor and low Q-Factor targets in our two examples. It can be seen from Figure 5.4 and Figure 5.6 that the bent wire target resonates longer in the frequency domain as compared to the ellipsoid target. Therefore, the bent wires and the ellipsoids are our high Q-Factor and low Q-Factor targets respectively.

As can be seen from Figure 5.5 and Figure 5.7, the performance of the CCA and GLRT methods are plotted as a function of SNR in decibels for each target's orientation. The performance of each technique is defined as the number of correct identifications (IDs) per 30 test trials at a specified SNR value.

It can be seen from the bent wire targets example that both the CCA and GLRT methods have identical performance for each target's orientation. At an aspect angles of $\phi=15^{o}$ and $\phi=45^{o}$, both the methods begin to correctly identify the reference target in every trial at a SNR of 2dB and 0dB respectively.

For the ellipsoid targets example, the performance of the CCA and GLRT techniques also matches closely to each other as shown in Figure 5.7. At an aspect angles of $\phi=15^{o}$ and $\phi=45^{o}$, both the detectors start to correctly identify the reference target in every trial at a SNR of 10dB and 2dB respectively. As expected, there is a slight drop in performance as compared to the bent wire example because of the lower Q-Factor of the ellipsoid. Also as predicted, the performance of both techniques decreases as SNR decreases.

In each of our two examples, five targets were being used for simulation. This means that there is 20% chance of classifying the reference target. It can be seen from Figure 5.5 and Figure 5.7 that the identification rate in 30 test trials for the bent wire target and ellipsoid target are above 20% even at a low SNR of -10dB except for $\phi=15^{o}$ for the ellipsoid target where the identification rate

drop to 13.33%. This demonstrated the robustness of the CCA technique as the identification rate in 30 test trials for the bent wire target and ellipsoid target are above 20% even at a low SNR of -10dB.

5.3.6 Conclusion

In this research, we have proposed a novel and robust statistical technique base on SEM representation for target discrimination. Numerical results using both high Q-Factor and low Q-Factor targets demonstrate the effectiveness of the CCA method as compare to the GLRT method in the presence of random noise. Applying this new technique to dielectric target will be the subject of further investigation.

5.4 Robust Target Identification Using a Modified Generalized Likelihood Ratio Test

This section is based on publication [J2].

5.4.1 Introduction

In order to correctly identify a remote target, an efficient and robust target signature identification technique is required. During the past, a number of target discrimination techniques that utilize the CNRs have been proposed. Perhaps the near optimal solution among them is the GLRT technique, which outperforms the E-pulse method in the presence of noise [24], [25]. It is well established that the resonance based target classifier only applies to the late time portion of the target response. However, for ATR applications, usually such information is not known *a priori* and incorrect determination of the commencement of the late time period for the unknown target response would significantly degrade the performance of the classifier.

In view of this problem, a modified GLRT target recognition scheme is proposed in this section. The enhanced GLRT method utilizes the WVD to determine the portion of the unknown target response on which to perform hypothesis testing. Therefore, it does not require *prior* knowledge of the commencement of the late time period for the transient response of the unknown target. The performance of our method is evaluated by using various simulated targets in free space under different environmental conditions. Simulation results show that the modified GLRT method is

comparable to the original GLRT technique when the beginning of the late time period for the unknown target response is accurately determined and surpasses the original GLRT technique when the commencement of the late time period for the unknown target response is wrongly determined.
It can be seen from Figure 1.1 that the feature based target classification process is broken down into two parts, the feature extraction and the discrimination/ classifier part. In this section, the late time information is needed for extracting the dominant poles of the reference target. But no further information of the late time is needed for the discrimination part.

5.4.2 Modified Generalized Likelihood Ratio Test

The first step in designing the modified GLRT technique is to use the WVD to determine the portion, as shown in Figure 5.8, of the unknown target response to perform the GLRT test. The WVD in Figure 5.8 was produced by the same target used in Section 4.3.3. It can be seen from Figure 5.8 and [67] that each of the resonance peaks (P1-P3) of the unknown target frequency response has a corresponding energy density distribution in the time-frequency domain and as time progresses, the energy of each resonances decreases as expected.

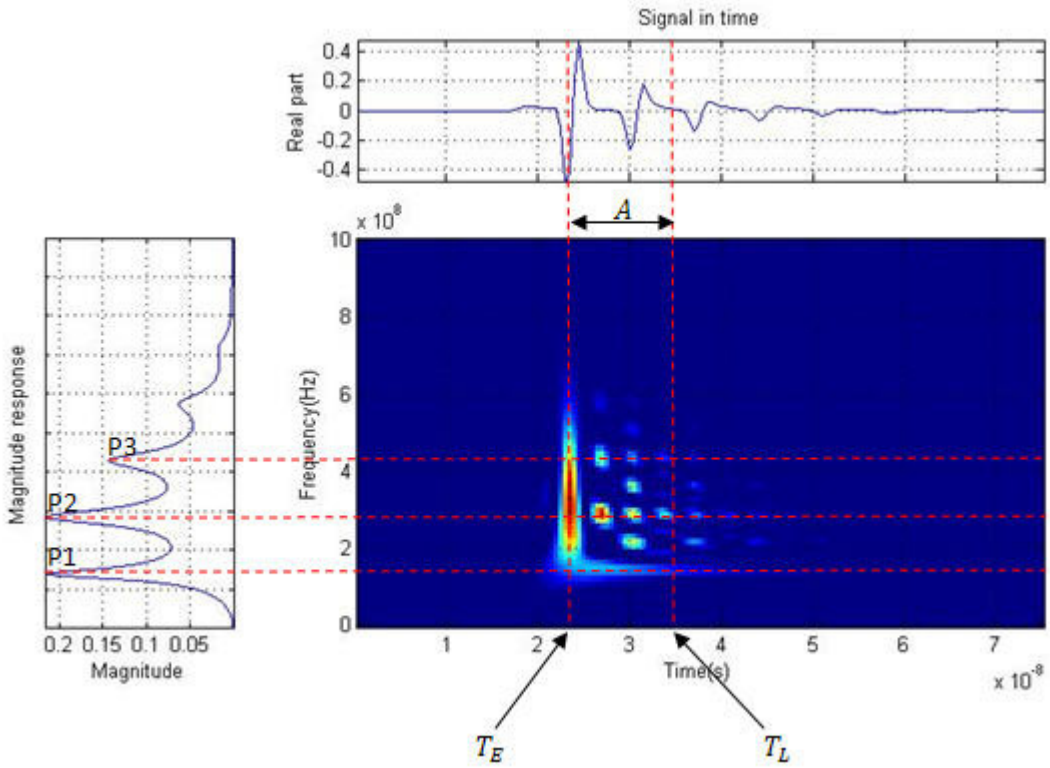

Figure 5.8: Using the WVD to determine the portion, *A*, of the unknown target response to perform the GLRT test.

Next, as a crucial step of the classifier design, the value of A must be determined. This corresponds to the region where most of the unknown target resonances' energies lie. This region is determined from the early time, T_E, to the late time, T_L. The proposed method of determining the values for T_E and T_L is based on empirical results on several targets. It is noted, from the WVD results of several targets, that every target will have a time, T_E, when the energy of the target response is maximum. Following that, the target resonances' energies traces will start to appear in the time-frequency domain.

In order to determine the values for T_E and T_L, the energy, E, of the unknown target response at each time sample has to be determined. This can be found by adding up the energies of the target transient response along the frequency axis of the time-frequency plot. T_E corresponds to the time when E is maximum and T_L corresponds to the time when E drops below the average energy, E_{avg}, of the signal in the time-frequency domain. E_{avg} is found by using the following equation:

$$E_{avg} = (\sum_{k=1}^{N} E)/D \qquad \textbf{(5.11)}$$

where D is the total number of data samples in the discrete time domain and A is the total number of samples between T_E and T_L.

Using Equation 2.18, the response from target g can be rewritten as

$$\mathbf{y}_a = \begin{bmatrix} y\left[T_{E_g} + (a-1)T_s\right] \\ y\left[T_{E_g} + (a-1)T_s + T_s\right] \\ y\left[T_{E_g} + (a-1)T_s + 2T_s\right] \\ \vdots \\ y\left[T_{E_g} + (a-1)T_s + (G-1)T_s\right] \end{bmatrix}, a = 1,2,\dots,A \quad \textbf{(5.12)}$$

where T_{E_g} is the early time for the transient response of target g, G is the total number of data samples, starting from T_{E_g}, in the discrete time domain, and A is the total number of $\mathbf{y}_a$ used to perform the modified GLRT test. Therefore, the modified GLRT leads to the following decision rule for P targets discrimination

$$\text{decide}\{y(t)\} = \text{target } g \text{ if the sum of } \left\| \left(\mathbf{Z}_g^H \mathbf{Z}_g\right)^{-\frac{1}{2}} \mathbf{Z}_g^H \mathbf{y}_a \right\|^2 \text{ is maximum} \quad \textbf{(5.13)}$$

5.4.3 Numerical Examples

To demonstrate the effectiveness of the proposed modified GLRT method, we will compare it against the GLRT algorithm.

5.4.3.1 Simulation Setup

In order to demonstrate the effectiveness of the modified GLRT technique as a function of SNR, several simulations using PEC targets in free space were conducted.

The first example considers five 1m long thin bent wire targets with different bending angles of θ=30°, θ=45°, θ=60°, θ=75°, and θ=90° as shown in Figure 5.1. It is noted that the bent wire has a fixed segment along the X axis and a rotating segment along the Y axis. The wires have equal lengths of 0.5m along both the X and Y axis.

The second example considers five ellipsoid targets with different lengths of L=0.56m, L=0.60m, L=0.64m, L=0.68m, and L=0.72m as shown in Figure 5.2. The ellipsoid surface satisfies Equation 4.5 where $a = \mathrm{L}/2$, $b = 5\mathrm{cm}$, and $c = 5\mathrm{cm}$.

The last example considers five wire models of aircraft with different rear wings' lengths of $\mathrm{r} = 0.1\mathrm{m}$, $\mathrm{r} = 0.2\mathrm{m}$, $\mathrm{r} = 0.3\mathrm{m}$, $\mathrm{r} = 0.4\mathrm{m}$, $\mathrm{r} = 0.5\mathrm{m}$ as shown in Figure 5.9. Also shown in Figure 5.1, Figure 5.2, and Figure 5.9, the orientations of the incident field E_ϕ are relative to each target.

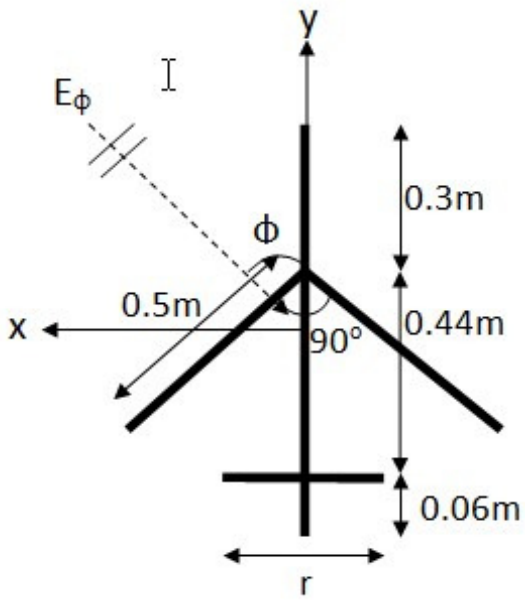

Figure 5.9: Geometry of the wire model aircraft target with a rear wing length of r.

In this section, we will classify the bent wire and the ellipsoid as our simple targets. The wire model aircraft target will be classified as our complex target as it has quite a few substructures.

The scattering data used in the experiment are the theoretical impulse responses of the targets. The impulse response was obtained by first acquiring the frequency response of the target using the MoM technique. The frequency response was then windowed using a Gaussian window to approximate the Gaussian incident pulse. Finally, the impulse response of the target was obtained by transforming the windowed frequency domain data to the time domain via an IFFT technique.
After obtaining the impulse responses of the targets, the poles of each target were extracted using the MPM algorithm. The extracted poles were then stored inside a targets' features reference

library. In this section, the poles were extracted from the impulse response, due to an impulsive plane wave incident from $\phi=45^{o}$, of the target.

The experimental setup for the simulation process is illustrated in Figure 5.10. In our experiment, we will fix the reference target in each example by letting the bent wire with a bending angle of $\theta=60°$, the ellipsoid with a length of L=0.64m, and the wire model aircraft with a rear wing length of $r = 0.3m$ to be the reference targets.

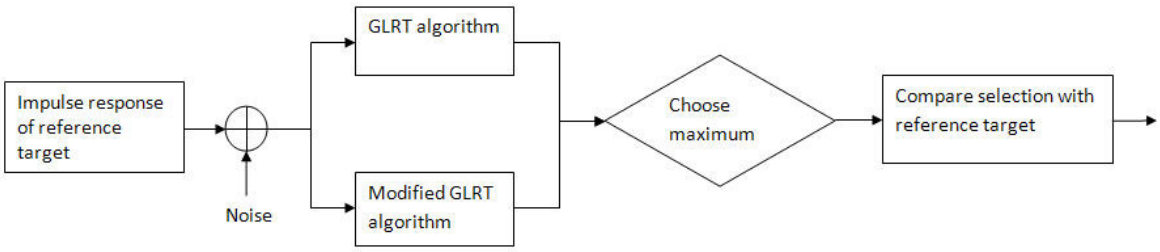

Figure 5.10: Experimental setup for demonstrating the performance of both the modified GLRT and GLRT techniques.

To simulate noisy environment, white Gaussian noise is added to the corresponding impulse signature of the reference target using Equation 5.9.

After adding noise to the signature, the corrupted impulse response of the reference target is then fetched into either the modified GLRT or GLRT detector, which then renders a decision as to which target is present. This process is repeated 100 times at each specified value of SNR. For the purpose of this experiment, the SNR values are chosen to range from -10dB to 20dB.

5.4.3.2 Bent Wire with Different Bending Angles

For our first example, we will consider five bent wire targets. In this example, 512 frequency samples were considered up to a maximum frequency of 1GHz, resulting to 1024 time samples. Figure 5.4 shows the frequency and impulse responses of the reference target, bent wire with a bending angle of $\theta=60°$, due to an impulsive plane wave incident from $\phi=45^{o}$. The 12 dominant complex conjugate poles for the five bent wire targets are listed in Table 5.1.

Although this is an example that uses simple targets, it can be seen from Table 5.1 that the five bent wire targets have quite similar CNRs as there is only a slight difference in the bending angles between the five targets. Therefore, this increases the difficulty of identifying the reference target when noise is introduced into the system.

Using Equation 2.4, the commencements of the late time periods for the transient responses of the reference target at incident angles of ϕ=15°, ϕ=30°, ϕ=45°, and ϕ=75° are estimated to be $T_L = 25.22nsec$, $T_L = 25.33nsec$, $T_L = 25.22nsec$, and $T_L = 26.08nsec$ respectively. These late times are used to perform the original GLRT test.

Prior to performing the modified GLRT test, WVD is used to determine the high resonance region, A, for the transient response of the reference target. Figure 5.11 shows an example of determining the value of T_E and T_L for the transient response of the reference target due to a plane wave incident from ϕ=45°. It can be seen from Figure 5.11 that T_E corresponds to the time when the energy, E, of the reference target response is maximum, at around 325, and T_L matches the time when E drops below $E_{avg} = 3.45$. Therefore, the total number of samples between T_E and T_L for this example is A=79. The values of A for the transient responses of the reference target at an incident angles of ϕ=15°, ϕ=30°, and ϕ=75° are $A = 87$, $A = 75$, and $A = 107$ respectively.

The performances of both the modified GLRT and original GLRT techniques as a function of SNR for four different target orientations are shown in Figure 5.12. In order to simulate the effect of incorrect late time determination for late time starting too early, $T_L = 16nsec$, $T_L = 16nsec$, $T_L = 18nsec$, and $T_L = 18nsec$ are arbitrary chosen for an incident angles of ϕ=15°, ϕ=30°, ϕ=45°, and ϕ=75° respectively. In order to simulate the effect of incorrect late time determination for late time starting too late, $T_L = 36nsec$ is used for all the four incident angles of ϕ=15°, ϕ=30°, ϕ=45°, and ϕ=75°.

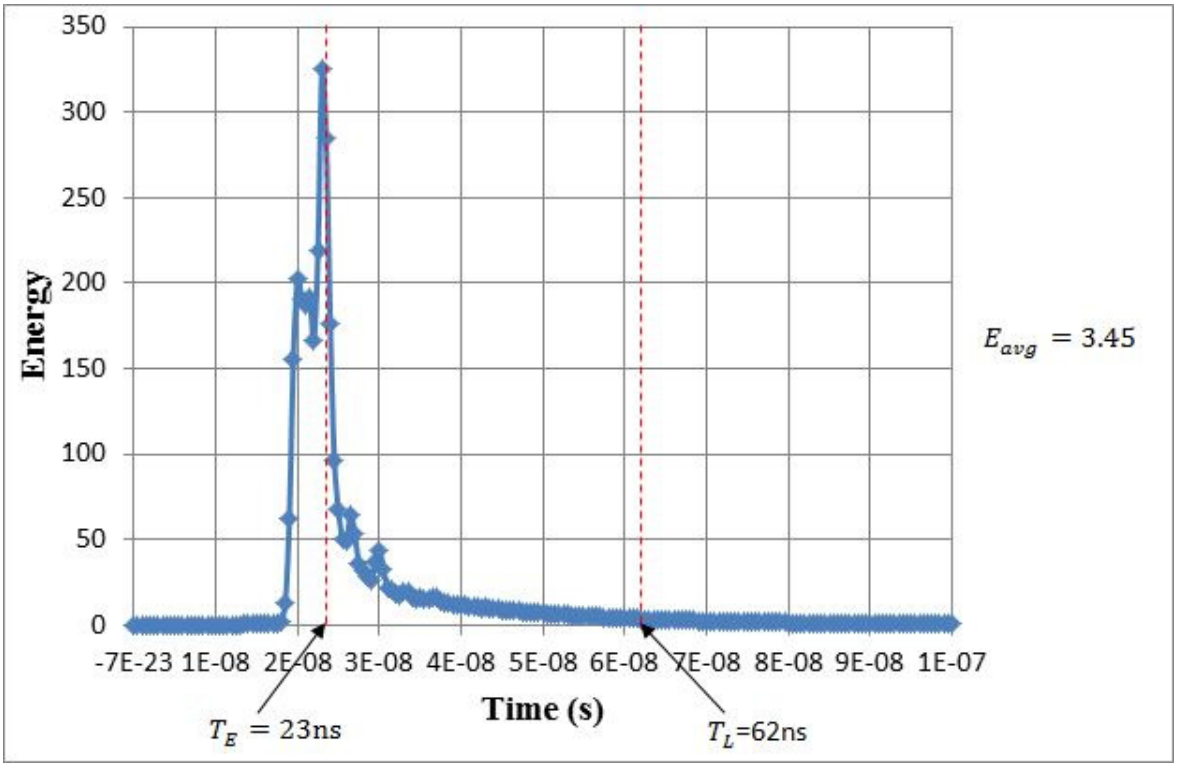

Figure 5.11: Determining the values of T_E and T_L using the energy, E, of the transient response of the bent wire target with a bending angle of θ=60°.

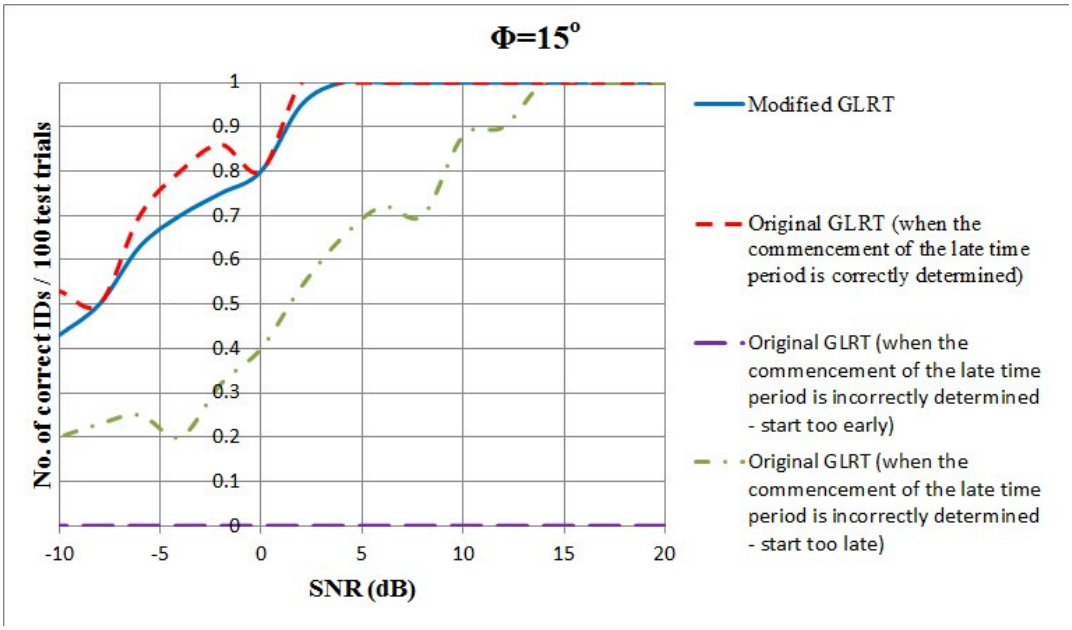

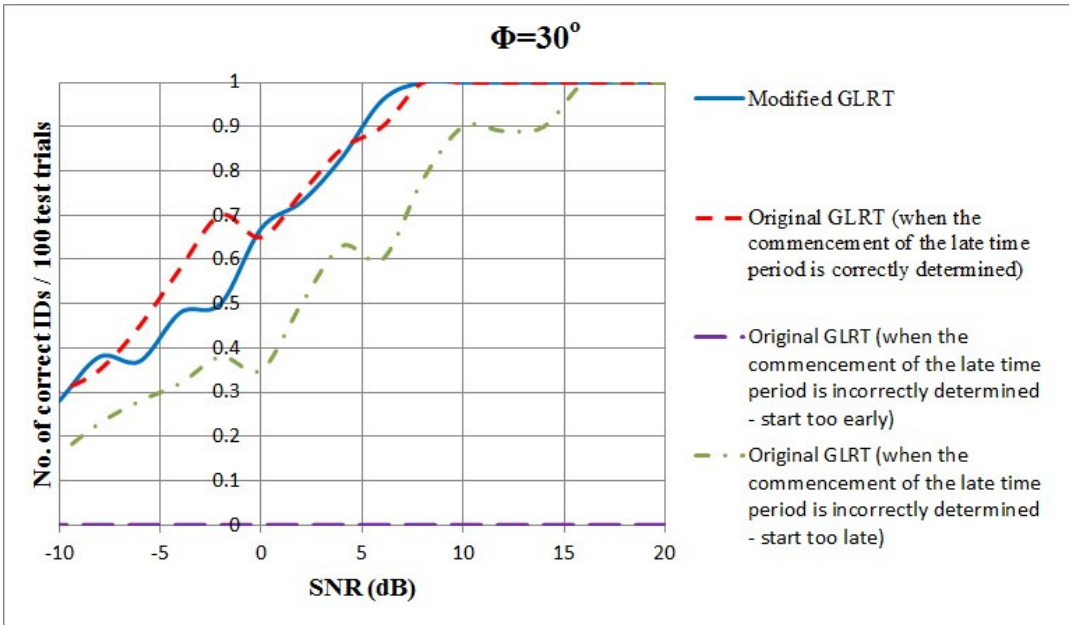
Φ=30°
No. of correct IDs / 100 test trials
SNR (dB)
Modified GLRT
Original GLRT (when the commencement of the late time period is correctly determined)
Original GLRT (when the commencement of the late time period is incorrectly determined - start too early)
Original GLRT (when the commencement of the late time period is incorrectly determined - start too late)

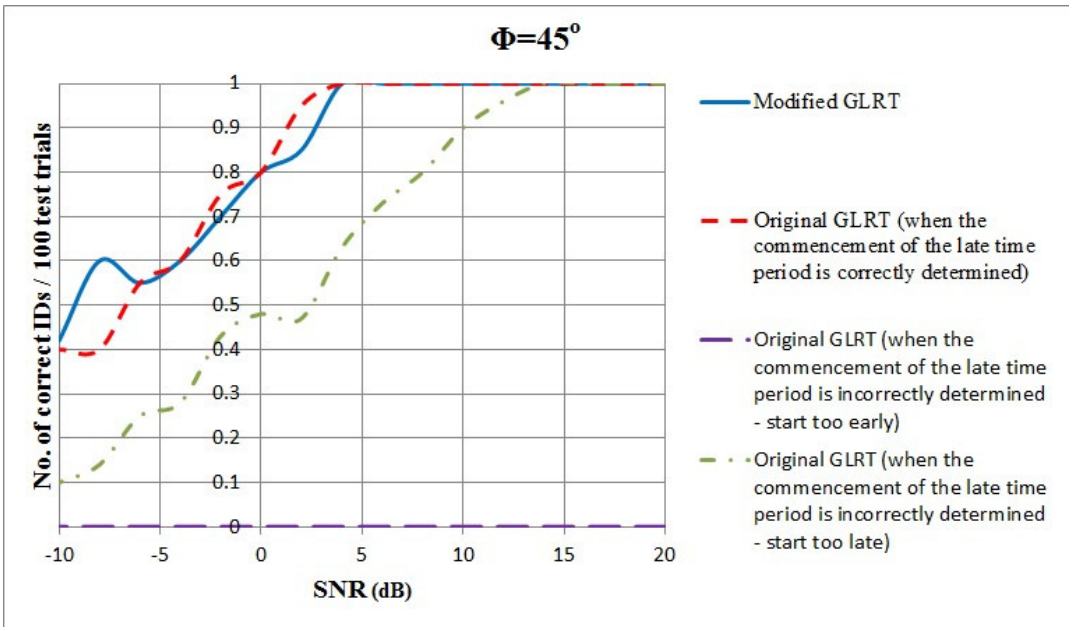
Φ=45°
No. of correct IDs / 100 test trials
SNR (dB)
Modified GLRT
Original GLRT (when the commencement of the late time period is correctly determined)
Original GLRT (when the commencement of the late time period is incorrectly determined - start too early)
Original GLRT (when the commencement of the late time period is incorrectly determined - start too late)

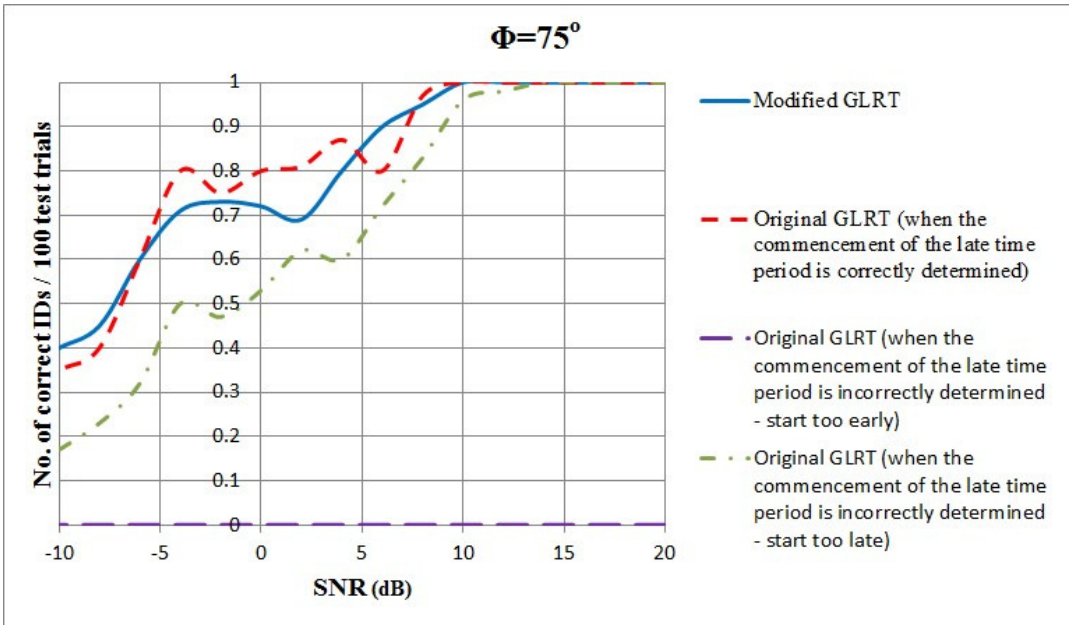

Figure 5.12: The performance of the modified GLRT and original GLRT methods as a function of SNR for four different incident angles using the five bent wire targets.

5.4.3.3 Ellipsoid Targets with Different Lengths

For our second example, we will consider five ellipsoid targets. In this example, 512 frequency samples were considered up to a maximum frequency of 4GHz, resulting to 1024 time samples. The frequency and impulse responses of the reference target, ellipsoid with a length of L = 0.64m, due to an impulsive plane wave incident from ϕ=45°, can be found in Figure 5.6. The 4 dominant complex conjugate poles for the five ellipsoid targets are listed in Table 5.2.

Using Equation 2.4, the commencements of the late time periods for the transient responses of the reference target at an incident angles of ϕ=15°, ϕ=30°, ϕ=45°, and ϕ=75° are estimated to be $T_L = 5.50nsec$, $T_L = 6.50nsec$, $T_L = 7.38nsec$, and $T_L = 9nsec$ respectively. These late times are used to perform the original GLRT test.

Prior to performing the modified GLRT test, WVD is used to determine the high resonance region, A, for the transient response of the reference target. Utilising the energy, E, of the reference target response, the values of A for the transient responses of the reference target at an incident angles of

ϕ=15°, ϕ=30°, ϕ=45°, and ϕ=75° are calculated to be $A = 64$, $A = 44$, $A = 52$, and $A = 58$ respectively.

The simulation's results for this example are shown in Figure 5.13 for different plane wave incident angles. In order to simulate the effect of incorrect late time determination for late time starting too early, $T_L = 1.75nsec$, $T_L = 2.75nsec$, $T_L = 4.50nsec$, and $T_L = 6nsec$ are arbitrary chosen for an incident angles of ϕ=15°, ϕ=30°, ϕ=45°, and ϕ=75° respectively. In order to simulate the effect of incorrect late time determination for late time starting too late, $T_L = 12.50nsec$ is used for all the four incident angles of ϕ=15°, ϕ=30°, ϕ=45°, and ϕ=75°.

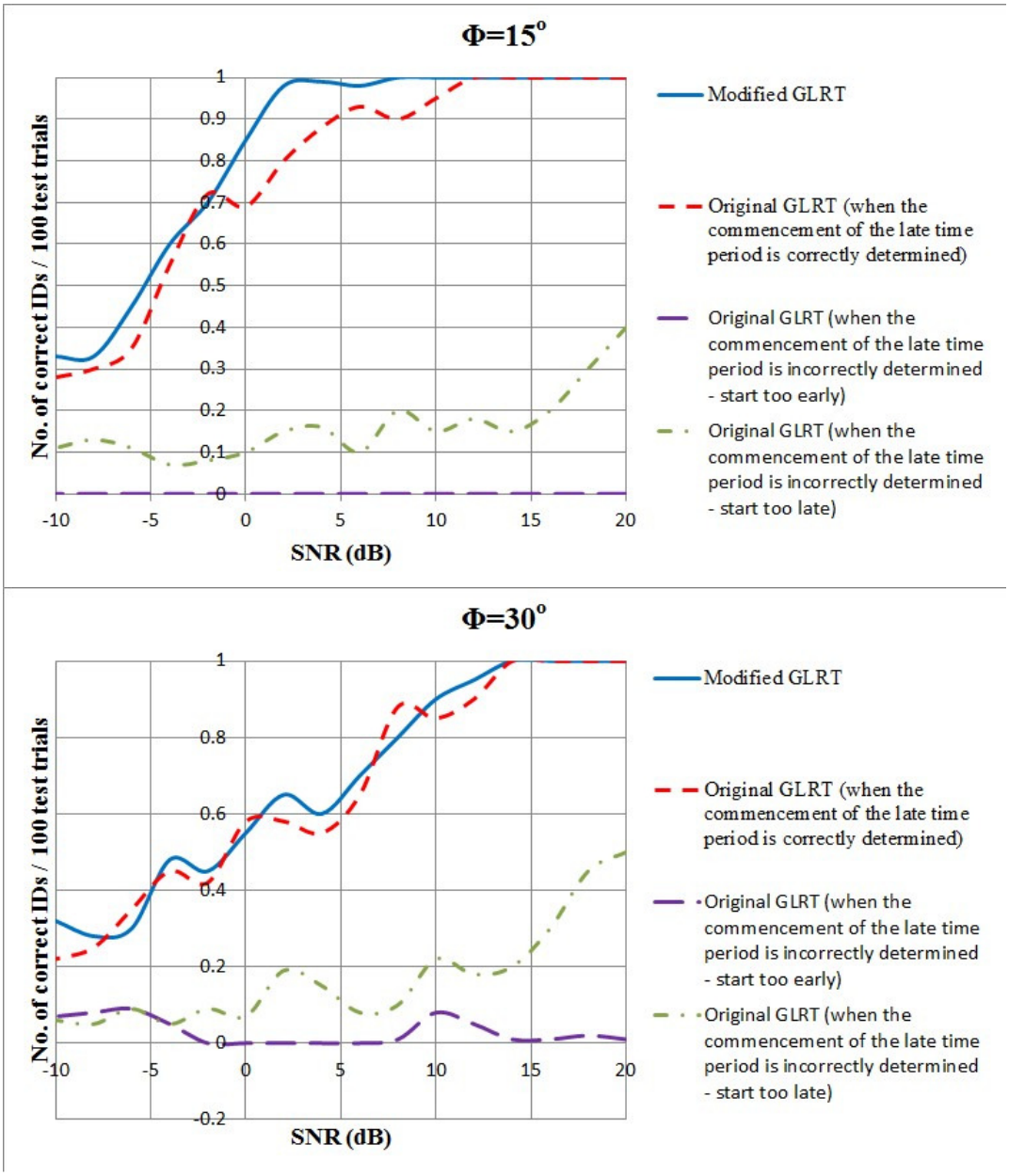
Φ=15°
No. of correct IDs / 100 test trials
SNR (dB)
Modified GLRT
Original GLRT (when the commencement of the late time period is correctly determined)
Original GLRT (when the commencement of the late time period is incorrectly determined - start too early)
Original GLRT (when the commencement of the late time period is incorrectly determined - start too late)
Φ=30°
No. of correct IDs / 100 test trials
SNR (dB)
Modified GLRT
Original GLRT (when the commencement of the late time period is correctly determined)
Original GLRT (when the commencement of the late time period is incorrectly determined - start too early)
Original GLRT (when the commencement of the late time period is incorrectly determined - start too late)

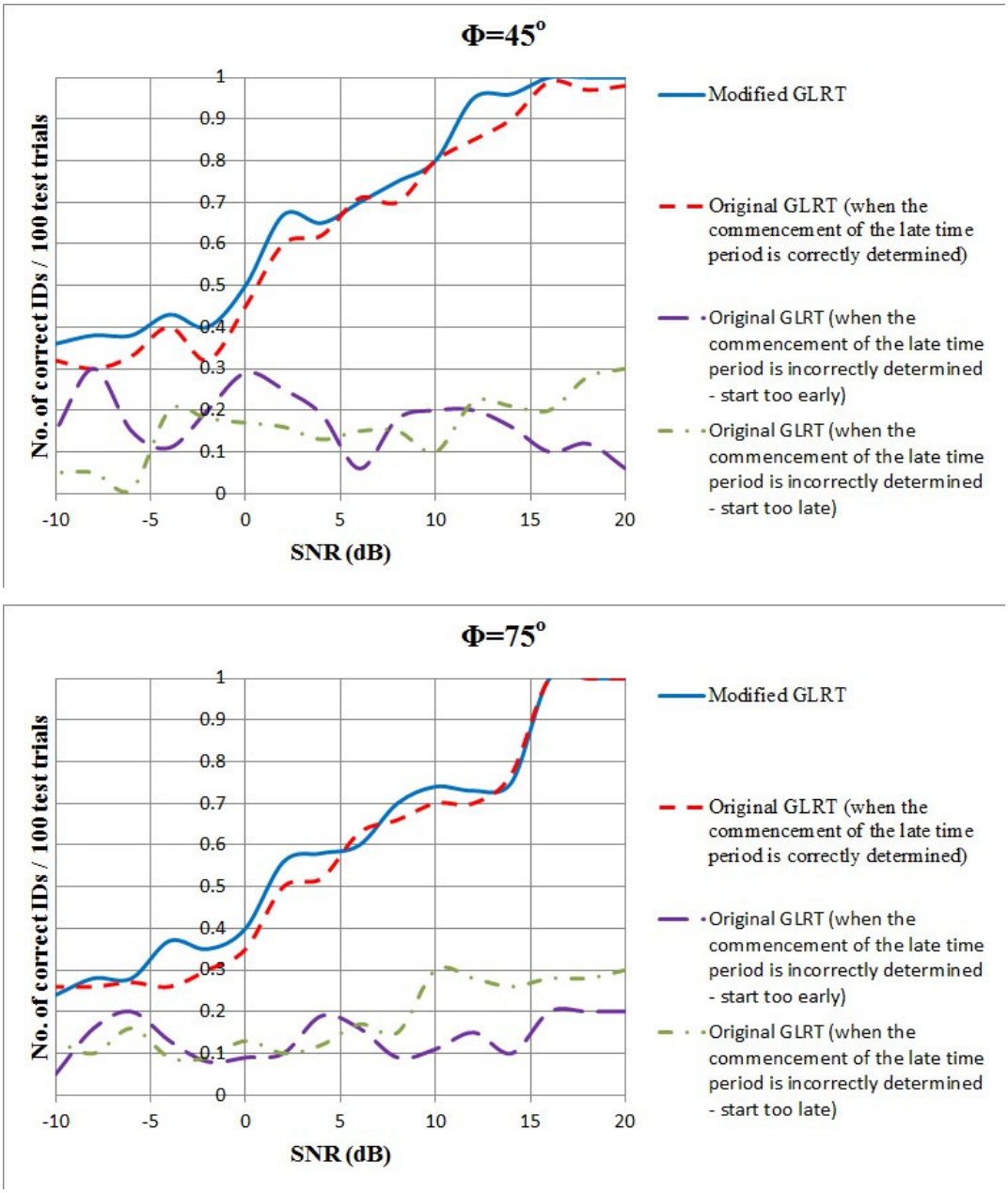

Figure 5.13: The performance of the modified GLRT and original GLRT methods as a function of SNR for four different incident angles using the five ellipsoid targets.

5.4.3.4 Aircraft Targets with Different Rear Wings

For our last example, we will consider five wire model aircraft targets. In this example, 512 frequency samples were considered up to a maximum frequency of 1GHz, resulting to 1024 time samples. The frequency and impulse responses of the reference target, wire model aircraft with a rear wing length of $r = 0.3$m, due to an impulsive plane wave incident from ϕ=45°, can be found in

Figure 5.14. The dominant complex conjugate poles for the five wire model aircraft targets are listed in Table 5.3.

Using Equation 2.4, the commencements of the late time periods for the transient responses of the reference target at an incident angles of ϕ=15°, ϕ=30°, ϕ=45°, and ϕ=75° are estimated to be $T_L = 56nsec$, $T_L = 60nsec$, $T_L = 64nsec$, and $T_L = 74nsec$ respectively. These late times are used to perform the original GLRT test.

Prior to performing the modified GLRT test, WVD is used to determine the high resonance region, A, for the transient response of the reference target. Utilising the energy, E, of the reference target response, the values of A for the transient responses of the reference target at an incident angles of ϕ=15°, ϕ=30°, ϕ=45°, and ϕ=75° are calculated to be $A = 94$, $A = 104$, $A = 110$, and $A = 136$ respectively.

The simulation's results for this example are shown in Figure 5.15 for different plane wave incident angles. In order to simulate the effect of incorrect late time determination for late time starting too early, $T_L = 40nsec$, $T_L = 42nsec$, $T_L = 46nsec$, and $T_L = 56nsec$ are arbitrary chosen for an incident angles of ϕ=15°, ϕ=30°, ϕ=45°, and ϕ=75° respectively. In order to simulate the effect of incorrect late time determination for late time starting too late, $T_L = 100nsec$ is used for all the four incident angles of ϕ=15°, ϕ=30°, ϕ=45°, and ϕ=75°.

Chapter 5: Robust Target Identification Techniques

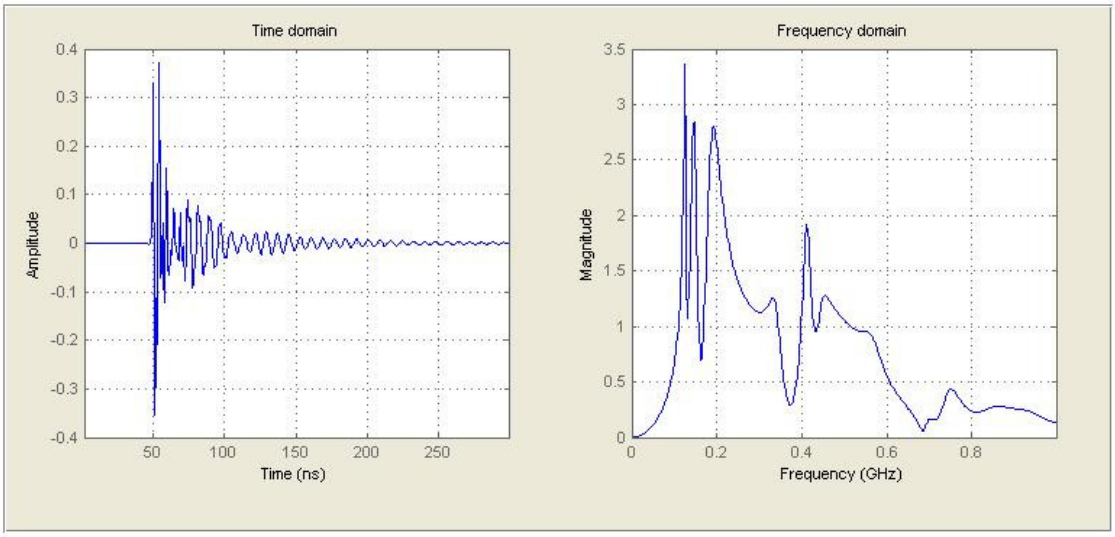

Figure 5.14: The backscattering frequency and impulse responses of the wire model aircraft with a rear wing length of $r = 0.3$m due to an impulsive plane wave incident from ϕ=45^o.

	Aircraft with r = 10cm	Aircraft with r = 20cm	Aircraft with r = 30cm	Aircraft with r = 40cm	Aircraft with r = 50cm
$\frac{s_{1,2}}{c}$	$-0.146 \pm j3.062$	$-0.054 \pm j2.863$	$-0.050 \pm j2.629$	$-0.044 \pm j2.440$	$-0.039 \pm j2.284$
$\frac{s_{3,4}}{c}$	$-0.052 \pm j3.147$	$-0.146 \pm j3.063$	$-0.145 \pm j3.062$	$-0.141 \pm j3.061$	$-0.136 \pm j3.058$
$\frac{s_{5,6}}{c}$	$-0.392 \pm j3.882$	$-0.375 \pm j3.883$	$-0.367 \pm j3.886$	$-0.362 \pm j3.888$	$-0.359 \pm j3.890$
$\frac{s_{7,8}}{c}$	$-0.451 \pm j7.434$	$-0.396 \pm j7.279$	$-0.338 \pm j7.135$	$-0.738 \pm j7.252$	$-0.233 \pm j6.847$
$\frac{s_{9,10}}{c}$	$-0.294 \pm j9.131$	$-0.232 \pm j8.823$	$-0.208 \pm j8.612$	$-0.200 \pm j8.446$	$-0.204 \pm j8.290$
$\frac{s_{11,12}}{c}$	$-0.511 \pm j9.374$	$-0.499 \pm j9.372$	$-1.086 \pm j9.752$	$-0.585 \pm j9.341$	$-0.560 \pm j9.355$
$\frac{s_{13,14}}{c}$	$-0.629 \pm j11.995$	$-0.614 \pm j11.893$	$-0.618 \pm j11.893$	$-0.641 \pm j11.785$	$-0.757 \pm j11.550$
$\frac{s_{15,16}}{c}$	$-0.501 \pm j15.210$	$-0.394 \pm j15.719$	$-0.411 \pm j15.565$	$-0.546 \pm j15.443$	$-0.539 \pm j15.158$
$\frac{s_{17,18}}{c}$	$-0.832 \pm j19.498$	$-0.738 \pm j19.535$	$-1.039 \pm j20.007$	$-0.795 \pm j19.501$	$-0.958 \pm j20.667$

Table 5.3: Natural resonant frequencies of the five wire model aircraft targets.

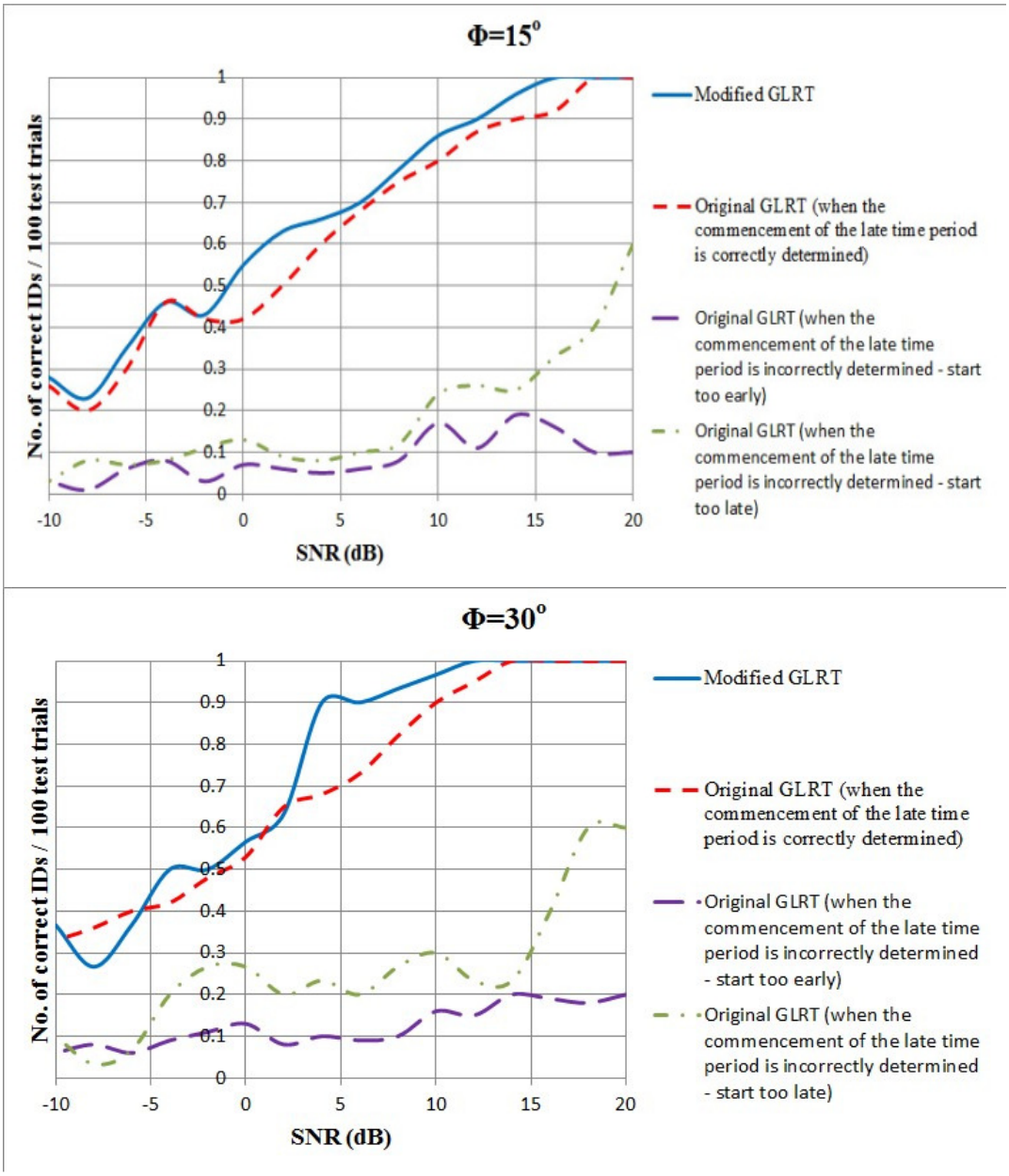
Φ=15°
No. of correct IDs / 100 test trials
SNR (dB)
Modified GLRT
Original GLRT (when the commencement of the late time period is correctly determined)
Original GLRT (when the commencement of the late time period is incorrectly determined - start too early)
Original GLRT (when the commencement of the late time period is incorrectly determined - start too late)
Φ=30°
No. of correct IDs / 100 test trials
SNR (dB)
Modified GLRT
Original GLRT (when the commencement of the late time period is correctly determined)
Original GLRT (when the commencement of the late time period is incorrectly determined - start too early)
Original GLRT (when the commencement of the late time period is incorrectly determined - start too late)

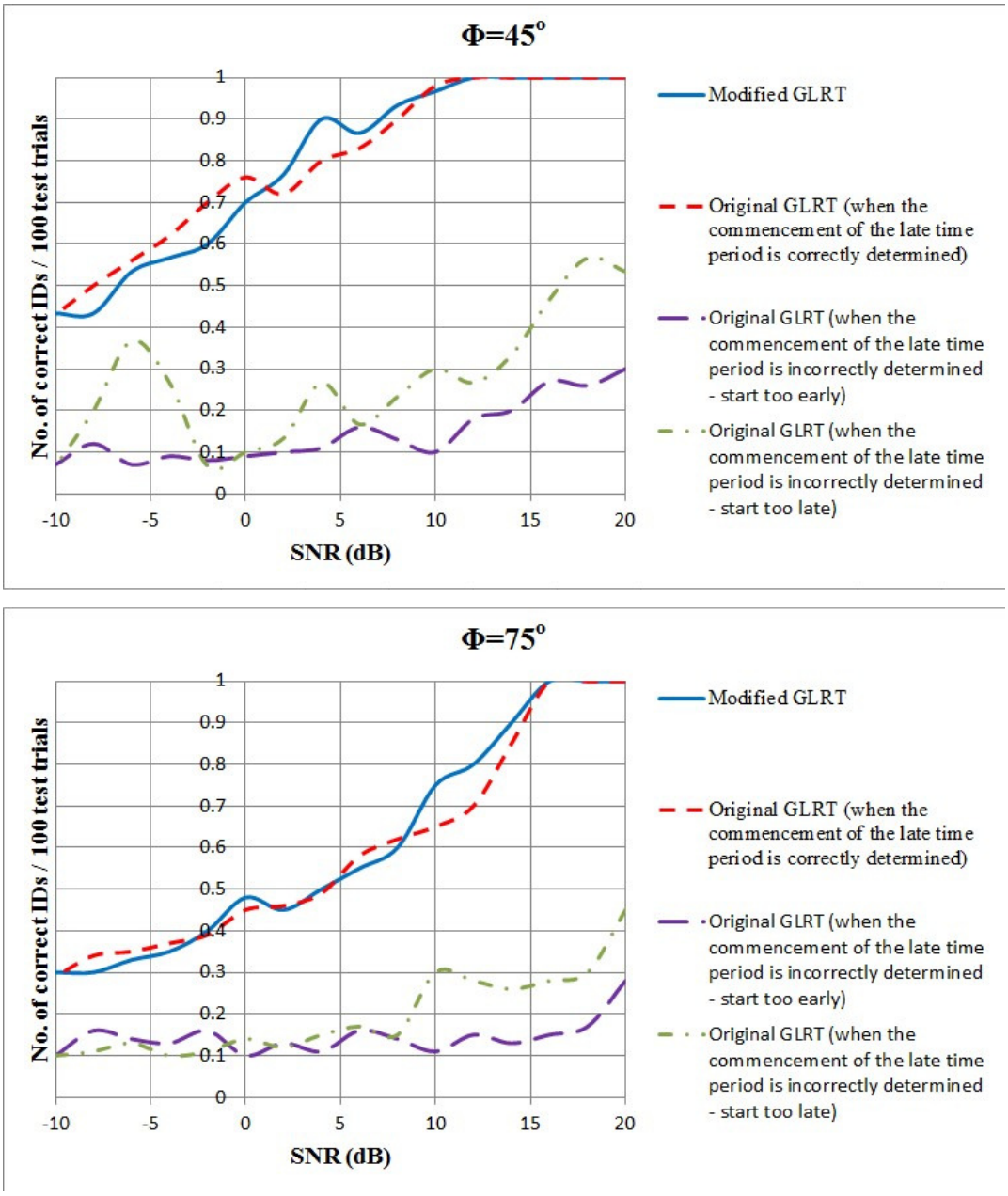

Figure 5.15: The performance of the modified GLRT and original GLRT methods as a function of SNR for four different incident angles using the five wire model aircraft targets.

5.4.4 Discussion

A Q-Factor is used to describe how under-damped a resonator is. Higher Q indicates a lower rate of energy loss relative to the stored energy of the oscillator. Therefore, the oscillations die out more slowly.

Chapter 5: Robust Target Identification Techniques

In order to demonstrate the effectiveness of the modified GLRT technique, we have utilised both the high Q-Factor and low Q-Factor targets in our simple target examples. It can be seen from Figure 5.4, and Figure 5.6 that the bent wire resonates longer in the frequency domain as compared to the ellipsoid target. Therefore, the bent wires and the ellipsoids are our high Q-Factor and low Q-Factor targets respectively.

As can be seen from Figure 5.12, Figure 5.13, and Figure 5.15, the performance of the modified GLRT and original GLRT methods are plotted as a function of SNR in decibels for each target orientation. The performance of each technique is defined as the number of correct identifications (IDs) per 100 test trials at a specified SNR value.

It can be seen from the bent wire targets example, Figure 5.12, that the performance of both the modified GLRT and original GLRT methods matches closely to each other, for each target orientation, when the commencement of the late time period for the transient response of the reference target is correctly estimated. At an aspect angles of $\phi=15^o$, $\phi=30^o$, $\phi=45^o$, and $\phi=75^o$ both the techniques begin to correctly identify the reference target in every trial at a SNR of 4dB, 8dB, and 4dB respectively.

It can be seen from the ellipsoid targets example, Figure 5.13, that the modified GLRT technique outperforms the original GLRT method at aspect angles of $\phi=15^o$ and $\phi=45^o$, even though the commencement of the late time period for the transient response of the reference target is correctly determined. At an aspect angle of $\phi=30^o$ and $\phi=75^o$, the performance of the modified GLRT and original GLRT techniques matches closely to each other and both the detectors start to correctly identify the reference target in every trial at a SNR of 12dB and 16dB respectively.

Last but not least, it can be seen from the wire model aircraft targets example, Figure 5.15, that the modified GLRT technique outperforms the original GLRT method at aspect angles of $\phi=15^o$, even though the commencement of the late time period for the transient responses of the reference target is correctly determined. At an aspect angle of $\phi=30^o$, $\phi=45^o$, and $\phi=75^o$, the performance of the modified GLRT and original GLRT techniques matches closely to each other and both the classifier start to correctly identify the reference target in every trial at a SNR of 14dB, 12dB, and 16dB respectively.

It can be seen from our simple target examples that there is a slight drop in the detectors' performance on the ellipsoid targets because the ellipsoid has a lower Q factor. The substructures and the small difference in the rear wings of the wire model aircraft targets have also deteriorate the performance of the classifiers. Also as predicted, the performance of both the modified GLRT and the original GLRT techniques decreases as SNR decreases.

It is demonstrated from both the simple targets and complex targets examples that the modified GLRT technique outperforms the original GLRT method when the commencement of the late time period for the transient response of the reference target is incorrectly estimated. If the commencement of the late time period is estimated to start too early, the inclusion of the early time component in the transient response of the reference target will deteriorate the performance of the original GLRT method as the original GLRT technique is based on SEM representation which models only the late time response of the target. If the commencement of the late time period is determined to start too late, the exclusion of some resonances which are used to reconstruct the transient response of the reference target will also affect the performance of the original GLRT method.

In summary, it is noted in the bent wire targets, ellipsoid targets, and wire model aircraft targets simulation results that the performance of the modified GLRT method either matches closely or exceeds the performance of the original GLRT technique when the commencement of the late time period is determined correctly. If the commencement of the late time period is determined incorrectly, the modified GLRT technique will outperform the original GLRT method by a considerable margin. Therefore, this has demonstrated the robustness of the modified GLRT technique although its computational cost is higher. The additional computational complexity involved including the formation of the WVD map and the construction of A GLRT tests in the classification process. By using a set of five candidate targets, the typical runtime for the classification of a test target in MATLAB, using a computer with Intel Core 2 Quad processor, is around 20 seconds (approximate 4 seconds for the formation of the WVD map and approximate 16 seconds for the construction of A GLRT tests).

5.4.5 Remarks

In this research, we have developed a robust resonance based target identification technique which does not require *prior* knowledge of the commencement of the late time period for the transient reponse of the unknown target. Numerical results using both the simple and complex targets have demonstrated the effectiveness of our method, modified GLRT test, as compare to the original GLRT technique in the presence of random noise. Improving the speed of the new technique and applying it to the dielectric target and more realistic target will be the subject of further investigation.

5.5 Conclusion

In the context of ATR, the design of a reliable and robust classifier plays an important role in the feature based target identification system. Therefore, it is the dream of researchers around the world to keep on enhancing the performance of the current classifiers. In this chapter, we have proposed two unique classifiers to improve the resonance based target identification process.

Numerical results have proven that the recommended CCA based and modified GLRT techniques are comparable to the well-known GLRT technique in the presence of noise. In some cases, the modified GLRT method even outperforms the original GLRT technique. Examples have also shown that *prior* knowledge of the commencement of the late time period for the transient reponse of the unknown target is not require by using the proposed modified GLRT. However, to further quantify the performance of the proposed resonance based target classifiers, further investigation using dielectric targets is needed.

Chapter 6: Conclusions and Future Works

Chapter 6: Conclusions and Future Works

6.1 Conclusions

The popularity of using CNRs as a feature set for radar target identification is no doubt due to the fact that they are theoretically independent of the aspect angle between the radar and the target, and they form a minimal set of parameters by which the target can be identified thus assisting the classification problem. In this thesis, the concert of radar target classification based on CNRs is further examined.

This thesis focuses on designing a reliable and robust resonance based target discrimination process by breaking down the resonance based target identification process into two parts. The first part which involves identifying the dominant poles of the target could be found in Chapter 4 and the second part which consists of designing a classifier that is capable of identifying the correct object from a set of targets under all weather conditions could be found in Chapter 5.

MPM has been widely used in the literature for extracting the resonant frequencies of the target due to its robustness to noise in the sampled data and computational ease. But the rank deficiency problem in the $\mathbf{Z}$ matrix, shown in Equation 2.15, of the MPM has degraded the performance of the MPM. A solution to the rank deficiency issue of the MPM has been presented in Chapter 4 and it is hoped that the proposed solution would enhance the performance of the MPM.

It is important for the CNRs to be properly excited before they could be extracted from the backscattered signature of the target. However, for certain aspect angles some poles cannot be excited sufficiently. Therefore, in order to ensure that all of the dominant CNRs of the target are extracted so as to avoid false alarms during the target identification process, target responses from multiple incident aspect angles and/or multiple incident polarizations are used. A novel technique based on multiple data sets and PCA is introduced in Chapter 4 to enhance the CNRs extraction process. Numerical examples have proven the feasibility of the proposed technique.

Determining the modal order of the system is one of the major problems related to CNRs extraction. Incorrectly determining the modal order of the system may result in spurious poles and affect the

identification results. Moreover, if the received signature is corrupted by noise, identifying the significant poles of the target will become an even more complex problem to solve. A post processing technique, based on examining the energies of the extracted CNRs, has been introduced in Chapter 4 to identify the dominant CNRs of the target for a particular aspect. The extraction for the dominant poles of the target is done without *prior* knowledge of the modal order of the system. Numerical results have demonstrated the viability of the proposed method.

In order to correctly identify a remote target, a robust target signatures identification technique is required. As evident from the literature, statistical techniques such as the GLRT have produced a better identification result, in the presence of noise, compared to some other SEM based identification methods such as the E-pulse technique. Two novel resonance based classifiers have been presented in Chapter 5 and their performances are measured against the original GLRT method. Numerical examples have demonstrated the performance of the proposed CCA based technique. Simulation results using various targets have also shown that the suggested modified GLRT method, which utilizes the WVD, is comparable to the original GLRT technique when the commencement of the late time period for the unknown target response is correctly determined and outperforming the original GLRT technique when the commencement of the late time period for the unknown target response is incorrectly determined.

In conclusion, a unique set of resonance based target recognition techniques have been proposed in this thesis and it is hope that the works presented in this research would enhance the ATR process.

6.2 Limitations and Future Works

The scope of this thesis has been limited to free space stationary PEC targets. The contributions made by this thesis may also be applied to dielectric targets, subsurface targets, and non-stationary targets. Upon the proposition of the SEM, efforts have largely focused on target recognition applications that involve radar targets in free space. The concept of target resonances for subsurface target was first fully addressed by Carin in a number of his works [68], [69]. Baum [70] has also studied the scattering and target resonances of buried metallic and dielectric target within a lossy media. Recently, microwave remote sensing that utilizes Baum technique has been applied to biological targets (i.e. breast tumor, hip prosthesis etc.) detection [71]-[74].

Chapter 6: Conclusions and Future Works

When the target is buried beneath a half-space, the scattering problem becomes increasingly complicated. Usually the excitation and the measured field points are located in the free space (air) and the target is embedded in the heterogeneous dispersive dielectric half-space. The 'total target' is the target together with the presence of the environment. As the depth and orientation of the target changes inside the environment, the characteristics of the 'total target' change as well. Furthermore, the scattered field from the object varies as the dielectric properties of the surrounding environment change.

As a first step to identify the target below a half-space, the authors of [74] have suggested using Baum's transform [11], [70] to classify an object below a homogeneous and lossy environment. Although it is a promising approach, it is noted that Baum's transform does not take the air-medium interface into consideration. Therefore, future works on subsurface target identification could go in this direction but include some techniques to remove the air-medium interface before applying the Baum's transform. Further investigations on using the poles extracted from the target in the homogeneous medium to classify the target below the half-space could also be conducted.

The scattering behaviour of the dielectric targets is much more complicated than that of the PEC targets. One of the most major differences is that there are additional resonant modes from internal bouncing that are in addition to the normal radiating modes [70]. Therefore, it is suggested to investigate the feasibility of applying the contributions make in this thesis to the dielectric targets in free space first before investigating the feasibility of applying them to the dielectric targets under the half-space.

As mentioned previously, the works presented in this thesis are limited to the stationary targets. Hence, future work could involve studying the resonances behaviour of the non-stationary targets and applying the contributions make in this thesis to them.

The impact of scatterer occlusion on the performance of the resonance based target identification system could also be the subject of further investigation.

Last but not least, white Gaussian noise is the only component that is being introduced into the system to quantify the performance of the proposed techniques in this thesis. Therefore, future work

could involve investigating the effect of other sources of interferences, such as clutter and multipath, on the performance of the proposed techniques presented in this thesis.

Finally, other than the above suggested future works, investigation on improving the speed of the proposed modified GLRT method could also be carried out.

List of References

List of References

[1] M. A. Morgan, "Target I.D. using natural resonances," *IEEE Potentials*, vol. 12, no. 4, pp. 11-14, 1993.

[2] W.-D. Wirth, *Radar techniques using array antennas*, London: Institution of Electrical Engineers, 2001.

[3] A. E. Souvorov, A. E. Bulyshev, S. Y. Semenov, R. H. Svenson, A. G. Nazarov, Y. E. Sizov, and G. P. Tatsis, "Microwave tomography: A two-dimensional Newton iterative scheme," *IEEE Trans. Microwave Theory Tech.*, vol. 46, no. 11, pp. 1654-1659, 1998.

[4] N. Joachimowicz, C. Pichot, and Jean-Paul Hugonin, "Inverse scattering: An iterative numerical method for electromagnetic imaging," *IEEE Trans. Antennas Propag.*, vol. 39, no. 12, pp. 1742-1752, 1991.

[5] D. Blacknell and H. Griffiths, *Radar automatic target recognition (ATR) and non-cooperative target recognition (NCTR)*, London: The Institution of Engineering and Technology, 2013.

[6] J. Chauveau, N. D. Beaucoudrey, and J. Saillard, "Determination of resonance poles of radar targets in narrow frequency bands," *Proceedings of the 4th European Radar*, pp. 122-125, 2007.

[7] C. E. Baum, "The singularity expansion method," in *Transient Electromagnetic Fields*, L. B. Felsen Ed., New York: Springer-Verlag, pp. 129-179, 1976.

[8] N. Shuley and D. Longstaff, "Role of polarisation in automatic target recognition using resonance descriptions," *IEEE Electronics Letters*, vol. 40, pp. 268-270, 2004.

[9] C. E. Baum, E. J. Rothwell, K. M. Chen, and D. P. Nyquist, "The singularity expansion method and its application to target identification," *Proceedings of the IEEE*, vol. 79, pp. 1481-1492, 1991.

[10] M. L. V. Blaricum and R. Mittra, "A technique for extracting the poles and residues of a system directly from its transient response," *IEEE Trans. Antennas Propag.*, vol. 23, pp. 777-781, 1975.

[11] C.-C. Chen and L. Peters, Jr., "Buried unexploded ordnance identification via complex natural resonances," *IEEE Trans. Antennas Propag.*, vol. 45, pp. 1645-1654, 1997.

[12] B. Drachman and E. Rothwell, "A continuation method for identification of the natural frequencies of an object using a measured response," *IEEE Trans. Antennas Propag.*, vol. 33, pp. 445-450, 1985.

List of References

[13] T. K. Sarkar and O. Pereira, "Using the matrix pencil method to estimate the parameters of a sum of complex exponentials," *IEEE Trans. Antennas Propag.*, vol. 37, pp. 48-55, 1995.

[14] T. K. Sarkar, S. Park, J. Koh, and S. M. Rao, "Application of the matrix pencil method for estimating the SEM (Singularity Expansion Method) poles of source-free transient responses from multiple look directions," *IEEE Trans. Antennas Propag. Mag.*, vol. 48, pp. 612-618, 2000.

[15] G. Turhan-Sayan and M. Kuzuoglu, "Pole estimation for arbitrarily-shaped dielectric targets using genetic algorithm-based resonance annihilation technique," *IEEE Electronics Letters*, vol. 37, pp. 380-381, 2001.

[16] E. Rothwell, C. Kun-Mu, and D. Nyquist, "Extraction of the natural frequencies of a radar target from a measured response using E-pulse techniques," *IEEE Trans. Antennas Propag.*, vol. 35, pp. 715-720, 1987.

[17] E. J. Rothwell and K. M. Chen, "A hybrid E-pulse/least squares technique for natural resonance extraction," *Proceedings of the IEEE*, vol. 76, pp. 296-298, 1988.

[18] Y. Hua and T. K. Sarkar, "On SVD for estimating generalized eigenvalues of singular matrix pencil in noise," *IEEE Trans. on Signal Processing*, vol. 39, pp. 892-900, 1991.

[19] Y. Hua and T. K. Sarkar, "Matrix pencil method for estimating parameters of exponentially damped/undamped sinusoids in noise," *IEEE Trans. on Acoustics, Speech, and Signal Processing*, vol. 38, pp. 814-824, 1990.

[20] Y. Hua and T. K. Sarkar, "Generalized pencil-of-function method for extracting poles of an EM system from its transient response," *IEEE Trans. Antennas Propag.*, vol. 37, pp. 229-234, 1989.

[21] L. W. Pearson, M. L. Van Blaricum, and R. Mittra, "A new method for radar target recognition based on the singularity expansion for the target," *IEEE Int. Radar Conf. Rec.*, Arlington, VA, USA, pp. 452-457, 1975.

[22] E. Kennaugh, "The K-pulse concept," *IEEE Trans. Antennas Propag.*, vol. 29, pp. 327-331, 1981.

[23] F. Fok, D. Moffatt, and W. Nan, "K-pulse estimation from the impulse response of a target," *IEEE Trans. Antennas Propag.*, vol. 35, pp. 926-933, 1987.

[24] J. E. Mooney, Z. Ding, and L. S. Riggs, "Robust target identification in white Gaussian noise for ultra wide-band radar systems," *IEEE Trans. Antennas Propag.*, vol. 46, pp. 1817-1823, 1998.

List of References

[25] J. E. Mooney, Z. Ding, and L. S. Riggs, "Performance analysis of a GLRT automated target discrimination scheme," *IEEE Trans. Antennas Propag.*, vol. 49, pp. 1827-1835, 2001.

[26] J. D. Taylor, *Introduction to ultra-wideband radar system*, Boca Raton: CRC Press, 1995.

[27] S. M. Rao, *Time domain electromagnetics*, San Diego: Academic Press, 1999.

[28] K. R. Menon, "Application of high frequency natural resonances extracted from electromagnetic scattering response for discrimination of radar targets with minor variations," *Ph.D. Thesis*, Department of Aerospace Engineering, India Institute of Science, 2001.

[29] R. Harrington, *Field computation by the Moment Method (2nd Edition)*, IEEE Press, 1993.

[30] J. D. Taylor, *Ultra wideband radar applications and design*, CRC Press, 2012.

[31] L. Felsen, "Comments on early time SEM," *IEEE Trans. Antennas Propag.*, vol. 33, pp. 118-119, 1985.

[32] S. Jang, W. Choi, T. K. Sarkar, M. Salazar-Palma, K. Kyungjung, and C. E. Baum, "Exploiting early time response using the fractional Fourier transform for analyzing transient radar returns," *IEEE Trans. Antennas Propag.*, vol. 52, pp. 3109-3121, 2004.

[33] M. A. Richards, "SEM representation of the early and late time fields scattered from wire targets," *IEEE Trans. Antennas Propag.*, vol. 42, pp. 564-566, 1994.

[34] D. W. Wang, Y. Su, X. Y. Ma, and S. G. Wang, "Natural resonance frequency extraction using an early-time and late-time responses combined technique," *Ultrawideband and Ultrashort Impulse Signals*, Sevastopol, Ukraine, pp. 201-204, 2004.

[35] D. Jiao, S. J. Xu, and X. L. Wu, "Extraction of natural frequency from measured late-time transient responses with rational minimax approximation in frequency domain," *Proc. Int. Conf. Microwave and Millimeter Wave Technology*, pp. 986-989, 1998.

[36] J. W. Nilsson and S. A. Riedel, *Electric circuits (9th Edition)*, New Jersey: Prentice Hall, 2011.

[37] A. V. Oppenheim, A. S. Willsky, and S. H. Nawab., *Signals & systems (2nd Edition)*, New Jersey: Prentice Hall, 1997.

[38] E. M. Kennaugh and D. L. Moffatt, "Transient and impulse response approximations," *Proceedings of the IEEE*, vol. 53, pp. 893-901, 1965.

[39] Y. Wang and N. Shuley, "Complex resonant frequencies for the identification of simple objects in free space and lossy environment," *Progress In Electromagnetics Research*, PIER 27, pp. 1-18, 2000.

List of References

[40] A. Mackay and A. McCowen, "An improved pencil-of-functions method and comparisons with traditional methods of pole extraction," *IEEE Trans. Antennas Propag.*, vol. 35, pp. 435-441, 1987.

[41] M. P. Ross, D. D. Dudley, A. J. Mackay, and A. McCowen, "Comments on 'An improved pencil-of-functions method and comparisons with traditional methods of pole extraction' [and reply]," *IEEE Trans. Antennas Propag.*, vol. 36, pp. 1192-1194, 1988.

[42] V. Jain, T. Sarkar, and D. Weiner, "Rational modeling by pencil-of-functions method," *IEEE Trans. on Signal Processing*, vol. 31, pp. 564-573, 1983.

[43] Y. Hua, A. B. Gershman, and Q. Cheng, *High-resolution and robust signal processing*, New York: Marcel Dekker, 2004.

[44] Q. Li, P. Ilavarasan, J. E. Ross, E. J. Rothwell, K. M. Chen, and D. P. Nyquist, "Radar target identification using a combined early-time/late-time e-pulse technique," *IEEE Trans. Antennas Propag.*, vol. 46, pp. 1272-1277, 1998.

[45] L. H. S. Anthony and N. Shuley, "Consequence of incorrect sampling procedures in resonance-based radar target identification," *IEE Electron. Letters*, vol. 40, pp. 507-508, 2004.

[46] H. L. Van Trees, *Detection, estimation, and modulation theory: Part I*, New York: Wiley, 1967.

[47] V. Blaricum, *Ultra wideband radar*, Boca Raton: CRC Press, 1991.

[48] L. Cohen, "Time-frequency distributions-a review," *Proceedings of the IEEE*, vol. 77, pp. 941-981, 1989.

[49] L. Cohen, *Time-frequency analysis*, New Jersey: Prentice Hall PTR, 1995.

[50] F. Hlawatsch and G. F. Boudreaux-Bartels, "Linear and quadratic time-frequency representations," *IEEE Signal Processing Mag.*, vol. 9, pp. 21-67, 1992.

[51] X.-Y. Jin, D. Zhang, and J.-Y. Yang, "Face recognition based on a group decision-making combination approach," *Pattern Recognition*, vol. 36, pp. 1675-1678, 2003.

[52] Q.-S. Sun, S.-G. Zeng, Y. Liu, P.-A. Heng, and D.-S. Xia, "A new method of feature fusion and its application in image recognition," *Pattern Recognition*, vol. 38, pp. 2437-2448, 2005.

[53] J. Yang, J.-Y. Yang, D. Zhang, and J.-F. Lu, "Feature fusion: parallel strategy vs. serial strategy," *Pattern Recognition*, vol. 36, pp. 1369-1381, 2003.

[54] R. Battiti, "Using mutual information for selecting features in supervised neural net learning," *IEEE Trans. Neural Networks*, vol. 5, pp. 537-550, 1994.

List of References

[55] J. Chauveau, N. D. Beaucoudrey, and J. Saillard, "Selection of contributing natural poles for characterization of perfectly conducting targets in resonance region," *IEEE Trans. Antennas Propag.*, vol. 55, pp. 2610-2617, 2007.

[56] P. C. Hansen, *Rank-deficient and discrete ill-posed problems – numerical aspects of linear inversion*, Philadelphia: Society for Industrial and Applied Mathematics, 1998.

[57] R. S. Adve, T. K. Sarkar, O. M. Pereira-Filho, and S. M. Rao, "Extrapolation of time-domain responses from three-dimensional conducting objects utilizing the matrix pencil technique," *IEEE Trans. Antennas Propag.*, vol. 45, pp. 147-156, 1997.

[58] E. J. Rothwell, J. Baker, K. M. Chen, and D. P. Nyquist, "Approximate natural response of an arbitrarily shaped thin wire scatterer," *IEEE Trans. Antennas Propag.*, vol. 39, pp. 1457-1462, 1991.

[59] H.-S. Lui and N. Shuley, "Resonance based radar target identification with multiple polarizations," *IEEE AP-S Int. Symp.*, New Maxico, USA, pp. 3259-3262, 2006.

[60] D. Moffatt and R. Mains, "Detection and discrimination of radar targets," *IEEE Trans. Antennas Propag.*, vol. 23, pp. 358-367, 1975.

[61] Hoi-Shun Lui and Nicholas V. Z. Shuley, "Sampling procedures for resonance based radar target identification," *IEEE Trans. Antennas Propag.*, vol. 56, pp. 1487-1491, 2008.

[62] H. Hotelling, "Relations between two sets of variates," *Biometrika*, vol. 28, pp. 321-377, 1936.

[63] W. Wang, T. Adalt, and D. Emge, "Target detection and identification using canonical correlation analysis and subspace partitioning," *IEEE ICASSP*, pp. 2117-2120, 2008.

[64] A. Pezeshki, M. R. Azimi-Sadjadi, and L. L. Scharf, "Undersea target classification using canonical correlation analysis," *IEEE Journal of Oceanic Engineering*, vol. 32, 2007.

[65] M. L. Marlow, "A canonical correlation analysis of savings and loan association performance," *Applied Economics*, vol. 15, pp. 815-820, 1983.

[66] James H. Harlow, *Electric power transformer engineering*, CRC Press, pp. 2-216, 2004.

[67] H. S. Lui and N. V. Z. Shuley, "Evolutions of partial and global resonances in transient electromagnetic scattering," *IEEE Antennas and Wireless Propag. Letters*, vol. 7, pp. 436-439, 2008.

[68] S. Vitebskiy, L. Carin, M. A. Ressler, and F. H. Le, "Ultra-wideband, shortpulse ground-penetrating radar: simulation and measurement," *IEEE Trans. Geoscience and Remote Sensing*, vol. 35, pp. 762-772, 1997.

List of References

[69] T. Dogaru and L. Carin, "Time-domain sensing of targets buried under a rough air-ground interface," *IEEE Trans. Antennas Propag.*, vol. 46, pp. 360-372, 1998.

[70] C. E. Baum, "Detection and Identification of Visually Obscured Targets," Taylor & Francis, 1999.

[71] Y. Huo, R. Bansal, and Q. Zhu, "Breast tumor characterization via complex natural resonances," *IEEE Int. Microwave Symp.*, pp. 387-390, 2003.

[72] Y. Huo, R. Bansal, and Q. Zhu, "Modeling of noninvasive microwave characterization of breast tumors," *IEEE Trans. Biomed. Eng.*, vol. 51, pp. 1089-1094, 2004.

[73] H. S. Lui, N. Shuley, S. Crozier, "A Concept for Hip Prosthesis Identification using Ultra Wideband Radar," *Proceedings of the 26th Annual Int. Conf. of the IEEE Engineering in Medicine and Biology Society*, pp. 1439-1442, 2004.

[74] H. S. Lui, N. V. Z. Shuley, and A. D. Rakic, "A novel, fast, approximate target detection technique for metallic target below a frequency dependant lossy halfspace," *IEEE Trans. Antennas Propag.*, vol. 58, pp. 1699-1710, 2010.

[75] F. Abujarad, A. Jostingmeier, and A. S. Omar, "Clutter removal for landmine using different signal processing techniques," *Proceedings Tenth IEEE Int. Conf. on Ground Penetrating Radar*, pp. 697-700, 2004.

[76] F. Abujarad and A. S. Omar, "Factor and principle component analysis for automatic landmine detection based on ground penetrating radar," *German Microwave Conf. (GeMiC)*, 2006.

[77] B. Karlsen, J. Larsen, H. B. D. Sorensen, and K. B. Jakobsen, "Comparison of PCA and ICA based clutter reduction in GPR systems for anti personal landmine detection," *Proceedings 11th IEEE Workshop on Statistical Signal Processing*, pp. 146-149, 2001.

[78] Q. Zhu and B. D. Steinberg, " Correction of multipath interference using CLEAN and spatial location diversity," *IEEE Ultrasonics Symp.*, vol. 2, pp. 1367-1370, 1995.

[79] R. L. Burden and J. d. Faires, *Numerical analysis*, Third ed. Boston: PWS-KENT Publishing Company, 1985.

[80] A. K. Shaw and K. Naishadham, "ARMA-based time-signature estimator for analysing resonant structures by the FDTD method," *IEEE Trans. Antennas Propag.*, vol. 49, pp. 327-339, 2001.

[81] P. Ilavarasan, J. E. Ross, K. M. Chen, and D. P. Nyquist, "Performance of an automated radar target discrimination scheme using E-Pulses and S-Pulses," *IEEE Trans. Antennas Propag.*, vol. 41, pp. 582-588, 1993.

List of References

[82] J. H. Wang, *Generalized Moment Methods in electromagnetics: Formulation and computer solution of integral equations*, John Wiley and Sons Inc., 1991.

[83] A. R. Djordjevic, T. K. Sarkar, and E. Arvas, "On the choice of expansion of weighting functions in the numerical solution of operator equations," *IEEE Trans. Antennas Propag.*, vol. 33, pp. 988-596, 1985.

[84] T. K. Sarkar, "Application of conjugate gradient method to electromagnetics and signal analysis," *Progress in Electromagnetics Research Series*, No. 5, 1991.

[85] R. Coifman, V. Rokhlin, and S. Wandzura, "The fast multipole method: A pedestrian description," *IEEE Trans. Antennas Propag.*, vol. 35, pp. 7-12, 1993.

[86] V. G. Nebabin, *Method and techniques of radar recognition*, Artech House, 1995.

[87] W. M. Boerner, "Use of polarization in electromagnetic inverse scattering," *Radio Science*, vol. 16, pp. 1045, 1981.

[88] M. C. Lin and Y. W. Kiang, "Target discrimination using multiple frequency amplitude returns," *IEEE Trans. Antennas Propag.*, vol. 28, pp. 1885-1889, 1990.

[89] J. S. Chen and E. K. Walton, "Comparison of two target classification techniques," *IEEE Trans. on Aerospace and Electronics Systems*, vol. 22, pp. 15-21, 1986.

[90] S. Vitebskiy and L. Carin, "Resonances of perfectly conducting wires and bodies of revolution buried in a lossy dispersive half-space," *IEEE Trans. Antennas Propag.*, vol. 44, pp. 1575-1583, 1996.

[91] Y. Wang, I. D. Longstaff, C. J. Leat, and N. V. Shuley, "Complex natural resonances of conducting planar objects buried in a dielectric half-space," *IEEE Trans. Geoscience and Remote Sensing*, vol. 39, pp. 1183-1189, 2001.

[92] H. S. Lui and N. V. Z. Shuley, "Radar target identification using a banded e-pulse technique", *IEEE Trans. Antennas Propag.*, vol. 54, pp. 3874-3881, 2006.

[93] N. F. Chamberlain, E. K. Walton, and F. D. Garber, "Radar target identification of aircraft using polarization-diverse features," *IEEE Trans. on Aerospace and Electronics Systems*, vol. 27, pp. 58-67, 1991.

[94] D. G. Dudley, "Progress in identification of electromagnetic systems," *IEEE Antennas Propag Newsletter*, pp. 5-11, 1988.

[95] C.-C. Chen, "Electromagnetic resonances of immersed dielectric spheres," *IEEE Trans. Antennas Propag.*, vol. 46, pp. 1074-1083, 1998.

[96] L. Y. Astanin, A. A. Kostylev, Y. S. Zinoviev, and A. Y. Parmurov, *Radar target characteristics: measurements and applications*, CRC Press, 1994.

List of References

[97] F. C. Committee, *FCC: First Report and Order*, 2002.

[98] J. Zhang, T. D. Abhayapala, and R. A. Kennedy, "Role of pulses in ultra wideband systems," *IEEE Int. Conf. on Ultra-Wideband*, pp. 565-570, 2005.

[99] C. O. Hargrave, I. V. L. Clarkson, and H. S. Lui, "Late-time estimation for resonance-based radar target identification," *IEEE Trans. Antennas Propag.*, vol. 62, pp. 5865-5871, 2014.

[100] T. Fawcett, "An introduction to ROC analysis," *Pattern Recognition Letters*, vol. 27, pp. 861-874, 2006.

[101] K. Haspert, J. Heagy, and R. Sullivan, "Template-based target identification and confusion matrices," *IEEE A&E Systems Mag.*, vol. 21, pp. 53-67, 2006.

[102] J. M. Hill, M. E. Oxley, and K. W. Bauer, "Receiver operating characteristic curves and fusion of multiple classifiers", *Proceedings of the Sixth International Conference of Information Fusion*, vol 2, pp. 815–822, 2003.

[103] J. A. O'Sullivan, M. D. Devore, V. Kedia, and M. I. Miller, "SAR ATR performance using a conditionally Gaussian model," *IEEE Trans. on Aerospace and Electronics Systems*, vol. 37, pp. 91-108, 2001.

[104] H. Zhang, Z. Fan, D. Ding, and R. Chen, "Radar target recognition based on multi-directional e-pulse technique," *IEEE Trans. Antennas Propag.*, vol. 61, pp. 5838-5843, 2013.

[105] J. A. G. Guerrero, D. P. Ruiz, and M. C. Carrion, "Classification of geometrical targets using natural resonances and principle component analysis," *IEEE Trans. Antennas Propag.*, vol. 61, pp. 4881-4884, 2013.

[106] S. Vitebskiy and L. Carin, "Moment-method modelling of short-pulse scattering from and the resonances of a wire buried inside a lossy, dispersive half-space," *IEEE Trans. Antennas Propag.*, vol. 43, pp. 1303-1312, 1995.

[107] E. Heyman and L. B. Felsen, "A wavefront interpretation of the singularity expansion method," *IEEE Trans. Antennas Propag.*, vol. 33, pp. 706-718, 1985.

[108] H. Shirai and L. Felsen, "Wavefront and resonance analysis of scattering by a perfectly conducting flat strip," *IEEE Trans. Antennas Propag.*, vol. 34, pp. 1196-1207, 1986.

[109] E. Heyman and L. B. Felsen, "Creeping waves and resonances in transient scattering by smooth convex objects," *IEEE Trans. Antennas Propag.*, vol. 31, pp. 426-437, 1983.

[110] L. B. Felsen, "Progressing and oscillatory waves for hybrid synthesis of source excited propagation and diffraction (invited review paper *IEEE Trans. Antennas Propag.*, vol. 32, pp. 775–796, 1984.

List of References

[111] C. E. Baum, “Substructure SEM,” in *Ultra-Wideband Short-Pulse Electromagnetics 7*, F. Sabath, Ed. et al. New York: Springer, ch. 72, pp. 681–689, 2007.